ÉCOLE DE TECHNOLOGIE SUPÉRIEURE
UNIVERSITÉ DU QUÉBEC

MASTER THESIS PRESENTED TO
ÉCOLE DE TECHNOLOGIE SUPÉRIEURE

IN PARTIAL FULFILLMENT OF THE REQUIREMENTS FOR
THE MASTER'S DEGREE WITH THESIS IN MECHANICAL ENGINEERING
M. A. Sc.

BY
Golnaz KHOSRAVI

PREDICTION OF BIOPARTICLES DISPERSION AND DISTRIBUTION IN A HOSPITAL ISOLATION ROOM

MONTREAL, 9th FEBRUARY-2016

BOARD OF EXAMINERS

THIS THESIS HAS BEEN EVALUATED

BY THE FOLLOWING BOARD OF EXAMINERS

Mr. Stéphane Hallé, Thesis Supervisor

Department of Mechanical Engineering at École de technologie supérieure

Mr. François Morency, Thesis Co-supervisor
Department of Mechanical Engineering at École de technologie supérieure

Pierre Bélanger, Chair, Board of Examiners
Department of Mechanical Engineering at École de technologie supérieure

François Garnier, Member of the jury
Department of Mechanical Engineering at École de technologie supérieure

THIS THESIS WAS PRESENTED AND DEFENDED

IN THE PRESENCE OF A BOARD OF EXAMINERS AND THE PUBLIC

2nd FEBRUARY-2016

AT ÉCOLE DE TECHNOLOGIE SUPÉRIEURE

“You are not a drop in the ocean. You are the entire ocean, in a drop.”

…….. Rumi

ACKNOWLEDGMENTS

Many people have contributed to the production of this thesis. I owe my gratitude to all those people who have made this dissertation possible and because of whom my graduate experience has been one that I will cherish forever.

My deepest gratitude is to my advisor Dr. Stéphane Hallé and my co-advisor Dr. François Morency. I have been fortunate to have advisors who gave me the freedom to explore on my own and at the same time the guidance to be on the right path. I am grateful for their patience, guidance, inspiration and continuous support throughout my master studies.

I would like to express my gratitude to my husband Ali and my brother-in-law Amir for his help and support. Special thanks to Maryam Ahmadi Golestan and Mehdi Kazeminia for their support at various stages of this research project. Last but not least, I am eternally grateful to my parents for their continuous encouragement and support throughout my life.

DEDICATION

To those who devote their life to the cause of “peace” “equality” and “freedom”

PRÉVISION DE BIOPARTICULES DISPERSION ET DISTRIBUTION DANS DANS UNE CHAMBRE D'ISOLEMENT D'HÔPITAL

Golnaz KHOSRAVI

RÉSUMÉ

L'extraction des bioaérosols dans une chambre d'isolement d'hôpital est importante pour réduire le risque de transmission de maladies infectieuses. La technique la plus courante pour protéger le patient, le médecin et les infirmières contre l'inhalation d'agents pathogènes est la ventilation. Le but de cette étude est de sélectionner, parmi plusieurs scénarios définis, le scénario de ventilation le plus efficace pour la chambre d'isolement étudiée. Pour atteindre cet objectif, l'influence du nombre de changement d'air par heure (ACH), l'angle d'injection (Θ) et la position de la grille d'extraction sur la concentration de bioaérosols expiré par un patient lors d'une toux, a été étudiée. La simulation numérique des écoulements (CFD) a été utilisée pour prédire l'écoulement d'air dans la chambre d'isolement et la concentration de bioaérosols. Une approche Euler-Lagrange a été utilisée pour étudier la dispersion des particules aéroportées et leurs dépôts dans la chambre modélisée. Le modèle mathématique pour l'écoulement d'air est basé sur les équations de Navier-Stokes moyennées (RANS) couplées au modèle de turbulence k-ε.

Un code CFD appelé Code-Saturne a été choisi. Les résultats numériques obtenus du Code-Saturne ont été comparés à des résultats publiés dans la littérature. Pour étudier la capacité du Code-Saturne à prédire le dépôt de particules, des particules d'un diamètre de 1 μm à 10 μm, ont été injectés dans un canal. La vitesse de dépôt obtenue du Code-Saturne a été comparée à des résultats empiriques. Les résultats ont montré que le Code-Saturne a la capacité de prédire adéquatement la dispersion des particules dans un écoulement turbulent. Pour déterminer le système de ventilation le plus efficace, l'efficacité d'élimination des particules (PRE) et la concentration des particules dans la zone d'inhalation ont été comparés pour tous les scénarios simulés. Parmi les six scénarios de ventilation, celui avec un ACH = 15 et un angle d'injection de 45° a été choisi comme étant le scénario de ventilation le plus efficace.

Finalement, l'influence du positionnement de la grille d'extraction a été étudiée. Trois scénarios ont été considérés. Un scénario avec une extraction murale au-dessus de la zone d'occupation, un scénario avec une extraction murale près du plancher et un scénario avec une grille au plafond. Les simulations ont montré que le positionnement de la grille d'extraction a une influence importante sur l'élimination des contaminants et que l'extraction par le plafond présente la meilleure efficacité d'élimination des particules.

Mots clés: CFD, Code-Saturne, Bioaérosols, Ventilation, Simulation, Chambre d'isolement.

PREDICTION OF BIOPARTICLES DISPERSION AND DISTRIBUTION IN A HOSPITAL ISOLATION ROOM

Golnaz KHOSRAVI

ABSTRACT

Removal of bioparticles from hospital isolation room is important in reducing the transmission risk of infectious diseases. An effective ventilation system is necessary to protect the patient, doctor and nurses from catching infectious diseases. The goal of this study was to select the most effective ventilation scenario for the investigated isolation room among the defined scenarios. To select the most effective ventilation scenario, the effect of air exchange rate (ACH), injection angle (Θ) and exhaust position on removing the exhaled bioparticles from a patient mouth during coughing process, was investigated. Computational Fluid Dynamic (CFD) was used for predicting the air flow pattern and bioparticle transmission. Bioparticle dispersion and deposition was modelled by an Eulerian-Lagrangian approach. The mathematical model for air flow was the Reynold Averaged Navier Stokes (RANS) equations with k-ε turbulence model. Code-Saturne was chosen as the CFD program and validated by numerical results and empirical equations. The numerical results obtained by Code-Saturne were compared to results publish in the literature. To investigate the Code-Saturne capability to predict particle deposition, particles with different diameter in the range of 1 μm to 10 μm, were injected in a channel. Non dimensional deposition velocity obtained using Code-Saturne was compared to the empirical results available in the literature. The results showed that Code-Saturne has the capability of predicting the air flow pattern, particle dispersion and particle deposition.

For analyzing the results and choosing the most effective ventilation system, particle removal efficiency (PRE) and normalized particle concentration in the inhalation zone were compared. Among the six ventilation scenarios with different ACH and Θ, scenario with ACH=15 and Θ=45° was selected as the most effective. Finally, effect of exhaust position was investigated. Three scenarios were defined. The first one with an exhaust mounted on a wall near the ceiling, the second one with an exhaust mounted on a wall near the floor and the last one with an exhaust mounted on the ceiling. It is observed that the exhaust position has great influence on the air flow pattern and particle removal. It is found that an exhaust mounted on the ceiling scenario has the best particle removal efficiency.

Keywords: CFD, Code-Saturne, Bioparticles, Ventilation, Simulation, Isolation room.

TABLE OF CONTENTS

Page

LIST OF TABLES

Page

LIST OF FIGURES

Page

LIST OF ABBREVIATIONS

C_c	Cunningham correction factor which account for the effect of slip	
C_j	Mean particle concentration in a cell	
$\overline{C}_{outlet}$	Time-averaged concentration of pollutants in the outlet	
$\overline{C}_{breathing\ Zor}$	Time-averaged concentration of pollutants in the breathing zone	
D	Particle mass diffusivity	$m^2.s^{-1}$
d_p	Particle diameter	m
dt	Particle residence time	s
F_D	Drag force per unit particle mas	$kg.s^{-2}$
$\vec{F}_a$	Other forces exerted on the particle per unit mass	N
$\vec{F}_s$	Saffman's force	N
$\vec{g}$	Gravitational acceleration vector	$m.s^{-2}$
g^+	Non-dimensional gravity	
K_b	Boltzmann constant	$J.K^{-1}$
μ_a	Fluid viscosity	$kg.m^{-1}s^{-1}$
$\dot{M}$	Number flow rate of each trajectory	
N_i	Number of particles	
p	Pressure	Pa
ρ	Density	$kg.m^{-3}$
ρ_p	Particle density	$kg.m^{-3}$
ρ_a	Air density	$kg.m^{-3}$
S_C	Schmidt number	

τ_w	Wall shear stress	$Kg.m^{-1}s^{-2}$
ϑ	Kinematic viscosity	$m^2.s^{-1}$
u	Fluid velocity in x direction	$m.s^{-1}$
$\vec{u}$	Fluid velocity vector with component of (u, v, w)	
$\vec{u}_p$	Velocity vector of the particle	
u_d^+	Non-dimensional deposition velocity	
u^*	Shear velocity of the fluid	$m.s^{-1}$
v	Fluid velocity in y direction	$m.s^{-1}$
V	Room volume	m^3
V_j	Volume of a computational cell for particles	m^3
V_p	Particle volume	m^3
w	Fluid velocity in z direction	$m.s^{-1}$
t	Time	s

INTRODUCTION

It is estimated that most people in urbanized countries spend more than 90% of their time in indoor environment [1]. So, the number of scientific studies about indoor air quality (IAQ) and its effects upon health has increased significantly in the past 10 years. U.S Environmental Protection Agency (EPA) ranks the indoor air pollution as the 5th environmental risks to public health in the US [1, 2, 3, 4]. The indoor air quality is represented by the pollutant concentrations in enclosed spaces. Indoor air quality affects the healthiness, the comfort, and the well-being of the occupants [5, 6]. Indoor pollutant such as dust, smoke, fungi and mists can penetrate into the respiratory system and cause negative health effects [1].

Indoor air quality problem exist in hospital sector just like in the other indoor places. However, in hospitals there is an elevated risk of infection with airborne infectious diseases from contagious patients [7, 8]. For example in a hospital outbreak in Canada, a super-spread of severe acute respiratory syndrome (SARS) epidemic happened due to airborne transmission [9]. In a hospital, some of the most important pathogen sources are: a potentially infectious patient, the personnel or the visitors and some hospital equipment like nebulizers [10].

More specifically, a patient in hospital isolation room can generate a significant amount of transmissible bioparticles such as mycobacteria, bacteria, viruses or fungi during a coughing process which includes a single cough event follows by breathing process. If the isolation room is not properly ventilated, airborne infectious diseases could spread easily and contaminate the personnel, the visitors or the other patients [11]. An airborne infection isolation room (AIIR) protects hospital workers, visitors and the other patients from exposure to infectious airborne transmitted from an infected patient [12, 13]. Airborne viruses, bacteria or microbes can be removed from isolation rooms by a highly effective ventilation system and a negative pressure differential with respect to the adjacent rooms. An appropriate

ventilation system in such rooms is one of the most important issue for engineers, which if fails can increase the pathogens spread within the hospital and thus contaminate more people and lead to hospital acquired infections [8, 14, 15].

According to ASHRAE Standard 170-2008, the recommended level of ventilation in a hospital isolation room is 10 air changes per hour (ACH) with two changes per hour of outdoor air (OA) [8]. These recommendations on the ACH should be respected to achieve a good air quality. To improve the air quality in an isolation room, the parameters which have influence on the ventilation effectiveness should be considered. Ventilation effectiveness and airborne dispersion strongly depends on some parameters such as the ventilation flow rates [17], the air distribution pattern [14, 18, 19], the position of air supplies (inlet) and exhausts (outlet) and the mechanism of atomization of airborne particles through breathing, coughing or sneezing [7, 10, 17 and 20]. An effective ventilation strategy is the one with particle removal efficiency (PRE) of at least 1 for enclosed spaces.

In order to improve the ventilation effectiveness, a good understanding of the fluid dynamic behavior of indoor air is needed. Ventilation measurements in full scale rooms can be expensive and may represent a health risk. Computational fluid dynamic (CFD) is an appropriate alternative which helps to study indoor air flow characteristics by solving conservation equations and predict airborne contaminant concentration and deposition for different ventilation scenarios.

The main objective of this project is to investigate the most effective ventilation scenario among a limited number of scenarios for removing the bioparticles exhaled by a patient mouth during a coughing process in a hospital isolation room. The scenarios were defined by changing three parameters; the air flow rate, the angle of incoming air and the exhaust position.

More specifically, it will:

- Introduce the previous works that studied the ventilation systems as a solution for decreasing bioparticle health risk to help us in reproducing some typical ventilation scenarios to remove the bioparticles effectively;

- Choose appropriate geometrical and mathematical model together with a numerical method for simulating airflow and bioparticle dynamic behavior into a 3 dimensional (3D) room during a cough process and propose different ventilation scenarios for investigations;

- Validate the 3D numerical simulation tools by comparing the air flow velocity, particle concentration and particle deposition velocity to available results in literature;

- Inject bioparticles into a 3D isolation room and investigate the air flow pattern and bioparticle dispersion for different ventilation scenarios;

- Compare the PRE values and particle concentrations to suggest the most effective ventilation scenario in diluting bioparticles for the room under investigation.

To choose the most effective ventilation strategy, the PRE values should be close to 1 or larger, the concentration of bioparticle in the inhalation zone should be as small as possible and the deposition of airborne particle should be limited.

To predict the dynamic behavior of a two-phase flow (fluid containing particles), an Eulerian-Lagrangian approach is used in which the particle phase is treated as a discrete phase and the fluid phase is considered as a continuum. In this work, the fluid phase is

modeled by the Reynolds Averaged Navier-Stokes (RANS) equations and the particle dispersion is modeled solving the momentum equation based on Newton's law. In the Lagrangian frame, the equation of motion, resulting from the different forces exerted on the particle, is solved for each particle to compute their individual trajectory [21]. In this Master's thesis, the airflow and particle dispersion models are predicted using an open source finite-volume based program, i.e., CFD package Code-Saturne (version 4.0.0) [22].

This memoir is structured as follows: Chapter 1 is devoted to the literature review, which presents the previous scientific articles available in scientific journals, relevant to bioparticle dispersion and effective ventilation systems. This chapter discusses the results of these previous works and their methodology to select the best method to find the most effective ventilation system for the investigated isolation room. Selected works to review are the researches focused on bioparticle transmission indoors and their risk for health. Also the literatures related to the cough process modeling are presented in this chapter. The other reviewed literatures focused on different ventilation strategies and the role of ventilation systems in improving the indoor air quality. The investigations that focused on the effective parameters on ventilation improvement in indoors particularly in hospital sectors were reviewed as well as the researches focused on the simulation of particle transport and distribution using CFD.

Chapter 2 defines the mathematical model and the methodology used to achieve our goals. This chapter begins with the problem definition. Then, an appropriate procedure for predicting the particle dynamic behavior is suggested. Finally, it introduces the useful metrics for evaluating the ventilation effectiveness.

Chapter 3 investigates the validity of Code-Saturne in predicting the airflow pattern and particle transport and deposition. First, it presents some comparison of the numerical results obtained by using the Eulerian-Lagrangian approach against the numerical results published in the literatures to validate the capability of Code-Saturne in prediction of air flow pattern

and particle dispersion. Then it compares obtained numerical results to some empirical results from literatures to validate the capability of the selected model in Code-Saturne to simulate accurately the particle deposition.

Chapter 4 presents the obtained numerical results and discusses them to find the most effective ventilation scenario in diluting the bioparticles for the defined hospital isolation room. It first presents the PRE results for meshes with different number of nodes to select a mesh that provides results accurately and efficiently. Then it represents the experimental design results and discusses the employed method for defining the scenarios with different air change rate (ACH) and angle of injected air (Ɵ) levels. The predicted air flow pattern and bioparticle distribution are also presented in this chapter. Thereafter, the results are compared to select the most effective ventilation scenario. For this purpose, the effects of two parameters: air change rate (ACH) and the angle of injected air in removing the bioaerosols from isolation room are studied and discussed. Finally, the effect of exhaust position is investigated and analyzed. The memoir ends with a general conclusion.

CHAPTER 1

REVIEW OF LITERATURE

The main objective of this chapter is to study and analyze the methods and outcomes of the relevant literatures about transmission of bioparticles. These literatures help us to define the problem and the geometrical model accurately and select an appropriate mathematical model and numerical method to find the most effective ventilation scenario for the defined isolation room. This chapter begins by a presentation of the transmission of bioaerosols in indoor environment and their risk for human health especially in the health care sector. Then an appropriate model for a cough process is determined. Thereafter, the ventilation strategies used by researchers for improving indoor air quality and the ventilation standards in hospitals are presented. Subsequently, results of seven investigations about indoors air dynamic behavior, in particular those that focus on improving the ventilation effectiveness in hospital isolation room, are presented. Finally, the methods used for modeling the quality of indoor air are mentioned.

1.1 Transmission of bioaerosols in indoor environment and their risk for health

Infection via inhalation of pathogens is termed airborne transmission. It occurs by spreading of either airborne droplet nuclei (typically 0.5 to 12 μm in diameter) or dust particles containing the infectious agents. Pathogens carried in this way can be widely dispersed by air flows and may become inhaled by a person close to the patient or may move a longer distance from the source patient. The distance that pathogens can move depends on factors such as their concentration, viability, diameter and aerodynamic behavior; as well as, environmental or physical conditions such as temperature, airflow and humidity [23]. Airborne transmission can cause nosocomial infections like tuberculosis, measles, chickenpox, severe acute respiratory syndrome (SARS) and flu (H1N1, bird flu, etc.). The cost related to the treatment of persons infected by airborne diseases represents a significant part of the health care system budget [24].

A large amount of droplets can enter the indoor air from a patient mouth by sneezing or coughing. First, these droplets are humid. After the release they start to dry-up and their diameter drop to 0.5-12 μm. Droplets with this new range of size are small enough to remain airborne and move passively through the air for a long period of time [9, 24]. According to Xie et al. (2007) [25] exhaled droplet nuclei are carried more than 6 m by sneezing while their initial velocity is around 50 m/s. Based on their results, coughing makes the droplet nuclei pass a distance more than 2 m while having an initial velocity equal to 10 m/s. Bolashikov et al. (2012) [8] reported that the initial peak of flow velocity generated by cough varies from 6 m/s up to 30 m/s.

The size and number of infectious airborne particle depend on the mechanism of generation, the age and the healthiness of the person who produced it. Different literatures present various amount for the size, number and the initial velocity of airborne particles. For example, Cole et al. (1998) [26] reported that coughing generates approximately 10^4 to 10^5 droplets. According to Marko Hyttinen et al. [33], sneezing generates up to 4×10^4 droplets, while a cough or talking for 5 min produce 3×10^3 droplet nuclei. Chao et al. (2009) [28] reported that the number of expelled droplets is 947 to 2085 per cough and 112 to 6720 during speaking.

Generally, the diameter of a virus is usually between 0.02-0.3 μm, a bacteria diameter is between 0.3-10 μm and fungal spore is 2-5 μm [24, 26]. Multiple pathogens are needed to create a sufficient level of infection for disease to be expressed. These pathogens need some larger aerosols like skin flakes, which are 13-17 μm in diameter or droplet with typical size of 20-40 μm in diameter, to be transported. About 95% of the respiratory generated droplets are smaller than 100 μm, while most of them are between 4-8 μm [27, 28, and 29]. Also, Yang et al. (2007) [30] reported that the coughing droplets size average is 8.35 μm. Papineni et al. (1997) [31], by means of improved diagnostics optical particle counting, showed that 80-90% of exhaled droplets in breathing or coughing are less than 1μm in diameter. Edwards

et al. 2004 [32] confirmed Papineni et al. [31] results by a similar experiment on 11 healthy human subjects. They suggested that inhaled particles during normal breathing are smaller than 1μm. Hyttinen et al. [33] in a review in 2011 reported that the size of coughed droplets is in the range of 0.6-16 μm and the average size is 8.4 μm. They mentioned that the size of droplet nuclei is between 0.6-5.4 μm, and 84% of them are smaller than 2.1 μm. Chao et al. (2009) [28] reported that the geometric mean diameter of the droplets exhaled during coughing is 13.5 μm and for speaking, it is around 16.0 μm.

1.2 Determine an appropriate model for a cough process

Considering the variety of the results about the size and number of exhaled particles during a cough, it is helpful to consider the studies that investigated the coughing droplet dynamic behavior in an isolation room. Zhang et al. [61] simulated a single cough in a 3D room. They injected 10^5 particles with a diameter of 1 μm from a patient mouth to investigate the particle dispersion by ventilation. Zhao et al. [35], injected particles with 1 μm diameter in two respiratory periods, with speed of 20 m/s to simulate two coughing process. Bolashikov et al. [8], simulated each cough by injecting CO_2 for 0.8s with an initial velocity of 28.9 m/s. Kao [17], modeled a cough with duration of 1s and particle velocity of 8 m/s when $t \leq 0.5s$ and particle velocity of $10e^{-7t}$ for $0.5s < t \leq 1s$. Balocco [20] simulated a cough by injecting particles with velocity of 28 m/s for 1s and then modeled the breathing with an injection of air flow with a velocity of 0.9 m/s. Also, Alani et al. [34] simulated a cough with an injection of 2700 particles in a 3D room and investigated particles dispersion after 5 min ventilation. Although there is a variety of assumption for simulating a cough, the particle size and cough duration are similar in these literatures.

Based on the studies that simulated a cough process and investigated exhaled particle dispersion in a 3D room, a cough process including a single cough followed by breathing process could be modeled by injection of 10^5 bioparticles with diameter of 1 μm and a

velocity of 10 m/s for 1s injection duration and subsequently injection of air flow with a velocity of 0.9 m/s for breathing process [8, 34, 35].

1.3 Ventilation strategies

For diluting the bioparticles exhaled during a cough process, selection of an appropriate ventilation strategy is important. Different ventilation strategies make different air flow patterns, which have a significant influence on the pollutant removal efficiency in a room. There are two kinds of ventilation systems, mechanical and natural ventilation. Mechanical ventilation systems are the only appropriate systems for hospital sectors. In mechanical ventilation systems, fresh air is introduced to the building by using fan power. There are three different mechanical ventilation strategies: mixing ventilation, displacement ventilation and laminar flow ventilation [54, 57]. In mixing ventilation, the fresh air is introduced into the room by diffusers mounted on the ceiling or close to it. The air is blown at a relatively high speed and mixed with ambient air to have a homogeneous temperatures and homogeneous contaminant concentrations in the room. In displacement ventilation strategy, the air flow is transferred from the residence site close to the floor, up to the ceiling where it is evacuated through the exhausts. Air is introduced into the lower part of the space at a low speed and with a temperature lower than the room air. In this strategy, the air near the ceiling is warmer than the average air in the lower parts. Activities in the room create convective air flows from the floor to the ceiling. The displacement ventilation system is a good option for indoors ventilating and cooling together. However, this strategy has its drawbacks for heating [14, 55]. Laminar flow ventilation aims to create a flow with minimum turbulences where the air goes directly from the inlet to the extraction grid. This ventilation strategy is usually used in special cases like clean rooms [17, 56, and 57].

1.4 Role of ventilation systems

Room ventilation includes the admission of a mix of outdoor and treated recycle air into the enclosed space, the uniform distribution of this air and the extraction of contaminated air [36]. The main role of ventilation system is to remove pollutants such as bioaerosol and to provide healthiness, thermal comfort and well-being of occupants [37, 38]. In buildings, the ventilation must also remove specific pollutants such as carbon dioxide, formaldehyde and ozone. The origin of indoor aerosol may be respiratory activities, fuel burning, laser printers, food preparation and clean-up activities to name a few. Among indoor aerosol, biological particles can have adverse effect on human health, and many studies investigated bioparticles dispersion in ventilated indoors [39]. The dispersion of pollutants strongly depends on factors such as air change rates [8, 19], air distribution pattern [14], pressure difference with the surroundings [19], and the positioning of the ventilation diffusers to name a few [17, 18, and 40]. One way to improve indoor air quality is to simply increase air change rates to push the particles out more effectively. However it uses a considerable amount of energy, which is in conflict with building energy efficiency requirements [41]. Also according to Occupational Safety & Health Administration (OSHA) increasing the ACH from 25 to higher levels has no effect on indoor air quality [42]. So it is helpful to explore the effect of the air distribution pattern and the position of the ventilation diffusers such as inlet and outlet on indoor air quality with a constant source of contamination. Traditionally, mixing ventilation was the main method for the ventilation of indoor environment. Recently, displacement ventilation and personalized ventilation were commonly applied mainly for their low energy consumption and the better quality they provide [43].

1.5 Ventilation strategies used for improving indoor air quality

The first investigations of the indoor air quality date back to 1960's decades. In those years, the main concern of researches was cigarette smoke, radon that is a radioactive gas that cause lung cancer and Sick Building Syndrome (SBS), or related building diseases [44, 45, and 46].

In recent years, the considerable increase of office equipment (computers, copiers, laser printers, etc.) and the widespread use of synthetic materials are among the causes responsible for the increasing problems of indoor air quality [47].

Yang et al. (2004) [48] studied the influence of ventilation strategies on the quality of indoor air in a chamber which is smaller than a real room. They have found that displacement ventilation creates a lower pollutant concentration level near the breathing zone than that by mixing ventilation. They concluded that with mixing ventilation, the contaminant is distributed more non-uniformly than with displacement ventilation. Therefore, they suggested that displacement ventilation performance is better for creating a healthy environment.

Bin Zhao et al. 2009 [49] indicated that, in the zone at height lower than 1 m, the ultrafine particles concentration in a room with a mixing ventilation mode is higher than that in a room with displacement ventilation, which is different for particles with micron size.

In another study by Jurelionis et al. (2015) [39], it is concluded that the location of the air diffusers and exhausts has a great effect on the quality of the ventilation process.

He et al. (2003) [50] published a study on the effects of contaminant source locations in a room ventilated by two ventilation strategies, displacement ventilation and mixing ventilation. They concluded that both systems are equally effective by measuring the normalized contaminant concentrations. Also, Cai et al. (2010) [51] found that the position of the contaminant source and the air extraction play an important role in the concentration of pollutants in indoor environment.

Qian et al. [14] investigated dispersion of exhaled droplet nuclei in a two-bed hospital ward with three different ventilation systems: mixing ventilation, downward ventilation and displacement ventilation. They concluded that displacement ventilation has been shown to provide better indoor air quality than the mixing ventilation in various environments such as offices. However, this conclusion is not applicable in hospital wards. They argued that the exhalation jet of a lying patient facing sideways can travel a very long distance along the exhaled direction assisted by the thermal stratification generated by the displacement ventilation. It could provide a high personal exposure level if the person is located in the exhalation jet area. So displacement ventilation is not suggested in hospital ward. From these investigations, it is concluded that although displacement ventilation strategy shows better performance in particles removal, it is not recommended for hospital sectors. Now it is important to have a look on the standards and guidelines for ventilation of hospital sectors.

1.6 Guidelines and standards

There are different guidelines and standards for the ventilation of health care facilities. Among them, the American Society of Heating, Refrigerating, and Air-Conditioning Engineers (ASHRAE) standard 170-2008 and Center of Diseased Control (CDC 2005) are the most usual ones [52, 53]. The ASHRAE 170 standard covers requirements to ensure adequate ventilation of healthcare facilities. This standard recommends at least 10 air changes per hour (ACH) for isolation rooms while this number according to CDC 2005 is 12 ACH.

1.7 Particular problem in the hospital sector and strategies for ventilation improvement

Hospitals are the places where patients and other healthy people such as medical staff and visitors are in interaction every day. In hospital, people are in higher risk of being infected by

airborne infectious disease from patients [8]. Therefore, ventilation in healthcare facilities is an important issue since it provides protection from harmful emissions or airborne pathogenic materials to both patients and healthcare workers in addition to thermal comfort [58].

Kekkonen et al. (2014) [13], tested the performance of different ventilation scenarios in removal of airborne infection in isolation rooms by tracer gas techniques in which they concluded that locating air exhausts nearer to the patient result in more efficient contaminant reduction. To reach this conclusion, they compared the ratio between the gas concentration at the outlet grille and near the patient.

In 2006, Cheong and Phua [7] arrived at the same conclusion that nearer exhaust to the patient increases the particle removal by calculating another ratio called the pollutant removal efficiency index (PRE). Bolashikov et al. (2012) [8] investigated the effect of overhead mixing ventilation on amount of staffs and occupants exposure to coughed bioparticles in a hospital patient room with double-bed. They measured the concentration of the tracer gas and concluded that the level of exposure depended strongly on the doctor positioning and the distance from the infected patient and position of the coughing patient. Also, they declared, at a point within 1.1 m from the contaminant source, the maximum contaminant concentration at 12 ACH was much higher as compared to the maximum contaminant concentration at 6 ACH, which could be explain by the complex flow interaction around doctor's body.

In 2011, Yau et al. [58] published a literature review about the ventilation of multiple-bed hospital in which they mentioned that a mechanical ventilation system significantly helps to improve the indoor air quality. They also concluded that mixing and displacement ventilations are the most prevalent strategies used for ventilation systems in hospital sectors.

Hyttinen et al. [33] in their literature review of experimental studies mentioned that for achieving a better protection of the healthcare workers, it is necessary to provide supply air from the ceiling in the front part of the room and make a direct air flow towards the patient. They declared that the results obtained about the location of exhaust air (outlet) whether it should be close to the patient head or ceiling level are not conclusive and need to be investigated more.

In 2010, Qian et al. [59] studied experimentally the distribution of expelled particles in an isolation room, with downward inlet and three different exhaust designs. They concluded that the ceiling-level exhausts are the most efficient strategy in removing expelled particles. Bin Zhao et al. [35] investigated the dispersion of droplets produced by the respiratory system. The results showed that droplets generated by normal breathing process move a relatively short distance, while droplets generated during coughing or sneezing can travel much longer distances, which increased the risk for workers and other patients to be affected by infectious patient.

From these investigations, it is concluded that the position of the diffusers are the most important factors that have effect on the ventilation effectiveness. Most of the researchers found that the exhaust position should be near the patient and on the ceiling to improve the ventilation effectiveness.

1.8 Modeling the quality of indoor air

There are two different methods to determine the airborne particles dispersion and distribution in indoors spaces. The first method is experimental studies, which provide information on particle transport and deposition in indoor spaces by specialized equipment such as Ultraviolet Aerodynamic Particle Sizer (UV-APS) and particle image velocimetry

(PIV). In this method, the potential danger for people during the measurements and the cost involved should be considered. In contrast, the second method, which is called computational fluid dynamics (CFD), provides a very cost-effective way to investigate the particle dynamic behavior in indoors environment [49, 60]. There are two approaches to model the two-phase flow problems and analyze the particle dispersion process with CFD. The first approach is the Eulerian-Eulerian model, in which the particle phase is considered as a continuum. The particle concentration is determined by solving the governing equations, which are derived from the mass conservation equation. The second approach is the Eulerian-Lagrangian model, in which the dynamic behavior of a single particle is determined by the trajectory method. In this approach, the air flow field is modeled by applying Reynolds averaged Navier-Stokes (RANS) turbulent models and the single-particle trajectory is modeled by solving the equation of motion. Various forces exerted on an individual particle drive the particle motion. With this model, it is necessary to analyze the dynamic behavior of a large number of sample particles to have statistically valid conclusions [61, 62].

The Eulerian-Eulerian approach involved Passive Scalar Model (PSM), Mixture Model (MIX) and Eulerian Model (EUL), while the Discrete Phase Model (DPM) belongs to the Eulerian-Lagrangian model. In PSM model, particles are considered as passive scalars, which means particles move in the same way as airflow and the inertia forces are ignored. The problem with this model is that only small particles could be assumed as passive scalar that do not have any interaction with the airflow. Discrete phase model (DPM) is a good alternative for PSM model, which is able to overcome the mentioned problem. In this model, all potential forces exerted on the particles are considered and the particle concentration could be determined from the individual particle trajectories [63]. DPM has been used in indoor airflow field prediction like in the Zhao et al. study in 2008 [21], Zhang et al. study in 2007 [61], Jiang et al. [63] work in 2012 and Alani et al [34] investigation in 2001. The major limitation of DPM is its need for much more computation time than Eulerian models. So considering this high computational cost, it is applicable for much diluted particle flows. In MIX and EUL models, both phases are treated as interpenetrating continuum and

interaction between the two phases are considered. Both of these models have been widely used in investigation of two-phase flow transportation [64, 65, and 66].

Choosing the Eulerian method or the Lagrangian method for simulating flows in a specific problem depends on the objectives and conditions of the problem. The most popular method for investigating particle concentration distribution in indoor spaces is the Eulerian method. For Lagrangian method, several researches declared that it can provide the detailed particle distribution, however it requires considerable computational efforts [61, 68, and 69]. In particular Zhang et al. [61] claimed that under steady state conditions, both Eulerian and Lagrangian methods were able to predict the particle concentration distributions in indoor environment. They concluded that the Lagrangian method is more capable in modeling particles transportation for unsteady diluted particle dispersion like modeling coughing state.

Zhao et al. [21] concluded that the Lagrangian model agrees well with the experimental data for the case studied, except at locations near the ceiling and inlet. They reported the largest relative error in particle concentration is 41.2% near the ceiling. They argued that the reason may be that the Lagrangian model assumes particles are trapped when reaching the walls. Jiang et al. [63] investigated particle dispersion and spatial distribution in a ventilated room using four different multiphase flow models, including PSM, DPM, MIX, and EUL. They concluded that only DPM could predict particle concentration distribution close to the experimental values. They argued that this model is the only one to take into account all the particle forces which are expected to affect the particle trajectories. Lai et al. [60], compared a new drift–flux Eulerian and a modified Lagrangian model for a single-zone chamber geometry. They concluded the two models agree very well for submicron particles.

In this study, we aimed to simulate the bioparticle dispersion and deposition, exhaled during a coughing process, in a ventilated isolation room to investigate the ventilation efficiency. In a coughing process the bioparticle concentration is low and we are in an unsteady air flow

condition. Zhang et al. [61] concluded that the Lagrangian method is more capable in predicting particles transmission for diluted particle dispersion in the unsteady condition. Thus, in this study the Lagrangian method was selected for the bioparticle dynamic behavior simulation.

CHAPTER 2

MATHEMATICAL MODEL AND METHODOLOGY

Now that the literature review has shown us that there is a need to improve ventilation system in isolation room to reduce the bioparticle hazard, a methodology to numerically investigate the ventilation systems will be propose in this chapter. The main objective is to propose geometrical and mathematical model plus a numerical method to simulate bioparticle dispersion and deposition after a cough into a ventilated isolation room. The first section of this chapter is dedicated to the problem definition. It begins with a description of the coughing process problem, the geometry and the mesh used for simulating coughing process. Then, the selected scenarios and the applied boundary conditions are described. In the next section, Code-Saturne software, the mathematical and numerical methods and the methods used for checking the validity and reliability of the code are presented. In the last section, the selected metrics for investigating the ventilation effectiveness are defined.

2.1 Problem definition

2.1.1 Coughing process problem

In this study, a coughing process includes a single cough event followed by the breathing process. Considering the literature review on the simulation of coughing processes, it was assumed that 10^5 particles were exhaled from the patient mouth in a single cough event [61]. According to the literature, the single cough event duration was assumed to be 1s [17, 20]. According to Xie et al. [25] the velocity of exhaled bioparticles in the coughing event was set to 10 m/s during 1s injection. For simulating the breathing process after the coughing event, the air velocity in the patient mouth was set 0.9 m/s [20, 25].

These bioparticles exhale from a patient mouth lying on a bed into an isolation room. The next section will define the geometry and the discretization of this isolation room.

2.1.2 Geometry and mesh

In this section the studied geometry is first defined. Then, the important zones of the studied hospital isolation room will be presented. The properties of the mesh and the procedure used to study the mesh effect on the results are described. The volume of the studied hospital isolation room was 50 m^3 (4 m length × 5 m width × 2.5 m height), with the floor center located at (0, 0, 0) m and a patient lying on the bed as shown in Fig.2.1.

In the basic geometry, there are two inlets and one outlet. The fresh air is delivered to the room via a 0.4 m × 0.3 m rectangular diffuser located at the top of the left wall (inlet 1) and the contaminated air is extracted from the room via a 0.4 m × 0.3 m diffuser mounted on the top of the right wall (outlet). A bed of 1 m × 2 m × 0.8 m is located in the room. The bed and the patient are modeled as a rectangular box. The patient in the figure is only there for reader comprehension. The bioparticles were expelled from a square inlet (0.04 m × 0.04 m) used to model the patient mouth, which was located on the bed top surface with center at (0, -2.1, 0.8) m (inlet 2). To explore the particle concentration in patient breathing zone, line D, which was situated above the patient mouth, was defined at (0,-2.1, $0 \leq z \leq 2.5$) m. The other important zone for investigating the particle concentration was the position of the doctor that was located at (-0.8, -2.0, $0 \leq z \leq 2.5$) m. In addition, four planes were defined for studying the air flow pattern and particle concentration: plane A with center at (0, 0 and 1.25) m, plane B with center at (0, 0 and 1.25) m in the middle of room, plane C with center at (0, -2.1 and 1.25) m in the patient breathing zone and plane G with center at (0, -2 and 1.25) m in the doctor position.

The particle concentration is a dimensionless metric. It is defined as follows:

$$C = \frac{N_i \times V_p}{V} \tag{2.1}$$

where N_i is the number of particles, V_p is the particle volume and V is the room volume.

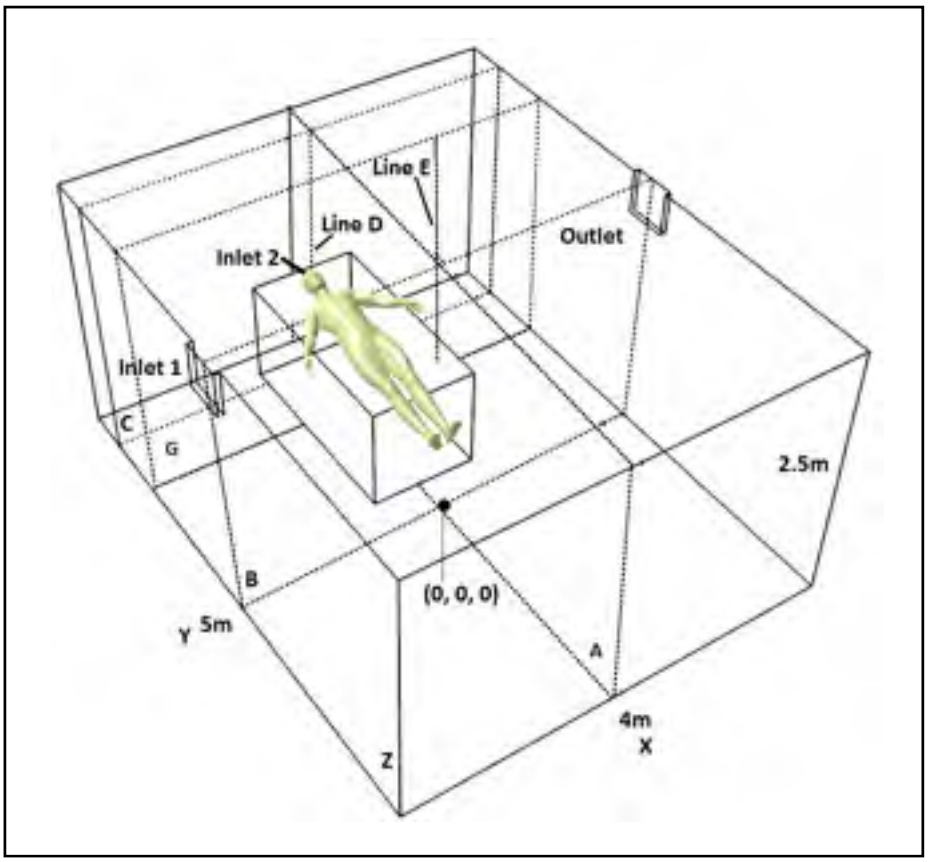

Figure 2-1 Hospital isolation room geometry with an exhaust mounted on the top of the left wall

For investigating the effect of the exhaust position on ventilation efficiency, two other geometries were defined from the basic geometry. Fig. 2.2 shows the first modified geometry with an exhaust located on the front wall near the floor, with center at (-1, -2.5, 0.5) m. Fig. 2.3 shows the second modified geometry with an exhaust mounted on the ceiling with center at (-1.2, -1.65, 2.5) m. For these two geometries, the studied zone positions are the same as the ones in the first geometry in fig. 2.1.

After defining the geometry, it is necessary to discretize the geometry and check that the results are not dependent on the constructed mesh.

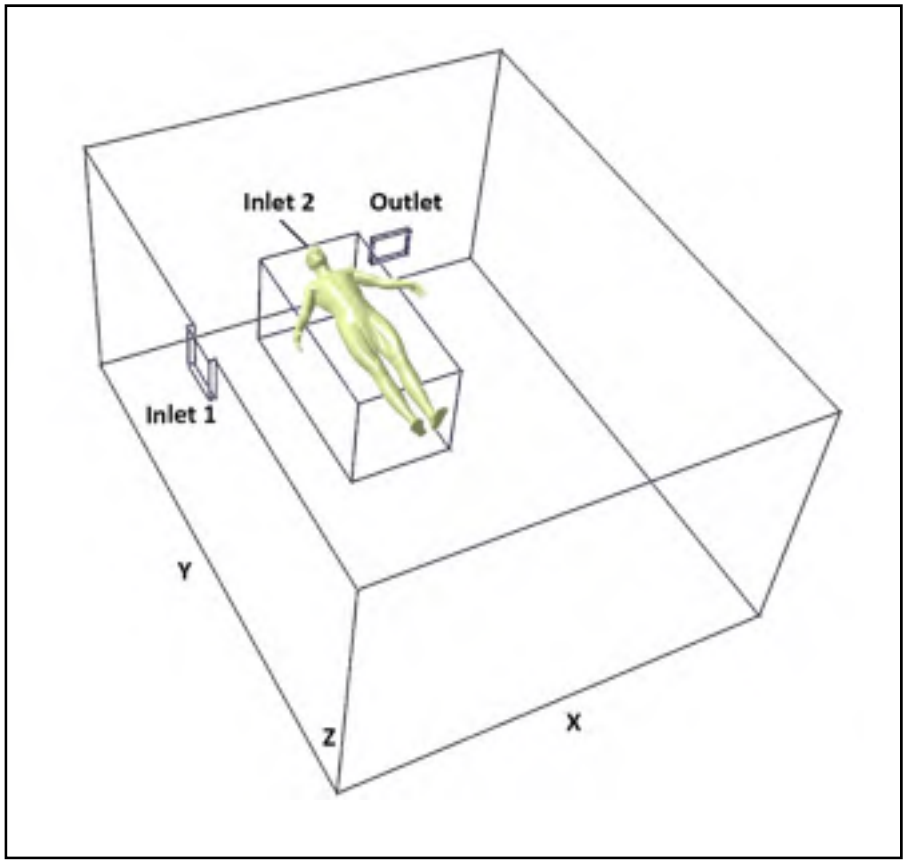

Figure 2-2 Hospital isolation room geometry with an exhaust mounted on the bottom of the front wall

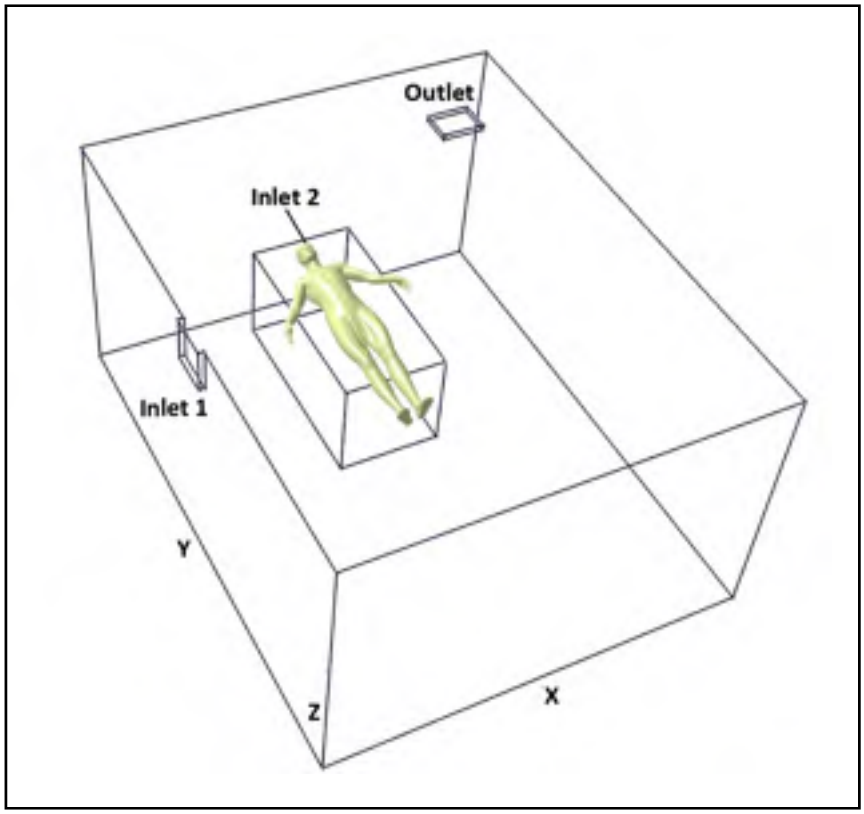

Figure 2-3 Hospital isolation room geometry with an exhaust mounted on the ceiling

Fig. 2.4 shows the mesh used for the simulation of bioparticles dynamic behavior in the hospital isolation room. The number of grid point in a discretized geometry influences the solution accuracy and the required CPU time. Therefore, it is important to first check the effect of grid points on both computational accuracy and efficiency. As the number of grid points decreases, the computational time and the results accuracy decrease. So the selected mesh for the study is the coarser mesh that does not have a significant influence on the results accuracy. In building engineering, a difference less than 5% in PRE results is acceptable to conclude that the mesh does not influence the results accuracy [1, 63].

To investigate the effect of the mesh on the numerical results, three meshes with different number of cells were chosen. Only the basic geometry is used for the mesh study. The

number of cells was chosen according to the previous similar works published in the literatures [10, 79].

- Dense mesh with 240 000 hexahedral cells;
- Moderately dense mesh with 120 000 hexahedral cells;
- Coarse mesh with 60 000 hexahedral cells.

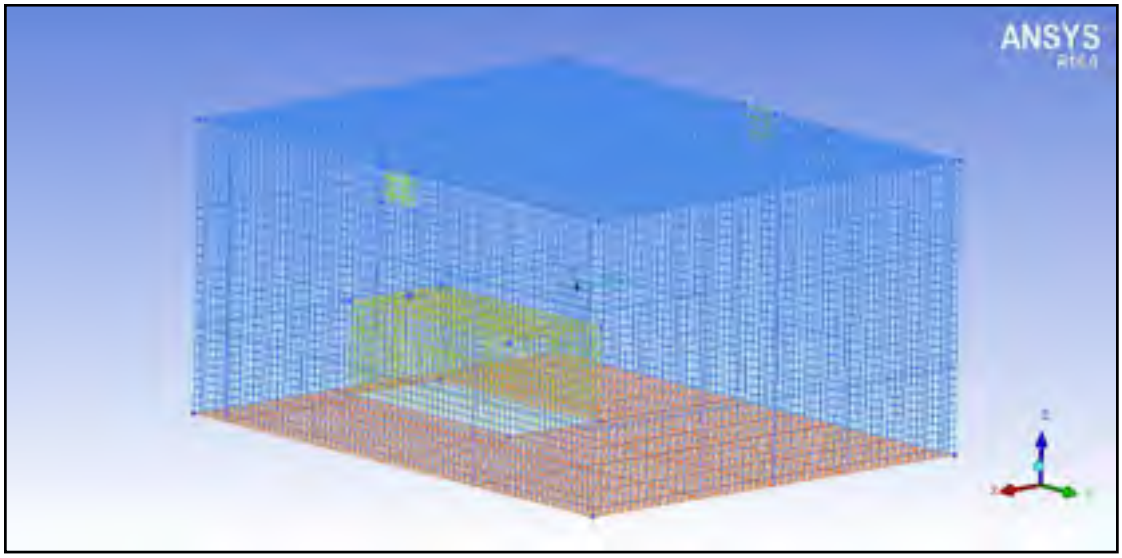

Figure 2-4 Hospital isolation room mesh with 120000 cells

The PRE was calculated for all of the above-mentioned meshes during the last 200s of a 600s simulation. In the last 200s, the results are stationary and do not change with time. The air flow was injected into the room from inlet 1 with a velocity of 2.77 m/s (ACH=24) and an injection angle of 45°. The Reynold number at inlet 1 is equal to 6.1×10^4. In total, 10^5 bioparticles were injected into the room via inlet 2 (patient mouth) in one second with a velocity of 10 m/s. After one second, the injection is stopped and the air velocity is reduced to 0.9 m/s for simulating the breathing process.

Among these three meshes, the moderately dense mesh with 120 000 cells was selected for the study simulations. The differences between the PRE result of this mesh and the one of the dense mesh were 3.78 %. As mentioned before, in building engineering, a difference less than 5% is acceptable for concluding that the mesh does not affect the results [1, 63]. Also, the calculation time associated with the dense mesh was about 66 hours with a 2.5 GHz i7 processor, while the computation time for the same problem with the moderately dense mesh in the same computer equipment took "only" 24 hours.

In the selected mesh, the distance of the first grid node from the floor is equal to 0.016m. So the y^+ for the near wall cell is equal to 10.

2.1.3 Design of experiment

To define the parameter effectiveness's on the results and choose a good range for the levels of these parameters, a two-level factorial design was used [80]. In this study, the effect of two parameters on PRE was investigated. The first parameter was the air flow rate (ACH) and the second one was the angle of the air flow injection at inlet (Θ). According to the literature, both of these parameters can change the air flow pattern in the hospital isolation room and thus the PRE [11, 19, 34, 59, 63, 76, and 79]. For each factor, the highest and lowest level were chosen. Table 2.1 shows the selected levels for each factor. Table 2.2 shows the factor setting for experimental design. For two factors with two levels, the total number of preliminary tests is equal to:

$$(number\ of\ levels)^{(number\ of\ factors\ with\ this\ level)} = 2^2 = 4 \qquad (2.2)$$

Table 2-1 Selected Factors and levels for experimental design

Factor	Lowest level (-1)	Highest level (+1)
θ	30°	45°
ACH	9	24

The levels of each parameter for four preliminary tests are shown in table 2.2. PRE values were calculated for each test. Effects of each parameter (and their levels) on the results were calculated. Knowing the effect of each parameter and levels helped us to choose the other levels and define the new scenarios for further investigation.

Table 2-2 Factor setting for experimental design

No.	θ	ACH
1	+1	+1
2	-1	-1
3	+1	-1
4	-1	+1

2.1.4 Ventilation Scenarios

According to the results obtained by experimental design, six scenarios were defined. Table 2.3 shows the selected ventilation scenarios.

Table 2-3 Selected ventilation scenarios with different levels of ACH and θ

Scenarios	θ	ACH
Scenario 1	45˚	24
Scenario 2	45˚	15
Scenario 3	45˚	12
Scenario 4	45˚	9
Scenario 5	30˚	24
Scenario 6	30˚	9

Also to investigate the effect of the outlet position on the ventilation efficiency, three new scenarios were defined in table 2.4.

Table 2-4 Selected ventilation scenarios with different outlet positions

Scenarios	θ	ACH	Exhaust position
Scenario A	45˚	15	On the right wall
Scenario B	45˚	15	On the front wall near the floor
Scenario C	45˚	15	On the ceiling

2.1.5 Boundary conditions

For hospital isolation room study, all variables were defined at the two inlets. The air was supplied to the room at inlet 1 in four different air change rates (9, 12, 15 and 24 ACH), and

in two different injection angles (30° and 45°). Table 2.5 shows the air flow velocity at inlet 1 for each ACH. For simulating the coughing process, 10^5 bioparticles with diameter of 1 μm and density of 1100 kg/m^3 [31, 61], were injected into the room for one second, from the patient mouth, at inlet 2.

Table 2-5 Air flow velocity at inlet 1 for each ACH

ACH	Air flow velocity (m/s)
24	2.77
15	1.73
12	1.38
9	1.04

The particle concentration was normalized by the concentration at inlet 2, therefore the particle concentration expelled by the patient was assumed to be 1. For the outlet, a Dirichlet boundary condition was set for pressure and a Neumann boundary condition was applied for velocity, i.e their normal derivative was equal to zero [1, 35]. Additionally, for solid walls, no-slip boundary condition was applied. The air was assumed to be isothermal and incompressible.

The Reynolds numbers were calculated based on the inlet hydraulic diameters and the air flow velocity. The Reynolds number at inlet 1 was in the range of 2.3×10^4 to 6.1×10^4, which means that the airflow was turbulent for all the applied ACHs namely 9, 12, 15 and 24. The Reynolds number at inlet 2 during particle injection was equal to 2.6×10^4, which was also in the turbulent flow range.

2.2 Procedures for predicting the particle dynamic behavior

After problem definition, it is important to choose the appropriate mathematical model and numerical method for simulating the bioparticle dispersion and deposition in the ventilated isolation room.

2.2.1 Code-Saturne Software

Code-Saturne [22] is an open source computational fluid dynamics software which was developed in 1997 at Electricité de France (EDF) R&D. This software is based on a co-located Finite Volume approach that accepts meshes with different types of cell such as tetrahedral, hexahedral, prismatic, pyramidal, and polyhedral. Also, it accepts different types of grid structures such as unstructured, block structured, hybrid, conforming and with hanging nodes. Code-Saturne solves the Navier-Stokes equations for 2D, 2D-axisymmetric and 3D flows, steady or unsteady, laminar or turbulent, incompressible or weakly compressible, isothermal or not, with scalars transport if required. There are several turbulence models available in Code-Saturne such as Large Eddy Simulations, Reynolds-Averaged Navier-Stokes (RANS) models, like the k-ε model and Reynolds Stress model. Particle-tracking with Lagrangian modeling is available in this code as a specific module [69].

2.2.2 Mathematical model

2.2.2.1 Air flow simulation

The Navier-Stokes equations are the basic relations in the field of fluid dynamics that can predict Newtonian flow dynamic behavior. We present here the governing equations for the prediction of incompressible Newtonian laminar flow movement:

1- Continuity equation

$$div\,\vec{u} = 0 \tag{2.3}$$

2- Equation of motions (Navier-Stokes equations)

$$\frac{\partial u}{\partial t} + div\,(u\vec{u}) = \frac{-1}{\rho}\frac{\partial p}{\partial x} + \vartheta\; div\; grad\; u \tag{2.4}$$

$$\frac{\partial v}{\partial t} + div\,(v\vec{u}) = \frac{-1}{\rho}\frac{\partial p}{\partial y} + \vartheta\; div\; grad\; v \tag{2.5}$$

$$\frac{\partial w}{\partial t} + div\,(w\vec{u}) = \frac{-1}{\rho}\frac{\partial p}{\partial z} + \vartheta\; div\; grad\; w \tag{2.6}$$

In above Equations, *u*, *v* and *w* are the fluid velocity in x, y and z direction, $\vec{u}$ is the fluid velocity vector with component of (*u, v, w*), *t* is the time, ϑ is the kinematic viscosity, ρ is the density and *p* is the pressure.

To predict the turbulent flow motion, it is necessary to replace in the above equations the flow variables *u, v, w* and *p*, by the sum of a mean and fluctuating component. So by putting $u = U + \acute{u}$, $v = V + \acute{v}$, $w = W + \acute{w}$ and $p = P + \acute{p}$, the Navier-Stokes equations for turbulent incompressible flow is achieved, where *U, V* and *W* are the mean values of velocity, *P* is the mean value of pressure, $\acute{u}, \acute{v}, \acute{w}\; and\; \acute{p}$ represent the turbulent flow fluctuations. Then, the time average of these equations gives the RANS equations:

$$\frac{\partial U}{\partial t} + div\left(U\vec{U}\right) = -\frac{1}{\rho}\frac{\partial P}{\partial x} + \vartheta\ div\ grad\ U + \left[\frac{-\partial\overline{u'^2}}{\partial x} - \frac{\partial\overline{u'v'}}{\partial y} - \frac{\partial\overline{u'w'}}{\partial z}\right] \quad (2.7)$$

$$\frac{\partial V}{\partial t} + div\left(V\vec{U}\right) = -\frac{1}{\rho}\frac{\partial P}{\partial y} + \vartheta\ div\ grad\ V + \left[\frac{-\partial\overline{u'v'}}{\partial x} - \frac{\partial\overline{v'^2}}{\partial y} - \frac{\partial\overline{v'w'}}{\partial z}\right] \quad (2.8)$$

$$\frac{\partial W}{\partial t} + div\left(W\vec{U}\right) = -\frac{1}{\rho}\frac{\partial P}{\partial z} + \vartheta div\ grad\ W + \left[\frac{-\partial\overline{u'w'}}{\partial x} - \frac{\partial\overline{v'w'}}{\partial y} - \frac{\partial\overline{w'^2}}{\partial z}\right] \quad (2.9)$$

The averaging process results in new unknown terms, such as $\rho\overline{u'v'}, \rho\overline{u'w'} and\ \rho\overline{v'w'}$, which are called the Reynolds stresses. The determination of the Reynolds stress terms requires extra equations that are solved with turbulence models [70, 71].

The most common turbulence models are: zero equation models like the mixing length model, two equations models like the k-ε model, the Reynolds stress equation model, the algebraic stress model and the large eddy simulation.

To simulate the airflow dynamic behavior, the k-ε model [69] was employed by using the scalable wall function for smooth walls. This turbulence model is a general description of turbulence in which two transport partial differential equations (PDE), one for the turbulent kinetic energy k, and the other one for the rate of dissipation of turbulent kinetic energy ε, are solved. Also, scalable wall functions overcome the problem associated with low y^+ values of the near-wall grid. The y^+ value of the grid points closest to the wall can no longer be in the log law region as presumed by wall functions. This occurs either with excessively fine grids or with moderately refined grids in the area close to the wall. [70, 72, 69].

2.2.2.2 Particle motion

Code-Saturne can predicts the trajectory of a discrete phase particle by integrating the force balance on the particle using the Lagrangian approach. This method solves the momentum equation in which the particle inertia is equated with the forces acting on the particle based on Newton's law:

$$\frac{d\vec{u}_p}{dt} = F_D\left(\vec{u} - \vec{u}_p\right) + \vec{g}\frac{(\rho_p - \rho_a)}{\rho_p} + \vec{F}_a \tag{2.10}$$

Where $\vec{u}_p$ is the velocity vector of the particle; $\vec{u}$ is the velocity vector of air; $F_D\left(\vec{u} - \vec{u}_p\right)$ is the drag force per unit particle mass which is the force exerted on the particle due to the velocity gradient between the fluid and the particle and acts in a direction opposing the flow; ρ_p and ρ_a are the particle and air density respectively; $\vec{g}$ is the gravitational acceleration vector and $\vec{F}_a$ represents the other forces per unit mass.

Since Re (based on particle diameter) is less than one for particles in the micrometer range, the drag force derived from the Stokes's law in slip condition is as follows

$$F_{drag} = F_D\left(\vec{u} - \vec{u}_p\right) = \frac{18\vartheta_a\rho_a}{\rho_p d_p^2 C_c}\left(\vec{u} - \vec{u}_p\right) \tag{2.11}$$

where ϑ_a is the fluid kinematic viscosity; d_p is the particle diameter and C_c is the Cunningham correction factor which account for the effect of slip. Small particles with diameter equal or less than the mean free path of the gas, settle faster than predicted by Stokes's law in continuum regime, due to the slip at the surface of the particle. So in slip condition, the drag force decreases compared to the one obtained by Stokes' law in

continuum regime. Thus, in slip condition, the Cunningham correction factor is used in order to correct this difference [73]:

$$C_c = 1 + \frac{2\lambda}{d_p}\left(1.257 + 0.4e^{-\left(\frac{1.1d_p}{2\lambda}\right)}\right) \quad (2.12)$$

where λ is the mean free path of the molecule which is equal to 66 nm at standard temperature and pressure, and $C_c = 1.1$ for particles with a diameter of 1 μm [73].

The second part of the right-hand side of Eq. 2.10, $\vec{g}\frac{(\rho_p - \rho_a)}{\rho_p}$, is the gravitational force minus the buoyancy force on the particle per unit mass. The last term, $\vec{F}_a$ represents other forces exerted on the particle which includes the Basset history term, the pressure gradient, the virtual mass force due to unsteady flow, the Brownian and Saffman's lift force caused by shear and thermophoretic force due to temperature gradient. The effect of these forces depends on the particle properties and flow condition. For fine particles in enclosed spaces, the Basset history, the pressure gradient and the virtual mass force are negligible. Also, regarding the isothermal assumption for this study, the thermophoretic force is negligible [21, 63 and 62].

The effect of Brownian motion can be optionally included in other forces ($\vec{F}_a$) for sub-micron particles, especially for non-turbulent models. The lift force, which is called the Saffman's force ($\vec{F}_s$) can also be included in other forces ($\vec{F}_a$) as an option for sub-micron particles. Lift force is only valid in an infinite domain and, therefore, should not be considered in the vicinity of a wall [83].

The equation of motion of the particles used for this study was based on the following assumptions:

1- The particles are rigid spheres.

2- The diameter of particles was 1μm and the simulation is in a ventilated room, thus the contribution of the Saffman's lift force and Brownian force in the movement of particles was small and could be neglected [62].

3- Because of the low concentration of the particle, collision between particles is negligible.

4- It was assumed in this study that the presence of particles in the fluid does not affect the structure of the turbulent flow (one-way coupling assumption). The one-way coupling assumption means that the fluid affects the movement of particles, but the particles do not influence the movement of fluid. This assumption is reasonable when the mass concentration of the particles is much smaller than the density of air, which is the fact in coughing simulation.

So the trajectory equation used in this study is:

$$\frac{d\vec{u}_p}{dt} = F_D\left(\vec{u} - \vec{u}_p\right) + \vec{g}\,\frac{(\rho_p - \rho_a)}{\rho_p} \tag{2.13}$$

The turbulent dispersion of the particles is modeled by a stochastic approach. In this approach, adopted by Code-Saturne, the trajectory equation for each particle was predicted by integrating the trajectory equation, using the instantaneous fluid velocity, $\left(\vec{u} + \overrightarrow{u'}\right)$ along the particle path. Here, the mean velocity of air flow, $\vec{u}$ was obtained by solving the RANS equations using the k-ε turbulence model. The instantaneous velocity was modeled by stochastic PDF (Probability Density Function) approach solving Langevin equation,

developed by Pope's team in 2000 [74]. The solution of this set of stochastic equations represents a Monte Carlo simulation. Therefore, this approach is equivalent to solving directly the corresponding equation for the PDF in the state-variable space [83].

In Code-Saturne there are two Langevin equations for modeling the turbulent dispersion. The first one is called standard equation, which is generally sufficient when the interaction between particle/turbulence is low (i.e. when the inertial effects are greater than turbulence effect). The second equation, called complete equation, corresponds to a Langevin equation in which the drift and diffusion coefficients involve more parameters. Since these two models have been found to be unable to reproduce the correct deposition velocity for small particles [83] (will be proven in the next chapter), none of them was used in this study. Thus, in the trajectory equation we just consider the mean velocity of air flow ($\vec{u}$) and the turbulence dispersion which cause the velocity fluctuations ($\overrightarrow{u'}$) was neglected.

To transfer the Lagrangian results to particle concentration distribution in enclosed spaces, the following equation is used:

$$C_j = \frac{\dot{M} \sum_{i=1}^{m} dt_{(i,j)}}{V_j} \tag{2.14}$$

where C_j is the mean particle concentration in a cell, V_j is the volume of a computational cell for particles, dt is the particle residence time, and subscript (i, j) represent the ith trajectory and the jth cell. $\dot{M}$ is the number flow rate of each trajectory. This method is called “the particle source in cell (PSI-C)” method [21].

2.2.3 Particle deposition

In the previous section it was mentioned that for small particles, Code-Saturne can predict the particle deposition accurately according to the empirical correlations, when we neglect the turbulent dispersion. Here the particle deposition mechanisms and the assumptions for predicting particle deposition are described. The particle deposition on the smooth surfaces in an enclosed space is due to different deposition mechanisms such as sedimentation, turbophoresis and diffusion, which includes turbulent diffusion and mass diffusion (Brownian motion) [75]. According to Gao et al. [76] the particle deposition on the floor in a 3D room is mainly caused by gravitational settling not by diffusion. Additionally, Lai and Nazaroff [77] reported that for particles with diameters of 0.5 μm and larger, the deposition velocity is approximately equal to the settling velocity. So, taking into account the particle diameter in this study $d_p = 1\mu\text{m}$, the diffusion mechanism and the turbophoresis are neglected and the gravitational settling is considered as the only deposition mechanism. As mentioned in section 2.2.2.2, in equation 2.13 the only considered force is gravitational settling and turbulent dispersion and Brownian forces are neglected.

For particle diameters equal to and less than 1μm, the particle loss coefficient for deposition, $\beta = V_d \frac{A}{V}$ (where A is the area of the room inner surface, V is the room volume and V_d is the deposition velocity), is on the order of 10^{-2}-10^{-1} (1/h) in the ventilated rooms. This value is about two-magnitude order lower than air exchange rates (1/h) in the ventilated rooms. So the particle deposition in such rooms is negligible [61].

In this study, considering the chosen particle diameter equal to 1 μm and the above mentioned investigations about particle deposition, the assumptions for predicting particle deposition were as follows:

1- For simulating coughing process, a large number of particles with a high velocity reach the ceiling and the surrounding walls in a short time. To prevent loss of a significant number of injected particles due to deposition based on the Lagrangian assumption, and also considering the negligible amount of deposition for d_p =1 μm in ventilated rooms [61], the deposition on the ceiling and the surrounding walls were neglected. Accordingly, rebound-type boundary conditions were set for the ceiling and the surrounding walls.
2- As mentioned in this section, the main deposition mechanism at the floor for d_p =1 μm is the gravitational settling [77]. Therefore a trap-type boundary condition was applied for the floor.

In the previous sections, the mathematical method for predicting the air flow behavior and particle dispersion and deposition were defined. Now, the numerical methods applied for solving the mathematical equations will be described.

2.2.4 Numerical method

For airflow simulation, a second order upwind discretization scheme is used for the turbulent equations, whereas, a second order centered scheme approach is used for the momentum equations. The SIMPLEC algorithm (SIMPLE-Consistent) [70] is employed for pressure-velocity coupling. The relaxation parameter for pressure is 1 and 0.7 for turbulent variables. The standard time scheme in Code-Saturne is a first-order scheme by default [69].

Particle trajectories were found by integrating the equations of motion with Runge-Kutta method:

$$dx_{P,i} = u_{P,i}dt \tag{2.15}$$

$$du_{P,i} = \frac{u_{S,i} - u_{P,i}}{\tau_P} dt + g\ dt \quad (2.16)$$

where x_P and u_P are the particle position and velocity. $u_{S,i}$ is the fluid velocity along the particle trajectory and τ_P is the particle relaxation time.

$$\tau_P = \frac{\rho_p {d_p}^2}{18\vartheta\rho} \quad (2.17)$$

The velocity of the fluid along the particle trajectory, u_S, is modeled by a stochastic diffusion process of Langevin type which is numerically solved by the Monte Carlo method [85].

To validate the Code-Saturne capability to predict the air flow pattern and particle dispersion and deposition, the literature results should be compared to results obtained by Code-Saturne.

2.2.5 Code-Saturne validation

In this section, the methodology used for Code-Saturne validation is described. First, the method used for the validation of the code capability to predict the air flow and particle distribution is introduced. Then, the strategy used for studying the Code-Saturne capability to predict particle deposition is presented.

2.2.5.1 Prediction of airflow and particle dispersion in a chamber

For Code-Saturne validation of the predicted air flow pattern, the air velocity in x direction over the chamber height in three locations was drawn and compared with Chen et al. [1] results. To validate the Code-Saturne prediction of the particle dispersion, the particle normalized concentrations were drawn vs. the chamber height in three locations and compared to Chen et al. [1] results. Particle concentration was normalized by the inlet

concentration. Thus, the inlet concentration was $C_i^+ = 1$. Chen et al. [1] results seems to be valid because they compared their results with experimental results.

2.2.5.2 Prediction of particle deposition

To validate the Code-Saturne capability to predict particle deposition, the non-dimensional deposition velocity u_d^+ graph versus non-dimensional particle relaxation time τ^+ in a 2D channel were drawn and compared with an empirical model predictions suggested by Wood [78]. This model is valid for small particle sizes in the range of 0.01 μm to 50 μm [78].

The simple empirical equation for non-dimensional deposition velocity u_d^+ suggested by Wood [78] is defined as:

$$u_d^+ = 0.057 S_c^{-2/3} + 4.5 \times 10^{-4} \tau^{+^2} + u_t^+ \tag{2.18}$$

where $S_C = \frac{\vartheta}{D}$ is the Schmidt number with D being the particle mass diffusivity given as:

$$D = \frac{K_b T}{3\pi\vartheta\rho d_p} C_c \tag{2.19}$$

where K_b Boltzmann constant.

In Eq. 2.18 the last term accounts for the contribution to particle deposition velocity by gravitational sedimentation in a 2D channel, which is defined as:

$$u_t^+ = \tau^+ g^+ \tag{2.20}$$

where g^+ is expressed with the following form:

$$g^+ = \frac{\vartheta}{u^{*3}} g \tag{2.21}$$

The non-dimensional deposition velocity u_d^+ for results computed by Code-Saturne is calculated by the following relationship:

$$u_d^+ = \frac{u_{deposition}}{u^*} = \frac{u_{settling}}{u^*} \tag{2.22}$$

$u_{settling}$ is obtained from Code-Saturne simulations. The non-dimensional particle relaxation time is defined as follows:

$$\tau^+ = \frac{\tau {u^*}^2}{\nu} = \frac{\rho_p {d_p}^2 C_c}{18\vartheta\rho} \times \frac{{u^*}^2}{\nu} \tag{2.23}$$

$$u^* = \sqrt{\frac{\tau_w}{\rho}} \tag{2.24}$$

where u^* is the shear velocity of the fluid and τ_w is the wall shear stress which obtained from Code-Saturne results.

2.3 Metrics selection

2.3.1 Ventilation effectiveness

For evaluating the ventilation effectiveness, the pollutant removal efficiency (PRE) is used. The PRE is defined as follows [7]:

$$PRE = \frac{\overline{C}_{outlet}}{\overline{C}_{breathing\ Zone}} \tag{2.25}$$

where $\overline{C}_{outlet}$ is the time-averaged concentration of pollutants in the outlet and $\overline{C}_{breathing\ Zone}$ is the time-averaged concentration of pollutants in the breathing zone. PRE is an indicator of the effectiveness of the ventilation system in removing the contaminant in enclosed spaces. The air flow pattern in the room influence the PRE value. In an ideal ventilation system based on the dilution principle, the PRE is equal to 1 [7]. PRE values above one shows an effective ventilation system that outperforms an ideal mixing ventilation strategy.

Particle concentration is another metric that helps to explore and compare the amount of existing particles in important zones such as the breathing zone at line D or the location of doctor at line E. Low particle concentration in these zones could show an increase in ventilation effectiveness. Also the fate of particles could help us to select the most effective ventilation system. A high percent of removed particles and a low percent of deposited particles could mean higher ventilation effectiveness.

The PRE value, the particle concentration, the fate of particles together with the energy consumption can help us to select the most effective ventilation system. Fig. 2.5 shows the

annual energy use vs. ACH. As observed in this figure, increasing ACH from 14 to 22 increase in energy consumption by 35% [84].

In this chapter, the coughing process, the geometry, the mesh and the ventilation scenarios were presented. Then, the k-ε turbulent model and the Eulerian-Lagrangian approach were proposed as the appropriate mathematical model. Thereafter, the selected numerical method for solving the equations was presented. Finally, the PRE and particle concentration plus the fate of particles were selected as the metrics that help us to analyze the results and select the most effective ventilation scenario among the defined scenarios. In this point, it is necessary to validate the selected mathematical and numerical capability in prediction of air flow pattern and particle distribution and deposition.

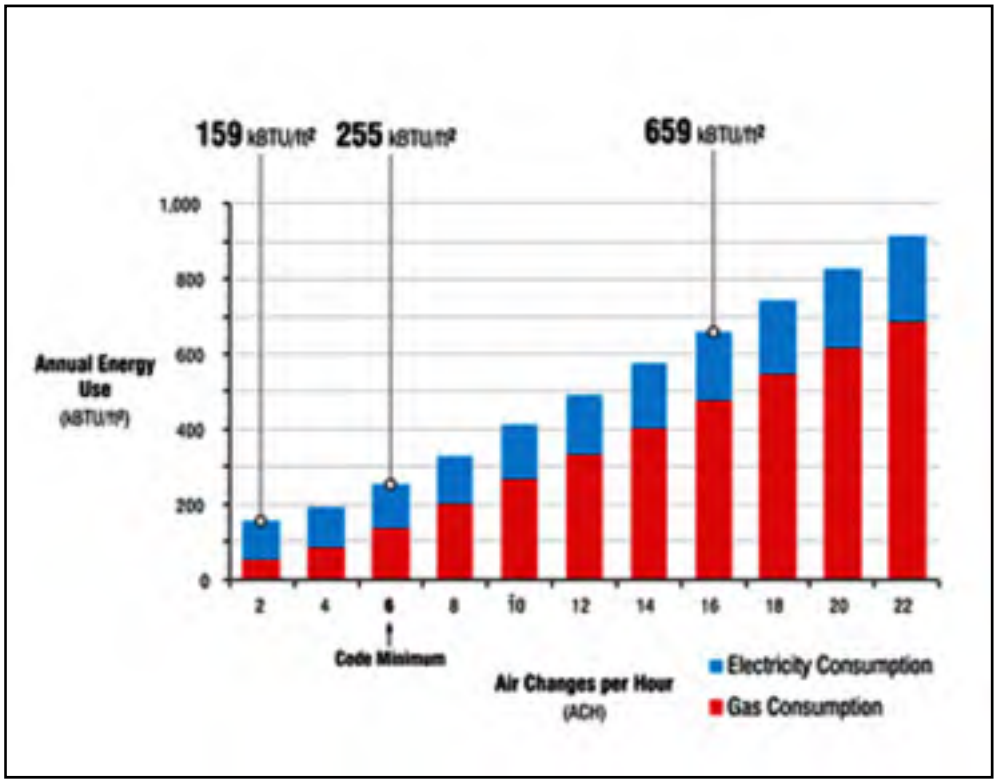

Figure 2-5 Energy consumption vs. Air Change per Hour (ACH) [84]

CHAPTER 3

CODE-SATURNE VALIDATION

For Code-Saturne validation, we are looking at velocity fields, concentration distributions, and depositions of airborne particles inside an enclosed space. Only a few studies suitable for validation are available in the literature. Chen et al. [1] study airflow dynamic behavior and particle concentration in a 3D chamber. Chen et al. results were obtained using a drift-flux model developed for predicting particle distribution in an enclosed space. For particle deposition, Wood provides an empirical prediction correlation [78] for particle deposition velocity in a 2D channel.

In this chapter, first, Chen et al. chamber geometry and used mesh will be presented. Then, the boundary conditions and the other assumption applied for solving the model equations will be defined. Thereafter Code-Saturne results will be compared to Chen et al. [1] for airflow pattern and particle dispersion. In the final section of this chapter, after introduction of the channel geometry and mesh and the applied boundary conditions, the deposition velocities obtained by Code-Saturne will be compared to Wood [78] results to validate Code-Saturne capability to predict the particles deposition.

3.1 Code-Saturne validation for prediction of air flow pattern and particle dispersion

In this section, the predicted air flow pattern and particle concentration obtained by Code-Saturne are compared to some results obtained by Chen et al. [1].

3.1.1 Chen et al [1] chamber geometry and mesh

Chen et al. [1] define the chamber geometry and performs a CFD study of particle dispersion using the Eulerian approach. Fig.3.1 shows a schematic of the chamber. The airflow and

particles were injected from the inlet. The dimensions of the chamber are 0.8 m in length, 0.4 m in width and 0.4 m in height. The inlet and outlet are 0.04 × 0.04 m squares. The inlet center is at (0, 0.2, and 0.36) meter and the outlet center is located at (0.8, 0.2, and 0.04) meter. As shown in Fig.3.1, the center plane is located in the middle of the room with z normal. Three lines on this plane are defined at x= 0.2 m, x= 0.4 m and x=0.6 m. the air flow velocity and particle concentrations were compared over these three lines. Plane F with center of (0.4, 0.2 and 0.2) m is located in the middle of the room according to x direction.

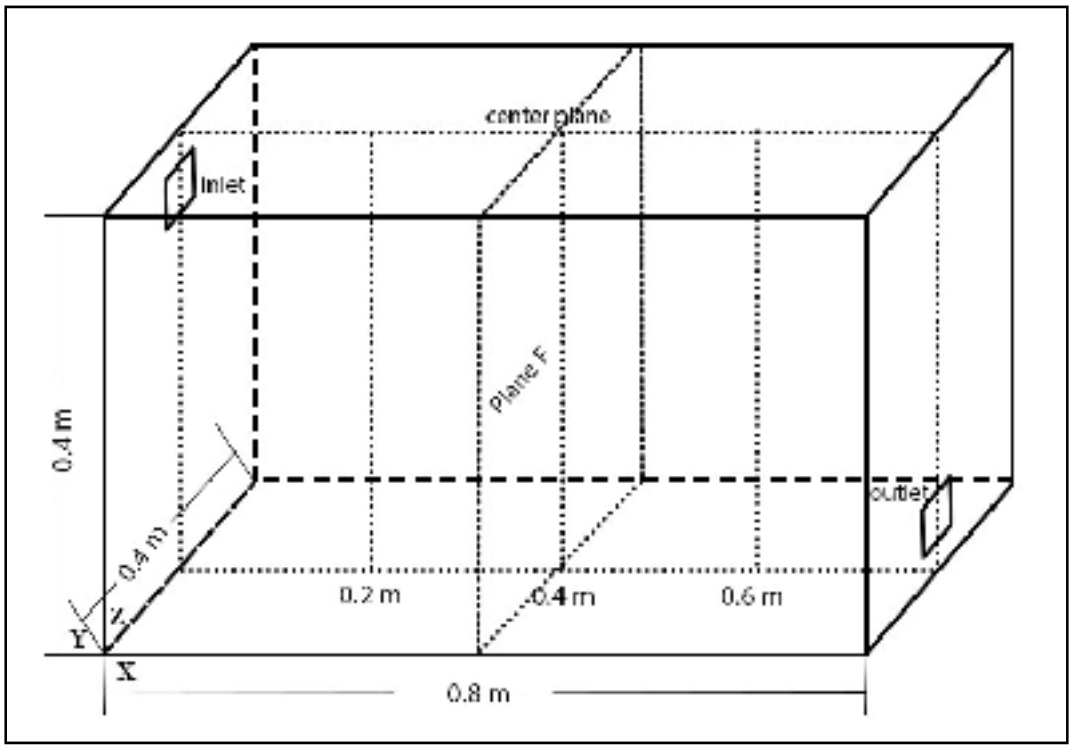

Figure 3-

As shown in Fig. 3.2 the chamber is discretized with hexahedral cells like the mesh used in Chen et al. The number of cells is 40 × 20 × 20, equal to those used in Chen et al. In addition, a finer mesh with 120 × 40 × 40 cells is used for checking the effect of the mesh size on the results.

3.1.2 Boundary conditions

A Dirichlet boundary condition was set at the inlet with a mean velocity of 0.225 (m/s). At the outlet, a Dirichlet boundary condition was set for pressure and a Neumann boundary condition was applied for velocity and other variables. The air was assumed to be incompressible and isothermal. The air density was 1.17 kg/m^3 and its viscosity was 1.83e^{-05} Pa.s. The air change rate is 10 ACH (1.28 m^3/h). Particles with a diameter of 10 μm and a density of 1400 kg/m^3 were injected continuously from the same inlet. The initial condition of the particulate phase in the chamber volume was specified as $C_i^+ = 0$ and particle initial velocity of 0.225 m/s. The particle tracking time was 1800 s.

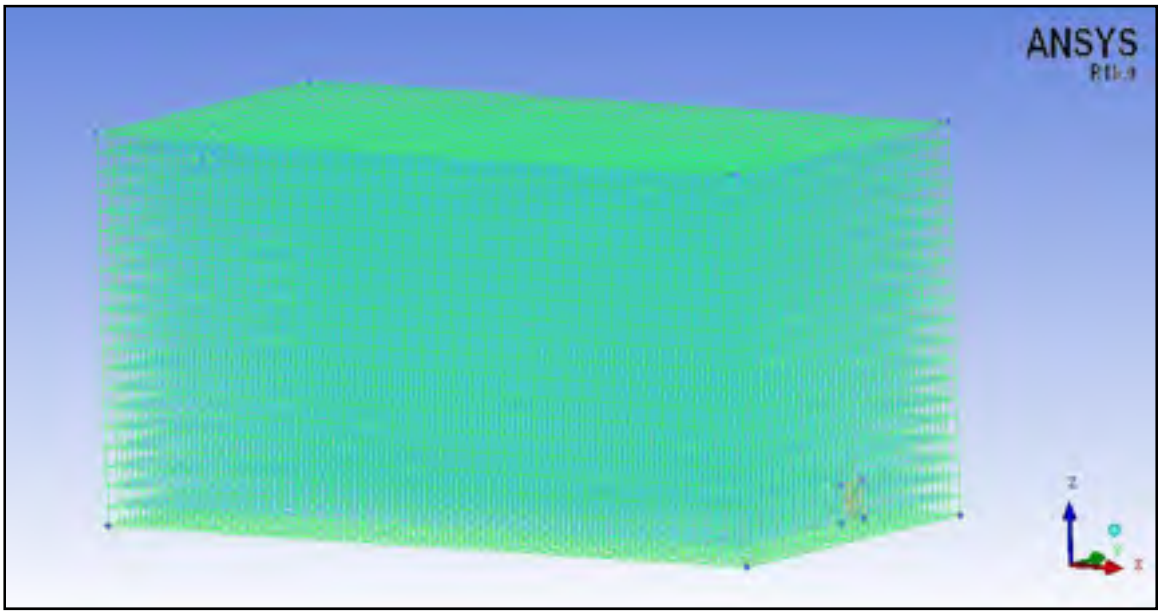

Figure 3-2 A schematic of the meshed chamber

3.1.3 Air flow pattern

For validating the Code-Saturne capability to predict the air flow pattern in the 3D chamber, the air velocity in x direction vs the chamber height, in three lines located on the center plane in z direction, with coordinates of (x= 0.2 m, y=0.2 m), (x= 0.4 m, y=0.2 m) and (x= 0.6 m, y=0.2 m) were drawn and compared with the results obtained in Chen et al. [1]. In Fig.3.3, results of this study with the coarse mesh is represented by the blue line, the black line shows the results obtained from a finer mesh and the orange line shows Chen et al. results.

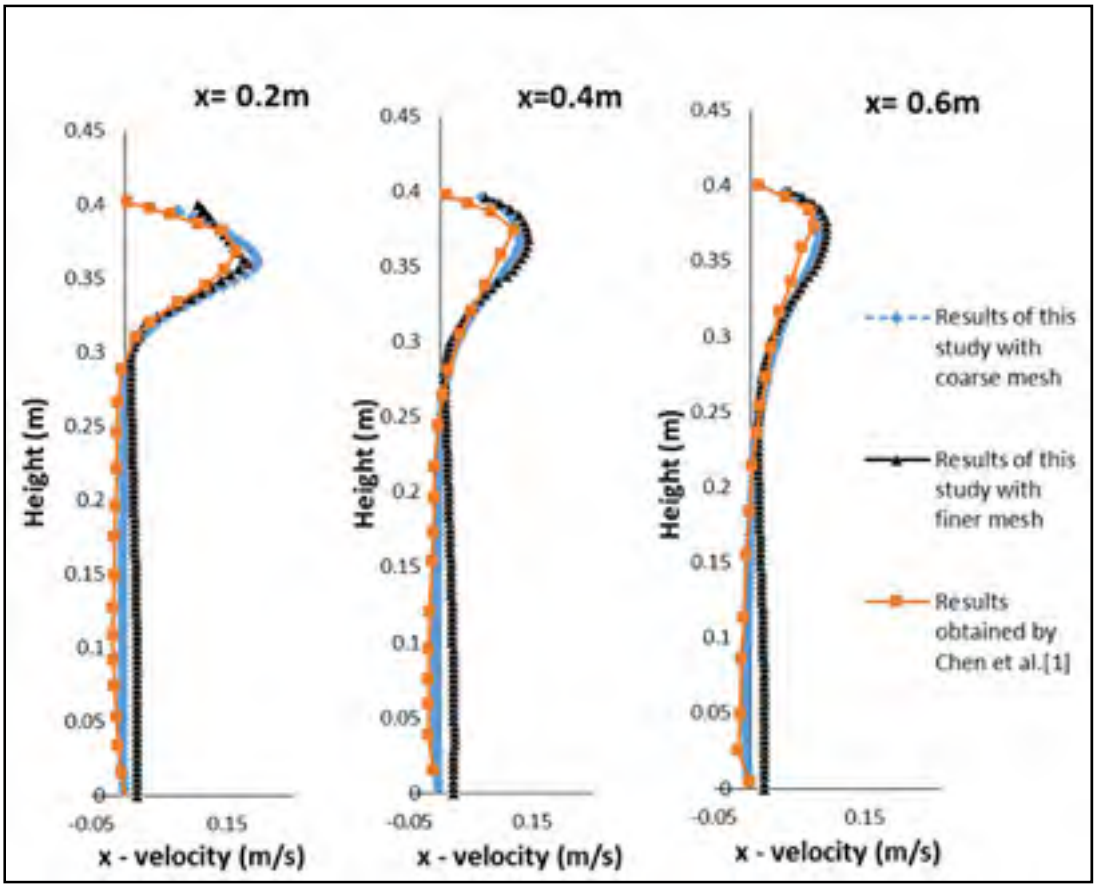

Figure 3-3 Comparison of Code-Saturne predicted and Chen et al. [1] x direction velocities at three different locations; a) x=0.2 m; b) 0.4 m and c) 0.6m

As shown in this figure, our results were acceptable to pursue further simulations, taking into account that the used turbulence model is not the same as the one used by Chen et al. Chen et al. used the RNG k-ε to simulate the turbulent air flow field while the k-ε model was used in this study. Although the RNG and the k-ε models are similar in formulation, there are some important differences in the constant coefficients used. Thus some differences at a height of 0.35m to 0.4m could be due to the difference in the models for simulating the air flow. Cortes et al. [83] reported such differences between these two models near the ceiling.

Also, discrepancy increased for the finer mesh close to the floor. Since the mesh close to the wall is very fine and thus y^+ is not in the log-law region the wall function could not predict the flow behavior near the wall precisely. So the results obtained with the coarser mesh is more accurate.

3.1.4 Particle dispersion

In this section, particles were injected into the 3D chamber and their normalized concentration, calculated by Code-Saturne, was compared with the results of Chen et al. [1]. Fig. 3.4 shows the comparisons of simulated particle normalized concentrations obtained using Code-Saturne for two mesh sizes (blue and black lines) with the simulation results of Chen et al. (orange line).

The comparison of particle normalized concentrations at three line locations with the cordinates of (x=0.2 m, y= 0.2m), (x=0.4 m, y= 0.2m) and (x=0.6m, y= 0.2m), showed that the results are acceptable to carry on the other simulations. The only significant difference between the results of this study and the results obtained by Chen et al. is in the region close to the floor.

In order to make sure that the observed near wall behavior in this study was not affected by the mesh size, we performed another simulation with a finer size mesh and observed the same behavior (Black lines on Fig. 3.4). Also to see the effect of the gravity, a simulation

was performed for the same situation with zero gravity assumption, and there was not any difference in particle concentration near the floor.

In this study, we used a Lagrangian approach, which has a higher concentration gradient near the floor compared to the Eulerian method used by Chen et al. Such a difference between Lagrangian and Eulerian approaches near the floor has been previously reported by Zhang et al. [61]. The maximum difference they reported was 58% which belonged to a position in the middle of the room at a height close to the floor. They argued that this difference between the two models is due to the lack of turbulence near the floor to disperse the particles. Here, we propose a slightly different argumentation.

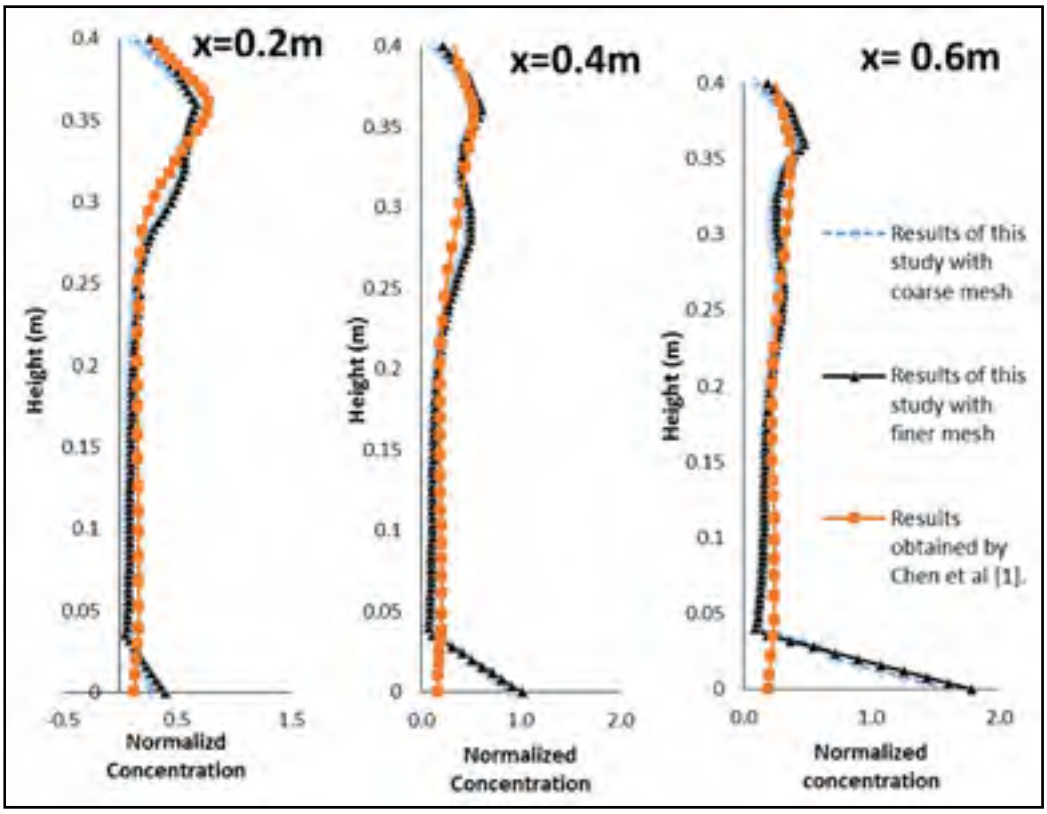

Figure 3-4 Comparis
concentration at thr

In the Lagrangian method, particles follow the mean airflow and disperse mainly by turbulent eddy viscosity. Close to the wall, the turbulence decreases. The mean airflow close to the floor dominates the turbulence, which can then cause a decrease in particle dispersion compared to the other locations. Consequently, a high concentration gradient is formed from this region to its vicinity. In contrast, particles, in the Eulerian approach, are treated as a continuum and the diffusion prevents forming of such a high concentration gradient. Also, considering the Fig.3.4, this concentration gradient increases with the distance from the inlet, which may be because of the stronger mean air flow rather than turbulence in regions far from the inlet.

But still, a physical explanation for the occurrence of the concentration gradient at the first place is needed. To investigate more the air flow behavior and particle concentration near the walls, the contours of velocity and particle concentration are drawn in a plane located in the middle of the chamber in the x direction. Fig. 3.5 shows the velocity contours in this plane. As shown in this figure the maximum velocity is around the ceiling. In Fig.3.6, the particle concentration contours are shown. This figure confirms that the particle concentration near the walls is high. To explain this accumulation near the surrounding walls and a region near the floor, the air flow vectors in the same plane are shown in Figs.3.7. As observed in Fig.3.7 (a), two vortices formed in the middle of the room. Figs. 3.7 (b) and (c) show this plane from the other viewing angles to help seeing the mentioned vortices in Fig. 3.7 (a).

These vortices were created due to the general fluid motion and dispersed the particles in these regions. Close to the surrounding walls and also in the region near the middle of floor in y-direction (regions with yellow border in Fig.3.7 (a)) with high particle concentration, stagnation regions occurred. No flow disperse the particles and particles tend to get trapped there, thus in these regions there were a high particle concentrations. In reality, the flow is unsteady, so these stagnation regions are more probably unstable in space and time. If the stagnation regions are unstable, the real particles do not get trap in these stagnation regions.

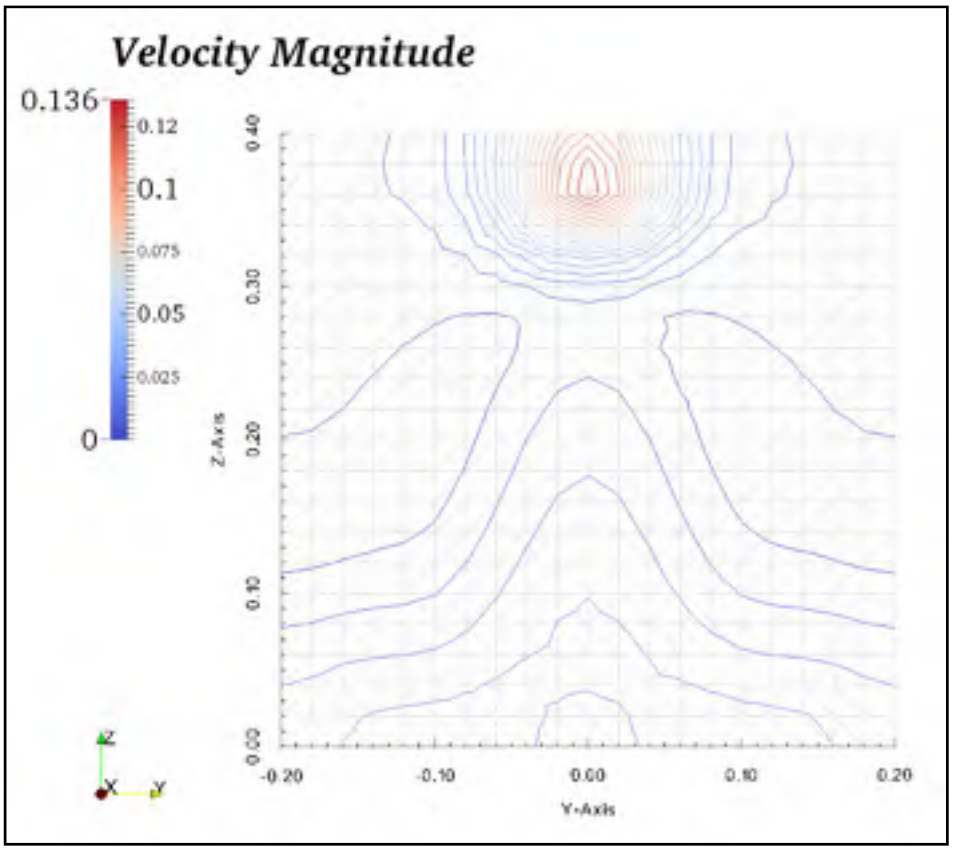

Figure 3-5 Velocity contours in plane F, located in the middle of the room in x direction

This problem was reported in another way in Sergio Chibbaro et al. [55] study. They studied the particle deposition in a 2D channel used the Langevin model in Code-Saturne. They reported that Code-Saturne overestimated deposition rate for particles smaller than 20 μm which could be explained by a high concentration of particles near the floor. They argued that the reason of this behavior is the Lagrangian assumption which states that all the particles are trapped when contact the wall. But they did not mention why a high concentration of particles accumulated near the wall and subsequently contact the wall. The reason could be again the lack of large-scale unsteady fluctuations of the velocity field near the wall. In this study, we have tried to use the complete Langevin equation in Code-Saturne for simulating the turbulent dispersion of particles. The percent of particle deposition in this

simulation was 75%, which is a high percentage. High concentration of particles near the wall increased the possibility of particle impaction to the floor and thus the deposition rate increased in order to Lagrangian assumption. To investigate more this problem, we conducted a channel flow simulation to examine Code-Saturne capability in predicting particle deposition.

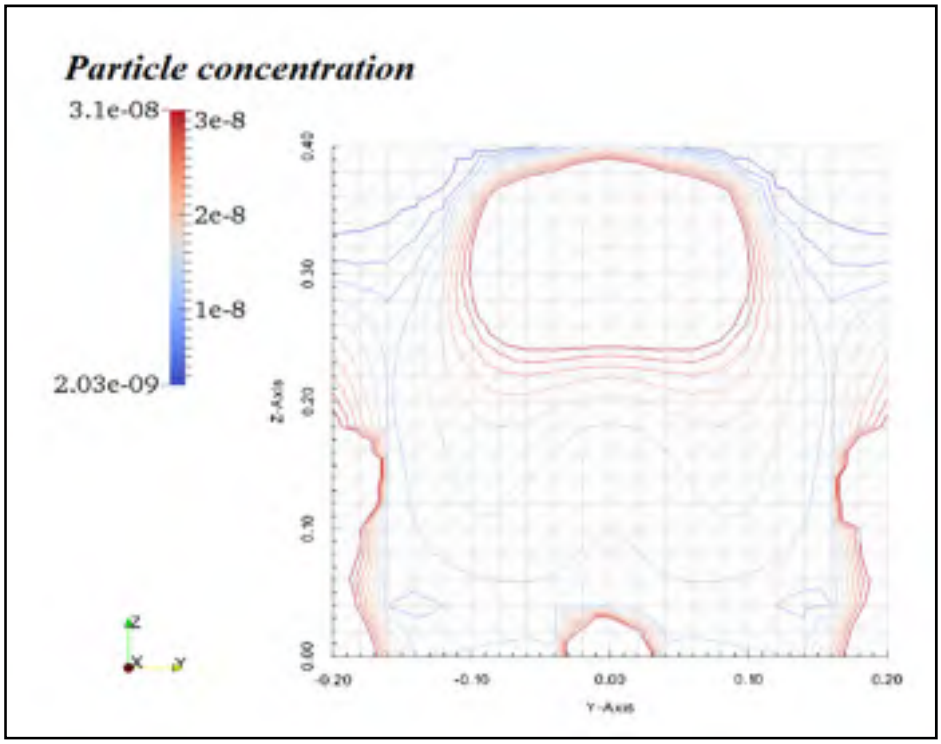

Figure 3-6 Particl
n

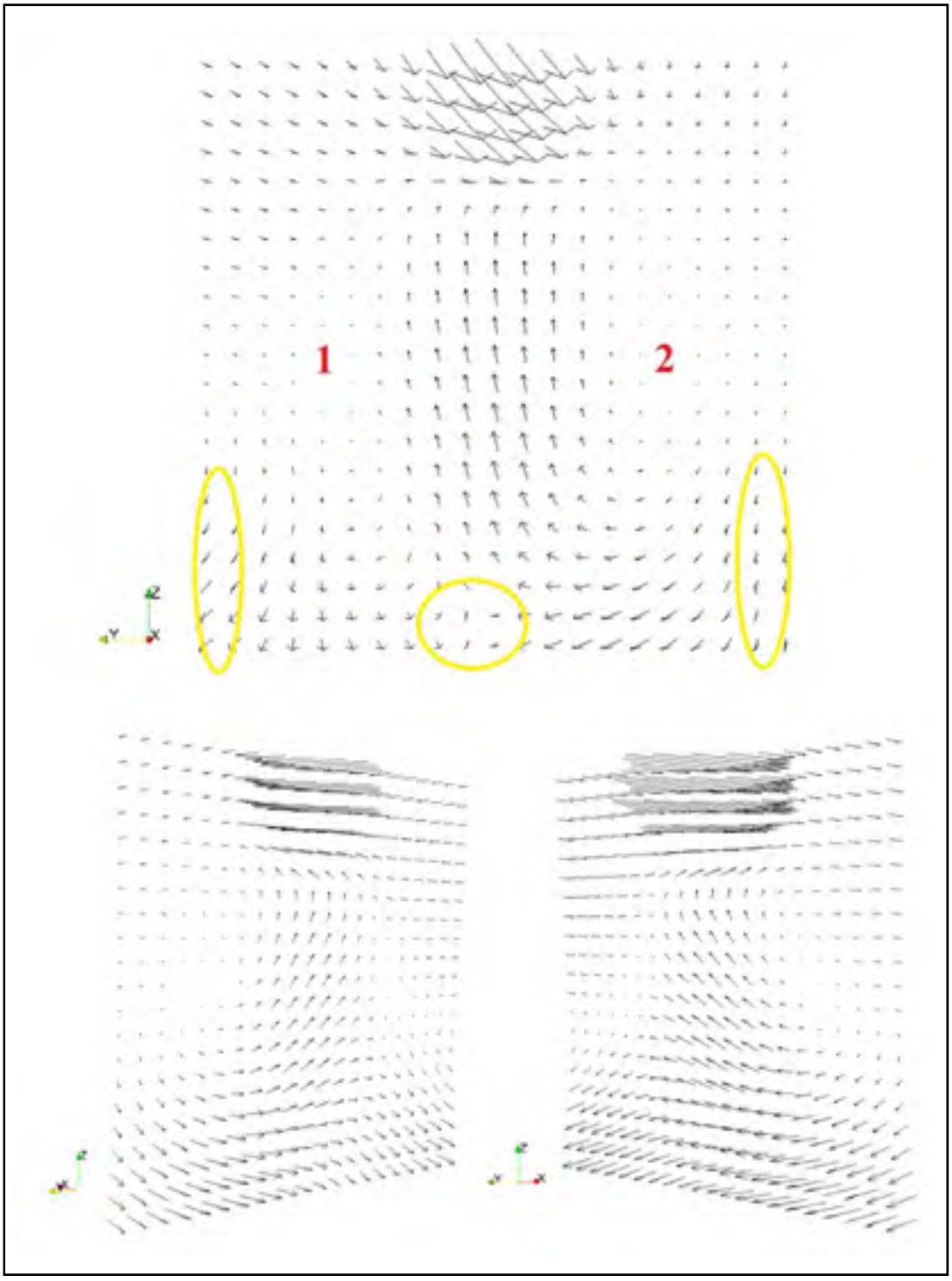

Figure 3-7 Air velocity vectors in the plane F, located in the middle of the room in x direction. a) From the front view b) From right view c) From left view

3.2 Validation of Code-Saturne prediction of particle deposition

In this section the capability of Code-Saturne in prediction of particle deposition is validated by comparing the results obtained using Code-Saturne to Wood [78] empirical results.

3.2.1 Channel geometry and mesh

Figure 3.8 shows the geometry of the 2D channel. The length (L) and width (W) of the channel were 5 m × 0.02 m respectively. Fig.3.9 shows the mesh used for the simulations. The channel was discretized with structured elements. The dimension of each cell in stream wise direction is 0.01 m. In lateral direction, there are 100 cells and the first grid point is located at 0.07 mm away from the wall.

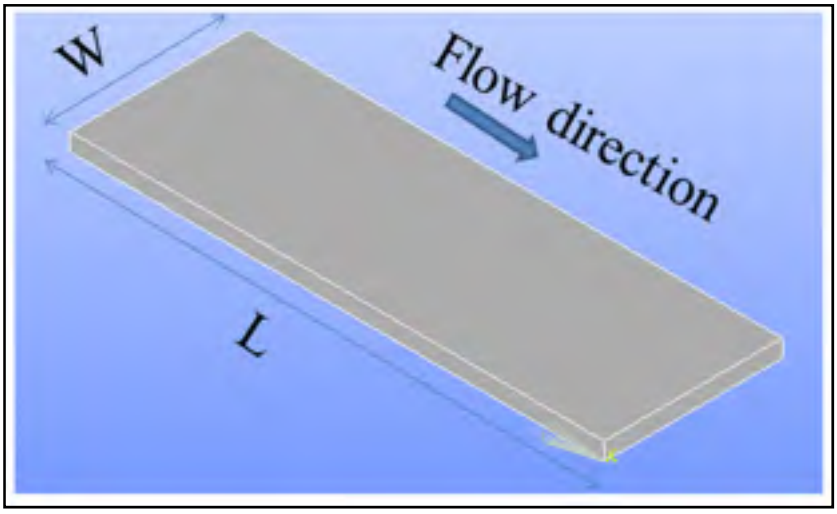

Figure 3-8 A schematic view of the channel geometry

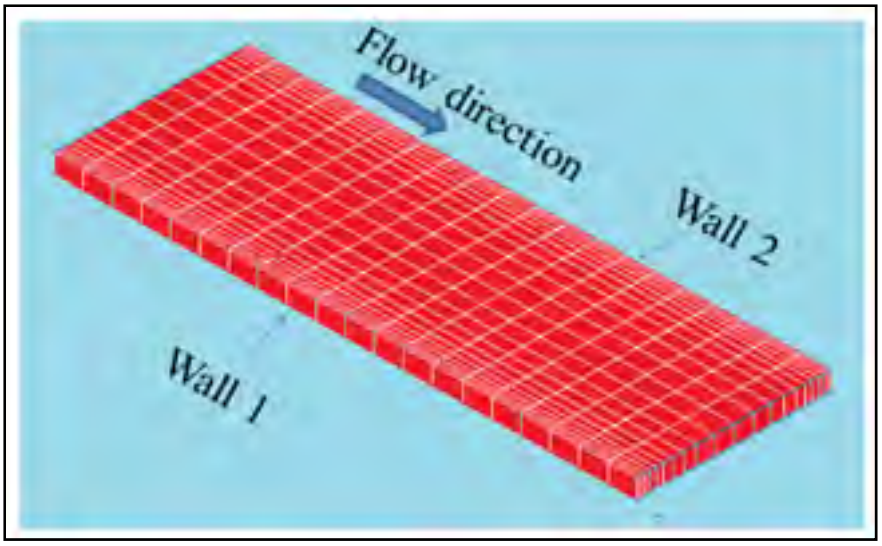

Figure 3-9 A schematic view of the channel mesh

3.2.2 Boundary condition

A 5 m/s air flow velocity was uniformly imposed at the inlet. The Reynolds number based on inlet velocity and channel width was equal to 1.33×10^4, which is in the turbulent flow range. The air density used in this study was $\rho = 1.225$ $(\mathrm{kg/m^3})$. The walls are considered as smooth walls with no-slip boundary condition.

3.2.3 Particle deposition

The non-dimensional deposition velocity u_d^+ graph versus non-dimensional particle relaxation time τ^+ were drawn and compared with an empirical model predictions suggested by Wood [78]. For this purpose, the deposition behavior of particles in the 2D channel was investigated by Code-Saturne, for a range of particles diameter between 0.1 µm-10µm.

Table 3.1 shows the calculated amount of non-dimensional particle relaxation time τ^+ from Eq. 2.23 for each particle diameter. In this equation the values of τ_{wall} was obtained from CFD results.

Table 3-1 Calculated amount of non-dimensional particle relaxation time τ^+ for each particle diameter.

Particle diameter (μm)	τ^+
10	2.28
5	0.578
3	0.212
1	0.0258
0.5	0.0073
0.1	0.000634

Fig. 3.10 shows the comparison of the results obtained by Code-Saturne with those obtained using Wood equation. Calculations were performed for two different conditions. First, the turbulent dispersion effect (Langevin effect) is considered and second, the turbulent dispersion effect on the particle trajectory is neglected.

Considering Fig. 3.10, the graphs show acceptable agreements when the turbulent dispersion is neglected and particles followed the mean-flow pattern. However, Code-Saturne overestimates the value of non-dimensional deposition velocity u_d^+ when we consider the turbulent dispersion effect. So, it is concluded that to simulate particles dispersion and deposition by Code-Saturne and to obtain acceptable results in the range of 0.1 -10 μm diameter, the turbulent dispersion should be neglected.

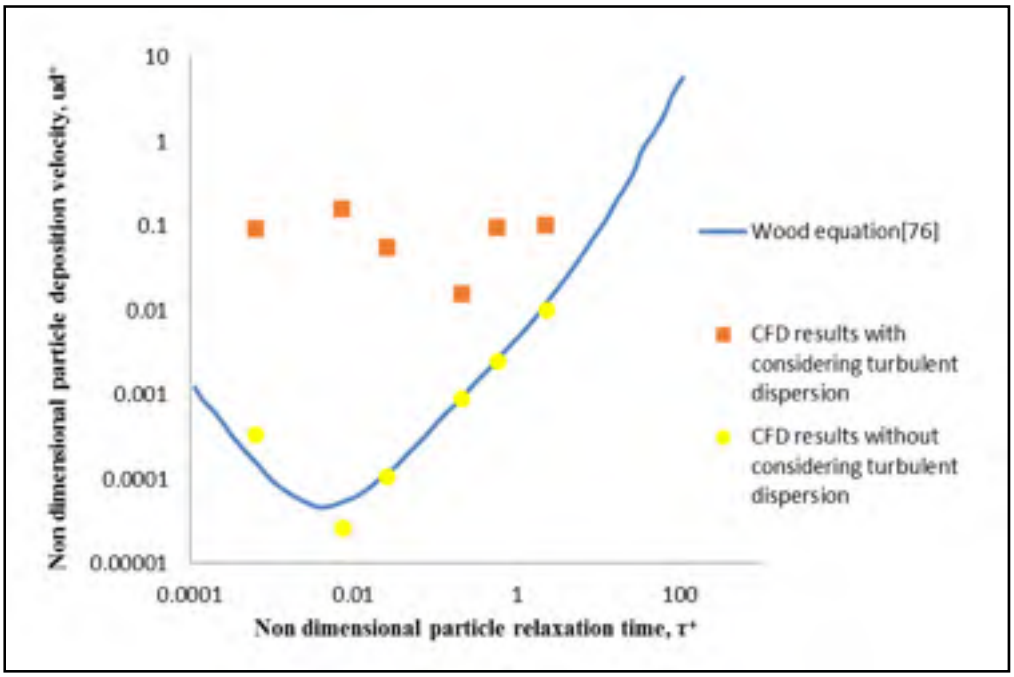

Figure 3-10 Comparison of CFD results and wood equation [78]

This chapter validated Code-Saturne use for predicting air flow pattern and particle dispersion and deposition except for regions near the walls. The air flow pattern predicted using Code-Saturne had an acceptable agreement with the literature. However, the difference in employed turbulence models made some differences near the ceiling. Also, the particle dispersion comparisons validated Code-Saturne capability in particle transport prediction. The Lagrangian model coupled with the k-ε model in Code-Saturne prediction created some stagnation regions that caused particle accumulation in these regions. So the particle concentration in these regions was higher than Chen et al. [1] results. From particle deposition prediction section, it is concluded that for particle diameters in the range of 1μm to 10μm, the turbulent dispersion effects must be neglected to have an acceptable agreement with literatures.

CHAPTER 4

RESULTS AND DISCUSSION

The main objective of this chapter is to present the numerical results and analyze them to find the most effective ventilation strategy for removing the bioparticles produced by a patient during coughing process from the defined isolation room. So the effect of inlet airflow velocity, injection angle and the exhaust position are investigated. To achieve this objective, the results related to the mesh selection and the justifications for choosing the mesh are presented. Then, the results of the design of experiment used to select the effective parameters and the number of levels are discussed, based on the computed efficiency to remove the bioparticles from the isolation room. Thereafter, the air flow dynamic behavior is shown by air flow velocity vectors. Then the bioparticle dispersion over time is shown to see their dynamic behavior from injection to 600s after ventilation. The most effective ventilation scenario, for the basic geometry, is selected among six defined scenarios with different ACH and injection angle Θ, by comparing the PRE values and the concentration of bioparticles in the breathing zones. Finally, the effect of exhaust position on the ventilation effectiveness is investigated by comparing the PRE values and the concentration of bioparticles, for the Θ and ACH that give the most effective ventilation for the basic geometry.

4.1 Results with different number of nodes

As mentioned in section 2.1.2.2, the goal is to select a mesh that will provide accurate results with reasonable simulation time. Three meshes with different number of nodes were chosen that were called dense mesh, moderately dense mesh, and coarse mesh. The PRE value computed on each mesh is compared, since this value shows the effectiveness of the ventilation strategy. Table 4.1 shows the PRE results during the last 200s of a 600s simulation, for different types of meshes. As observed, the PRE difference between the dense mesh and the moderately dense mesh is equal to 3.87%. The computation time for the dense

mesh is 3 times longer than the one for the moderately dense mesh. It is thus reasonable to choose the moderately dense mesh for further simulations.

Table 4-1 PRE values for different types of mesh

Type of mesh	PRE (during the last 200s of a 600s simulation)
Dense mesh	1.29
Moderately dense mesh	1.24
Coarse mesh	1.12

4.2 Experimental design results

As mentioned in section 2.1.3, to choose effective parameters and levels for investigating the ventilation effectiveness, the factorial design of experiment was used. Table 4.2 shows the PRE values for four defined preliminary scenarios.

Here, there are 4 simulations that can help us to choose other effective levels. Fig. 4.1 shows the value of PRE vs θ for two different levels of ACH. From this figure, it can be concluded that the effect of ACH on the PRE is more significant than effect of θ. In addition, as observed in this figure, the effect of θ on the PRE values changed slightly with increasing ACH from 9 to 24. Furthermore, Fig. 4.2 shows the effect of these two parameters and their interaction effect on the PRE value. This figure confirms that ACH parameter has the biggest effect on the PRE and that the effect of interaction was small. The first order regression equation for this design of experiment is as follow:

$$PRE = 0.8050 + 0.1200\ \theta + 0.2850\ ACH + 0.03000\ (\theta \times ACH) \quad (4.1)$$

This equation is valid for ACH=9 to 24 and θ=30º to 45º.

Table 4-2 PRE results for four preliminary scenarios

No.	θ [(-1)=30º, (+1)=45º]	ACH [(-1)=9, (+1)=24]	PRE(during the last 200s of 600s ventilation)
1	+1	+1	1.24
2	-1	-1	0.43
3	+1	-1	0.61
4	-1	+1	0.94

In this equation, there is a coefficient for each parameter that shows the effect of that parameter on the PRE. From eq. (4.1), it is concluded that ACH has the biggest effect on the PRE values due to its larger coefficient. From these results, it is possible to define the ventilation scenarios with different effective parameters and levels.

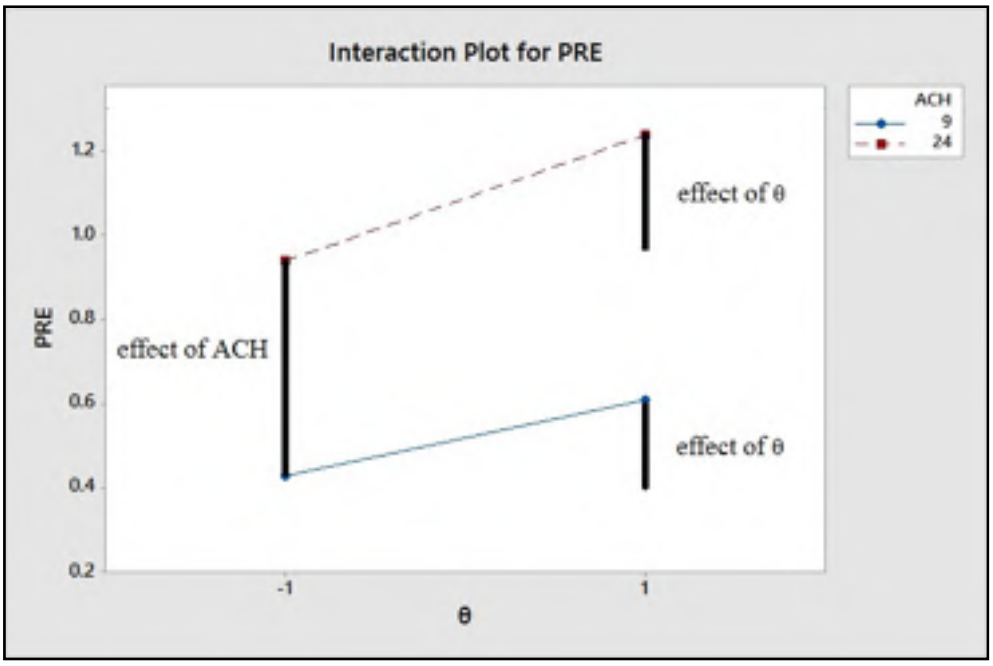

Figure 4-1 The value of PRE vs θ for two different levels of ACH

According to the results of the design of experiment investigation, θ and ACH, influences the PRE value. Since the ACH parameter had a larger effect on the results, it required more exploration. So, we chose two more levels for ACH parameter; the first is ACH=12 which is the recommended level in ASHRAE standard 170 [32] and the next level is 15. Considering the low values of PRE with θ=30° and nearly the same effect of θ for both ACHs=24 and 9, it is reasonable that we omit this level of θ for the new simulations. Thus, six scenarios are selected for investigating the ventilation effectiveness in the hospital isolation room (Table 2.3).

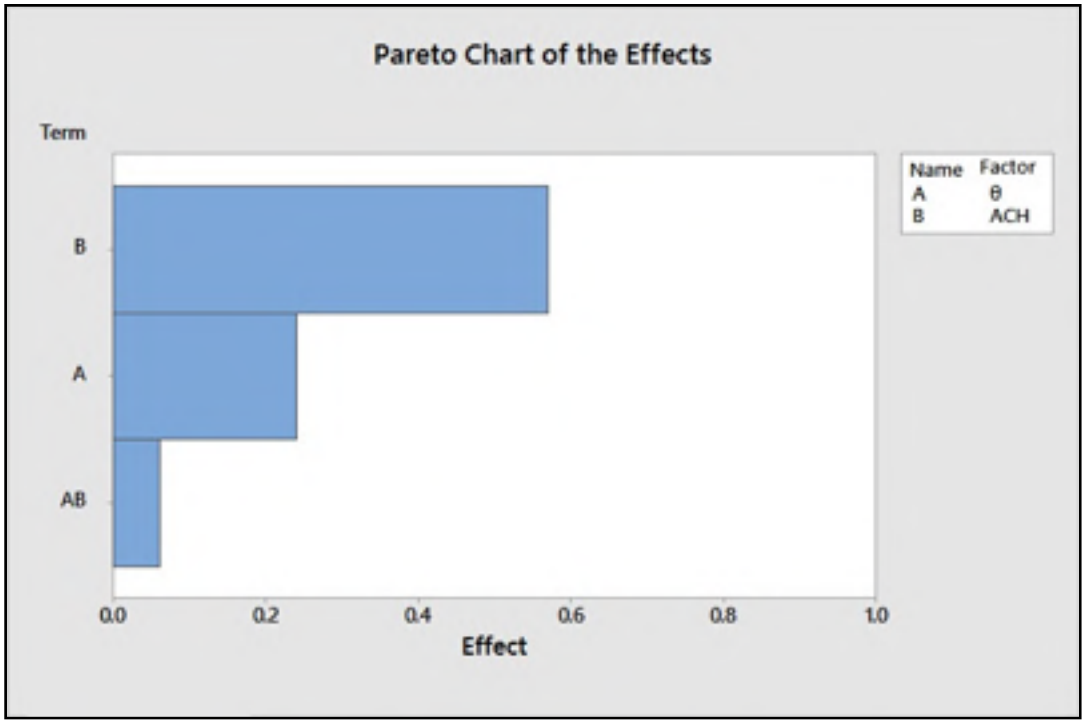

Figure 4-2 Effect of the parameters and their interaction effect on the PRE value

4.3 Air flow pattern in the ventilated hospital isolation room

The air flow pattern of the first scenario is presented in Fig 4.3 to help to understand the air velocity behavior in the hospital isolation room. In this scenario, the air was injected into the room from inlet 1 with a velocity of 2.77 m/s (ACH=24) and an injection angle of 45^{o}. Fig. 4.3 shows the velocity vectors in the first seconds of ventilation. The air is initially at rest in

the room. In this figure, we can observe that the flow entered the room with an angle of 45˚ toward the floor. The flow then hit the opposite wall and went to the upper part of the room, where it was distributed throughout a part of the room between inlet and outlet. A small fraction of the air was extracted via the outlet mounted on the right wall.

As observed in this figure, the air flow was not yet distributed into the part of the room where the bed is located. So the air flow was not affected by the bed. The reason could be the bed location since the bed is not in front of the inlet.

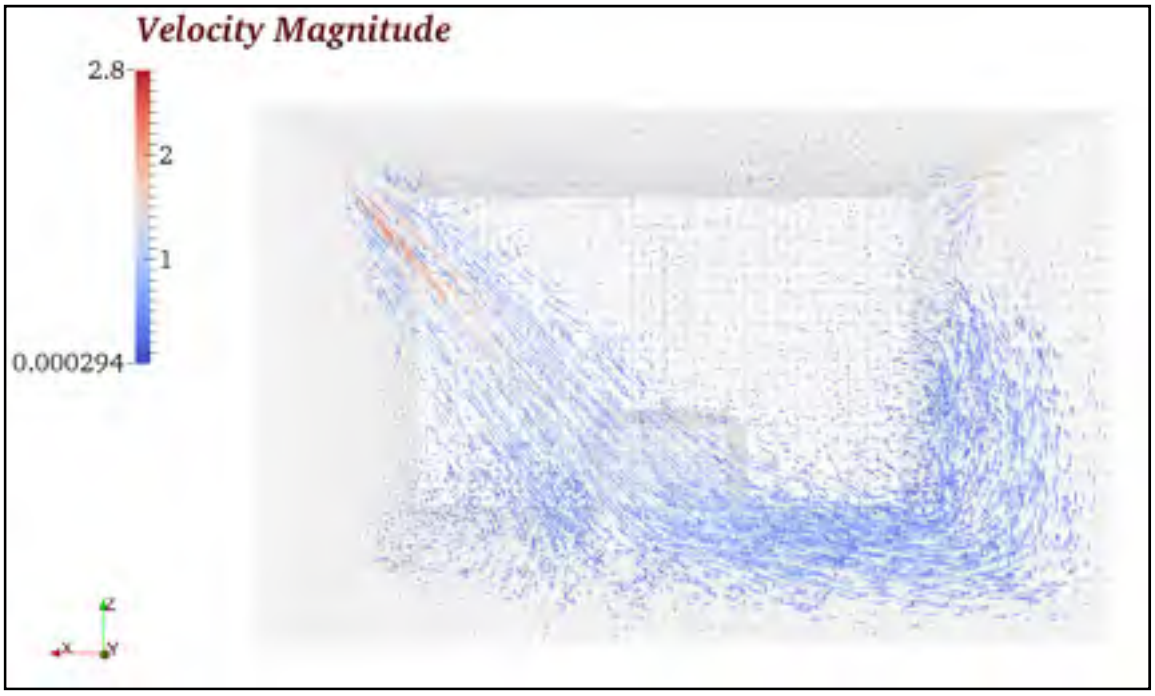

Figure 4-3 Airflow pattern, for ACH=24, Θ=45°, at t=10s of ventilation

Fig. 4.4 shows the velocity vectors after 600s of ventilation for the same scenario. As observed in this figure, the air is in motion everywhere in the room. There was a substantial air mixing between the supply air and the air in the room. In this figure, the velocity vectors spread out all around the room when we compare them with the velocity vectors in Fig. 4.3

that were just distributed within an area between inlet and outlet. As observed in Fig. 4.4 supply air after 600s of ventilation hit the bed and the floor. Then, it went to the upper parts of the room.

Fig. 4.5 shows the changes in the air flow pattern with time, from t=10s to t=600s for scenario 1 in plane C. The location and the number of formed vortices in the patient zone change with time. Vortices are the regions in a fluid in which the flow is mostly rotating around an axis line. As observed in Fig. 4.5 (a), there were two vortices when the ventilation was just started and both were destroyed after a while. After 100s of ventilation, four vortices were formed at the right side of the plane C in Fig. 4.5 (b). Then, all of them were destroyed except number 2. After 200s of ventilation, the number of vortices diminished to two vortices, one located near the ceiling and another one in the middle of the right side of the plane C in Fig. 4.5 (c). After 300s of ventilation, two vortices were formed close to the ceiling and also one in the bottom of the right side of the plane C in Fig. 4.5 (d). Then, after 400s of ventilation, the number of vortices was yet three among which two were located near the right-side wall and one near the floor (Fig.4.5 (e)). After 500s of ventilation, one vortex was formed near the ceiling and another one close to the floor at the right side of the Fig. 4.5 (f). Finally after 600s of ventilation, there were two vortices up at the right side of the Fig. 4.5 (g) and two vortices down close to the bed. Fig. 4.5 shows that during 600s of ventilations, different vortices were formed in this region, some of them moved through the other areas and some destroyed. These vortices could help disperse the bioparticles throughout the room more effectively. Thus formation of these vortices could increase the pollutant dispersion efficiency.

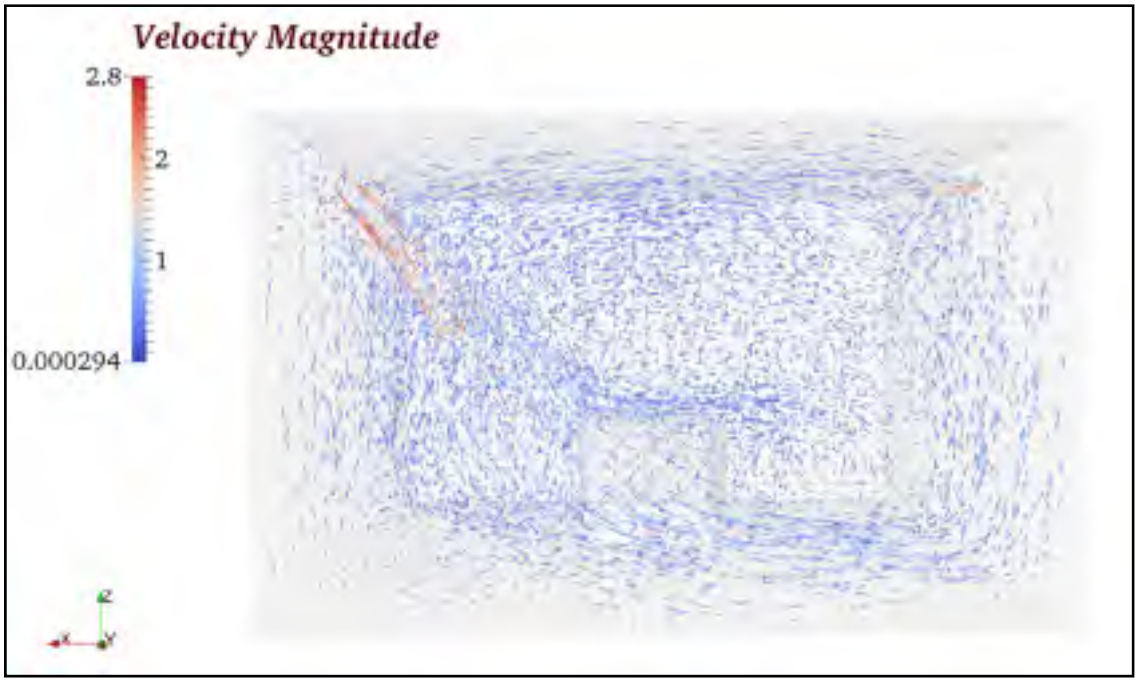

Figure 4-4 Airflow pattern, for ACH=24, Θ=45°, at t=600s of ventilation

Fig 4.6 shows the differences between the air flow patterns when Θ is 30°, with the pattern in which Θ is 45°. Velocity vectors in plane B are shown in Fig. 4.6 (a) and (b), for Θ = 30° and Θ = 45° respectively, with the same ACH (=24), prior to patient coughing. As shown in this figure, the injection angle influenced the air flow pattern. The fresh air flow was injected as a jet flow, until it was deflected by the floor in both situations, but the jet flow for the ventilation scenario with Θ = 45°, impacted the floor in further location in the x direction. Also, for Θ = 45°, the jet flow was bigger than the jet flow for Θ = 30°. Moreover, the velocity vectors near the exhaust for Θ = 45° were bigger than the ones in the same location for the ventilation scenario with Θ = 30°.

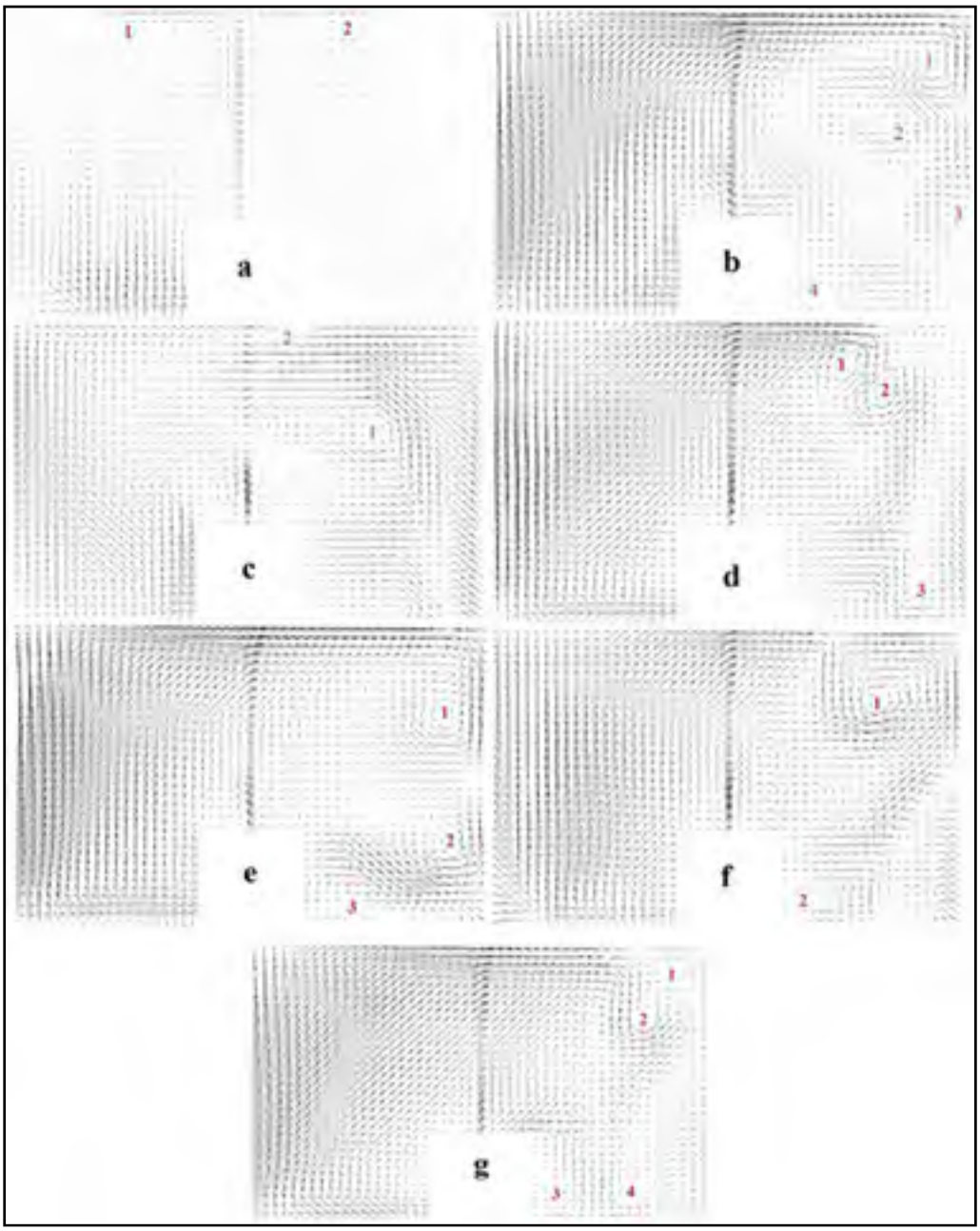

Figure 4-5 Air flow velocity vectors at plane C, for ACH=24 and Θ=45^{o}, (a) t=10s (b) t=100s (c) t=200s (d) t=300s (e) t=400s (f) t=500s (g) t=600s of ventilation

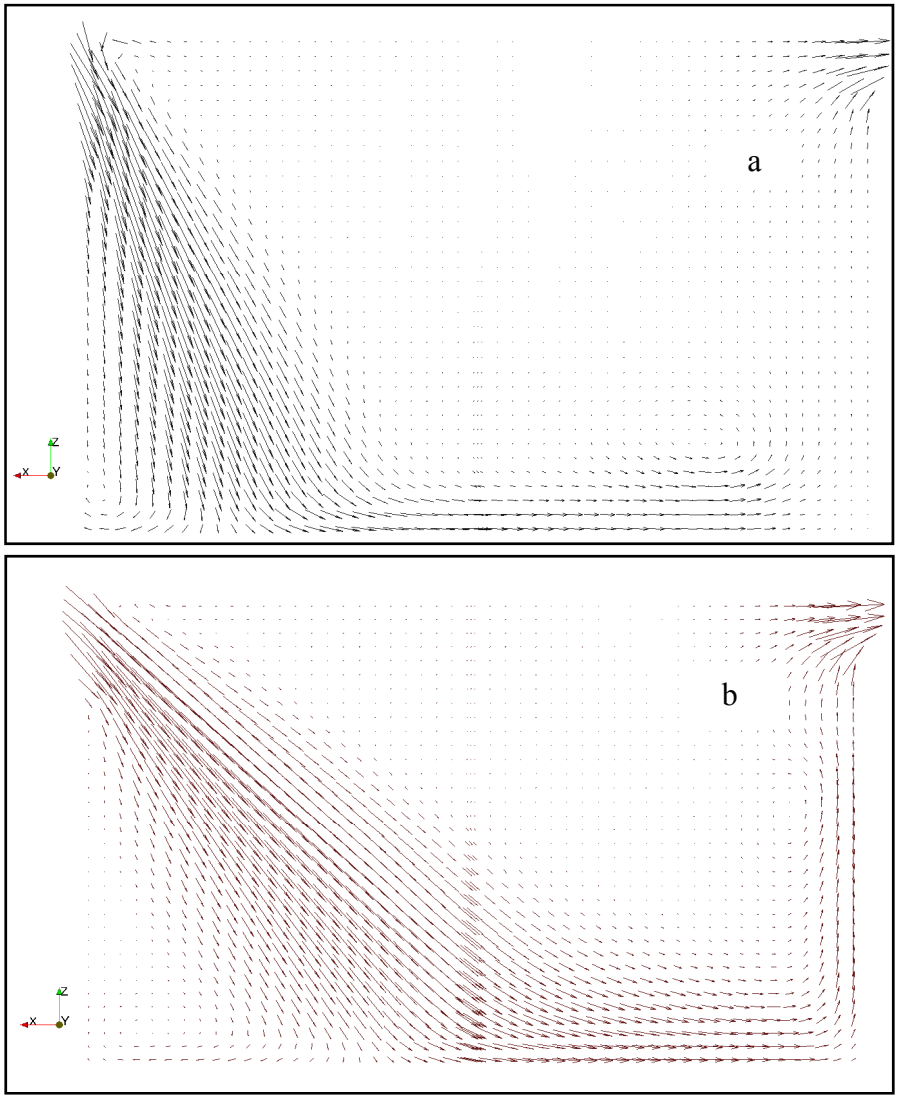

Figure 4-6 Comparison
Θ=30° and b) AC

4.4 Bioparticle distribution

As mentioned in chapter 3, 10^5 bioparticles were injected into the hospital isolation room from the patient's mouth, for a duration of 1s and a velocity of 10m/s to simulate the coughing process. Fig. 4.7 shows the injected particles after 1s. As shown in this figure, particles go up and impact the ceiling. A core of particles is formed above the patient mouth that extended in a conical shape from the patient mouth to the ceiling (classical air jet

behavior). Two lines of particles extended on both side of the cone. It was assumed that the particle rebound on the ceiling.

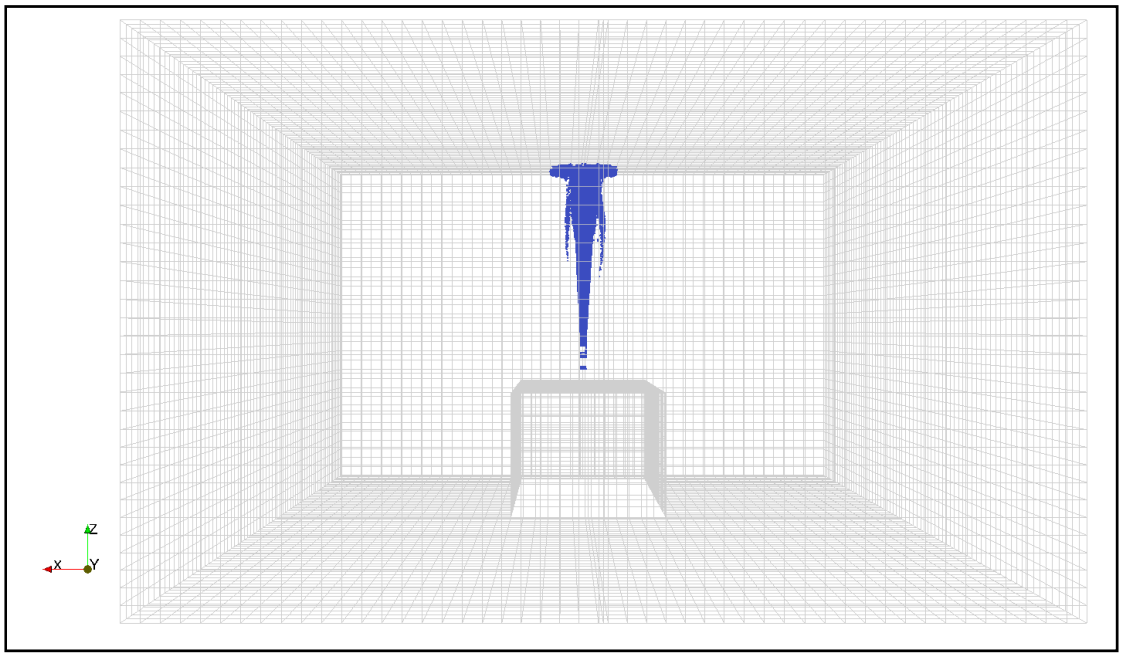

Figure 4-7 Bioparticle distribution after 1s injection ACH=24, Θ=45°

Figs. 4.8 to 4.11 show the bioparticle distribution in the ventilated isolation room over time. The ventilation scenario for these figures is: Ach=24 and Θ=45°. As shown in these figures, over time the bioparticles distributed within the room. Also, the number of remaining particles in the room environment gradually decreased from Figs. 4.9 to 4.11. This could be mainly due to the exit of particles from the room through the outlet and also because of a low percentage of particles deposited on the floor. Fig. 4.8 shows the particles distribution after a few seconds of ventilation. As observed in this figure, particles were going down after impacting the ceiling. Fig. 4.9 shows that most of the particles were distributed at the right side of the room after 100s of ventilation. After 400s of ventilation particles were distributed almost uniformly within the room and the number of remained particles decreased (Fig. 4.10). Finally, as shown in Fig. 4.11, after 600s of ventilation, a small number of particles remained within the room. The other scenarios showed the same behavior with difference in the number of the remaining particles in the room environment over time.

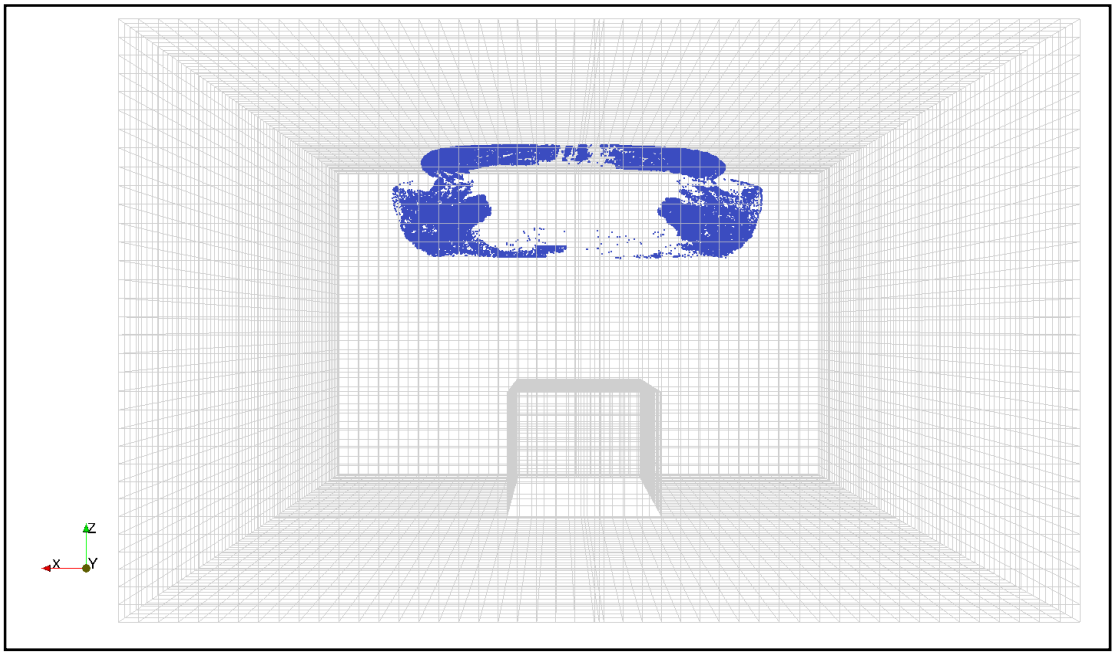

Figure 4-8 Bioparticle distribution in the 3D room with ACH=24, Θ=45° a few seconds of ventilation

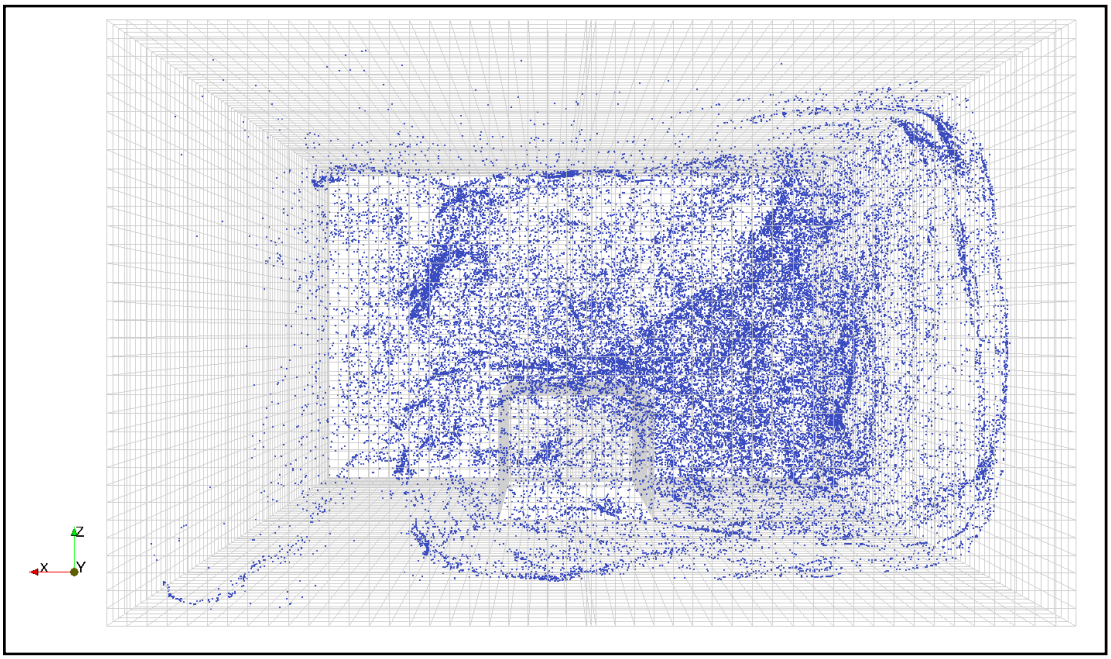

Figure 4-9 Bioparticle distribution in the 3D room with ACH=24, Θ=45° after a few 100s ventilation

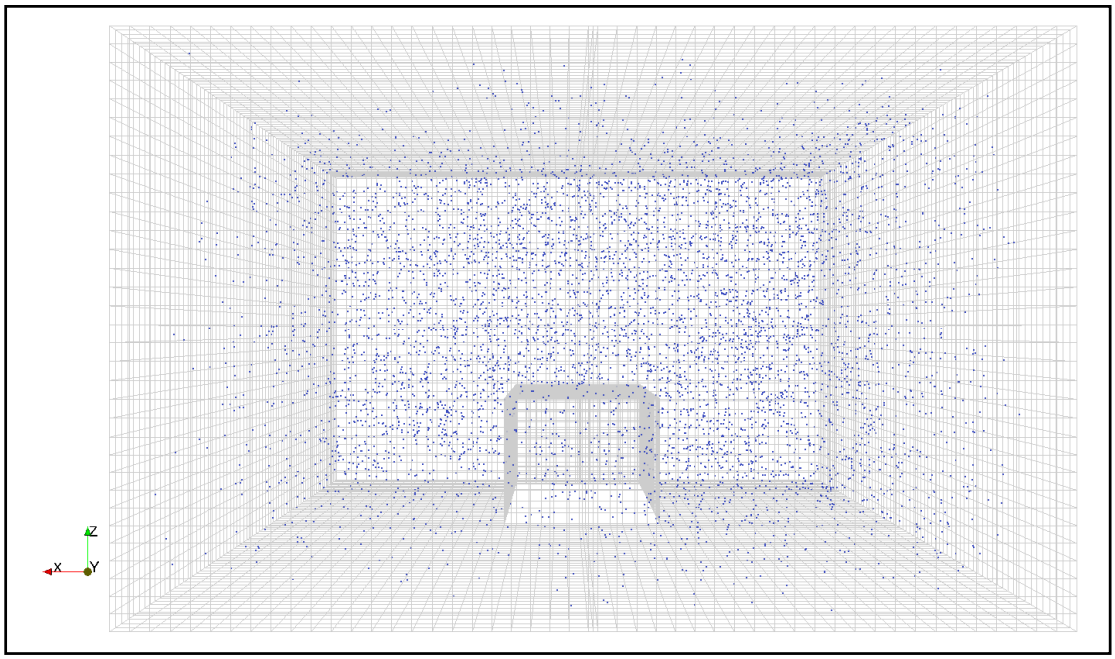

Figure 4-10 Bioparticle distribution in the 3D room with ACH=24, Θ=45° after 400s ventilation

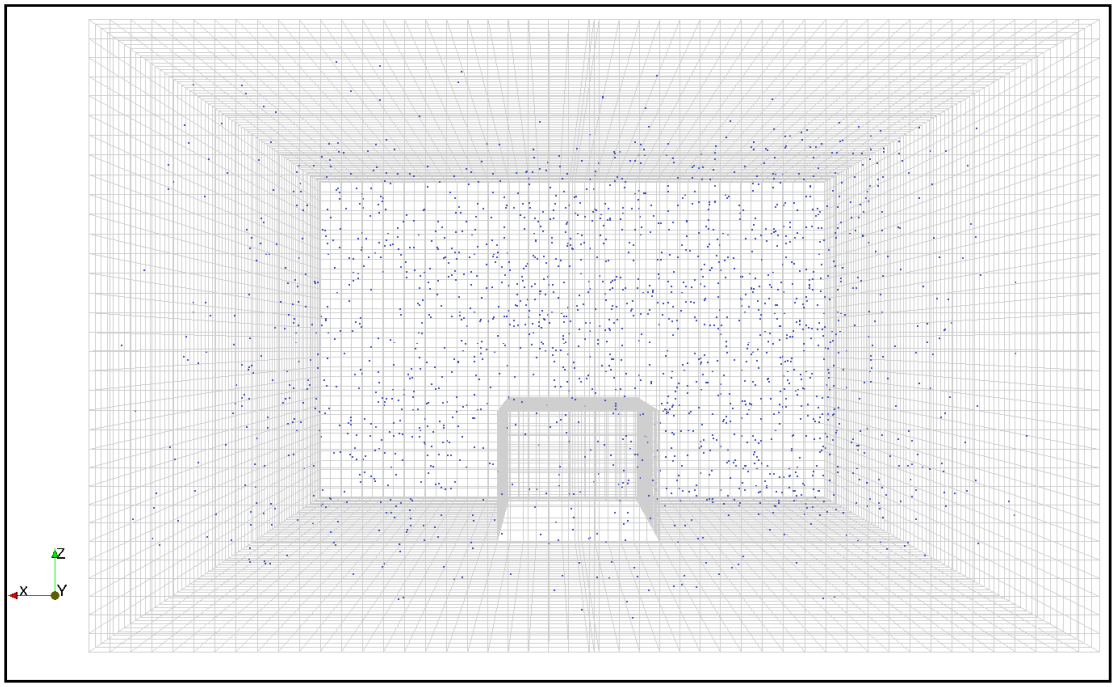

Figure 4-11 Bioparticle distribution the 3D room with ACH=24, Θ=45° after 600s ventilation

To analyze the particle distribution in the patient's head zone, the particle volume concentration contours are helpful. Figs. 4.12-4.16 show the particle concentration contours in the plane C (with 4m length and 2.5m height, situated at y=-2.1m) from particle injection moment to 600s after ventilation. The ventilation is performed by the following condition: ACH=24 and Θ=45^{o}. As seen in these figures, the particle concentration over patient's head in plane C decreased over time. Fig. 4.12 shows the particle concentration contours just after the bioparticle injection. This figure shows that the particle concentration is high in the middle of the plane over patient mouth through the ceiling. As shown in Fig. 4.13, the maximum particle concentration zone was near the ceiling after 1s of ventilation.

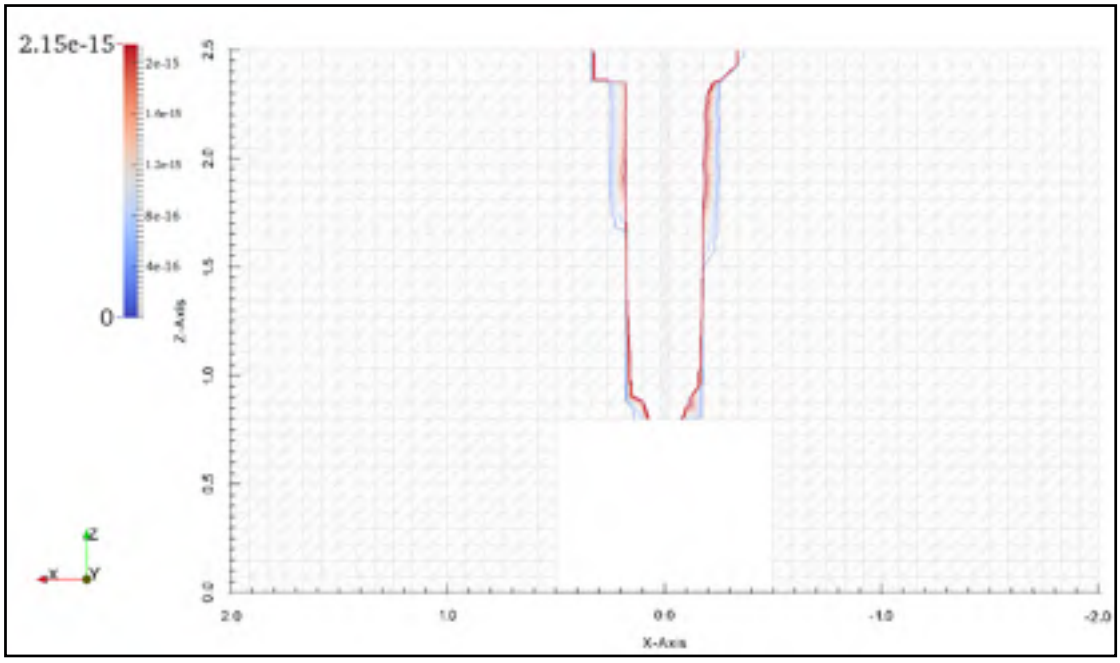

Figure 4-12 Contours of particle concentration in the plane C for ACH=45, Θ=45^{o} after 1s of injection

Fig. 4.14 shows that the particle concentration in the right side of the room and also in the top of the room was higher than the other parts after 100s of ventilation. High particle concentration in the right side of the room was seen in the Fig. 4.9 as well. As observed in Fig. 4.15, the particle concentration in the right hand side of the room is decreasing faster than the left hand side after 200s of ventilation. Since the exhaust is located on the right-side wall and the number of particles was decreasing over time considering the Figs. 4.8-4.11, we can conclude that particles are removed from the right-side wall. As shown in Fig. 4.16, the particle concentration fell abruptly after 400s of ventilation. Considering the Fig. 4.10, which shows the uniform particle distribution in the isolation room, it could be concluded that this decrease in particle concentration is due to particle exiting from the exhaust. It is not because of particle displacement to the other parts of the room. Fig 4.17 shows that after 600s of ventilation, the particle concentration in this zone became very low.

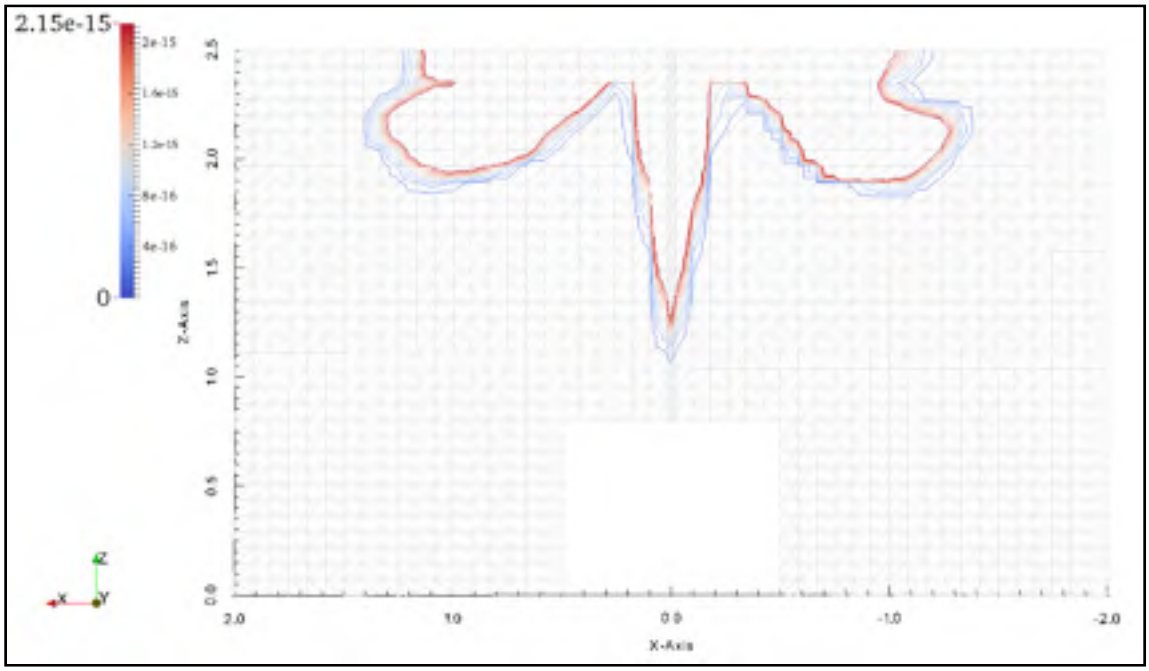

Figure 4-13 Contours of particle concentration in plane C for ACH=24, Θ=45° after 1s of ventilation

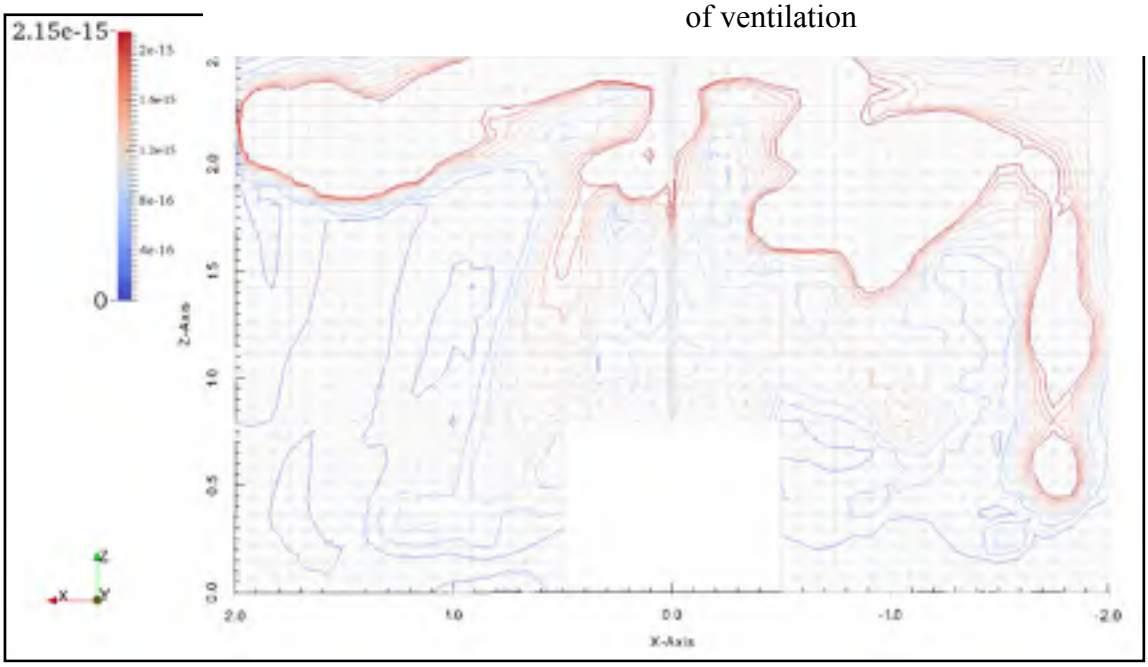

Figure 4-14 Contours of particle concentration in plane C for ACH=24, Θ=45°, after 100s of ventilation

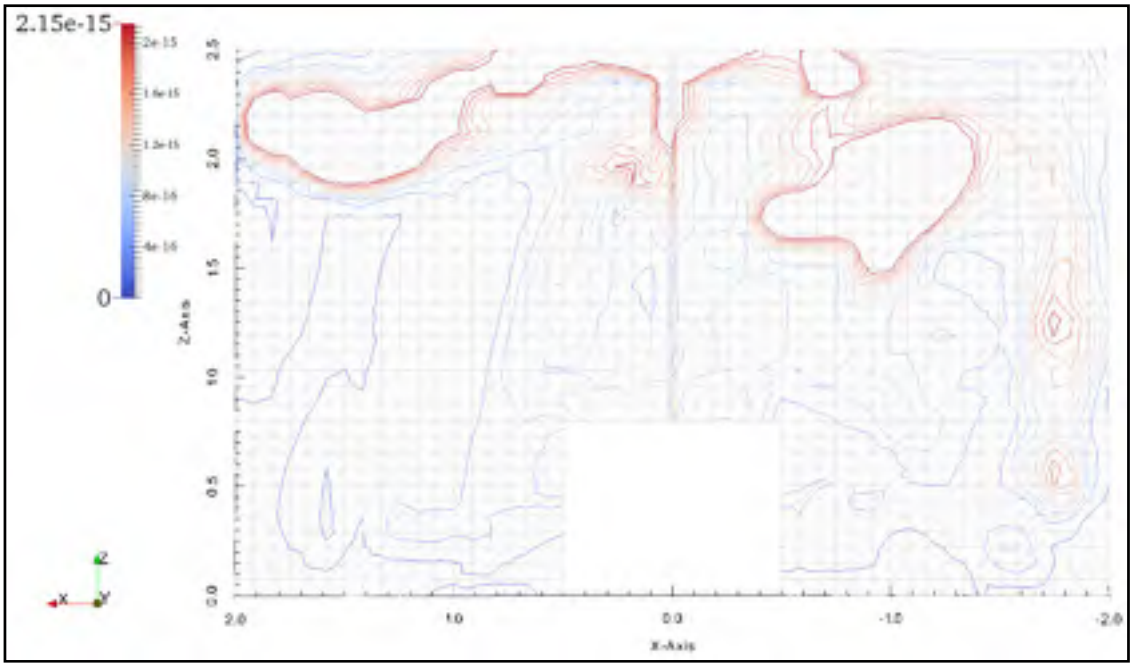

Figure 4-15 Contours of particle concentration in plane C for ACH=24, Θ=45°, after 200s of ventilation

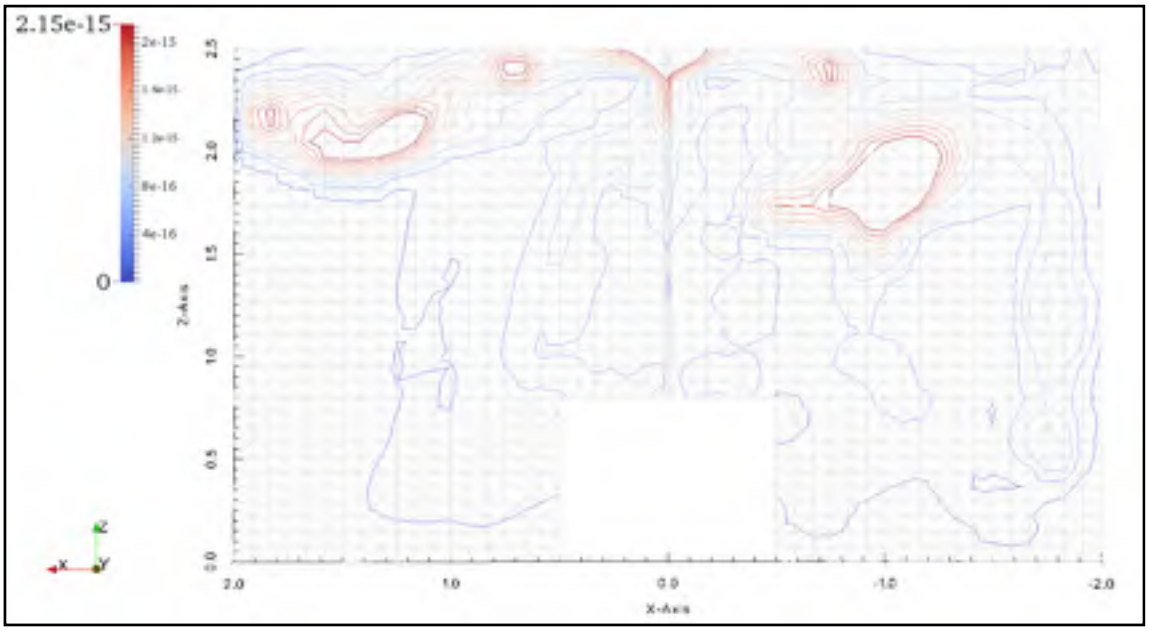

Figure 4-16 Contours of particle concentration in the plane C for ACH=24, Θ=45° after 400s of ventilation

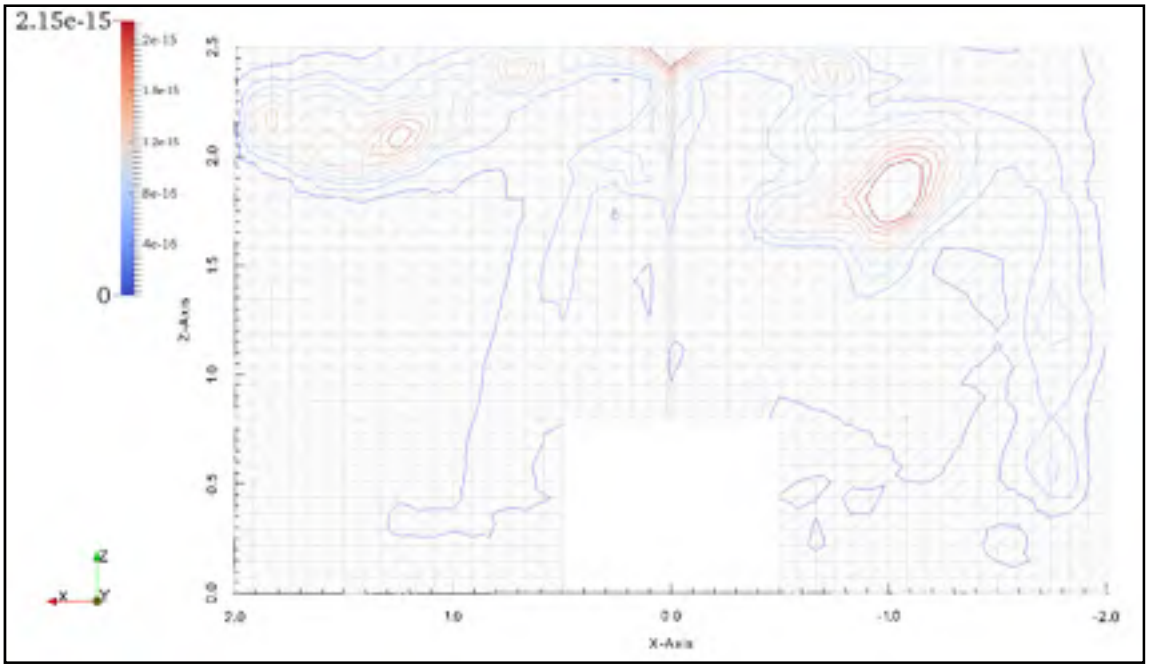

Figure 4-17 Contours of particle concentration in the plane C for ACH=24, Θ=45° after 600s of ventilation

For further investigation of the particle distribution over the patient mouth, particle concentration contours were drawn in plane A with center of (0, 0, 1.25) m. Fig. 4.18 shows the particle concentration contours after 1s particle injection. Here, we can see again a conical region with maximum particle concentration over the patient mouth through the ceiling. Fig. 4.19 shows the particle concentration contours after 100s of ventilation. As observed in this figure, the particle concentration is high in some regions above the bed. Fig. 4.20 and 4.21 show the particle concentration contours after 200s and 600s of ventilation, respectively. As shown in these two figures, the particle concentration over the bed is decreasing over time. The conclusion from these figures is that the particle concentration in the region around the bed front did not increase over time. It shows that the particles were removed through the exhaust by the ventilation.

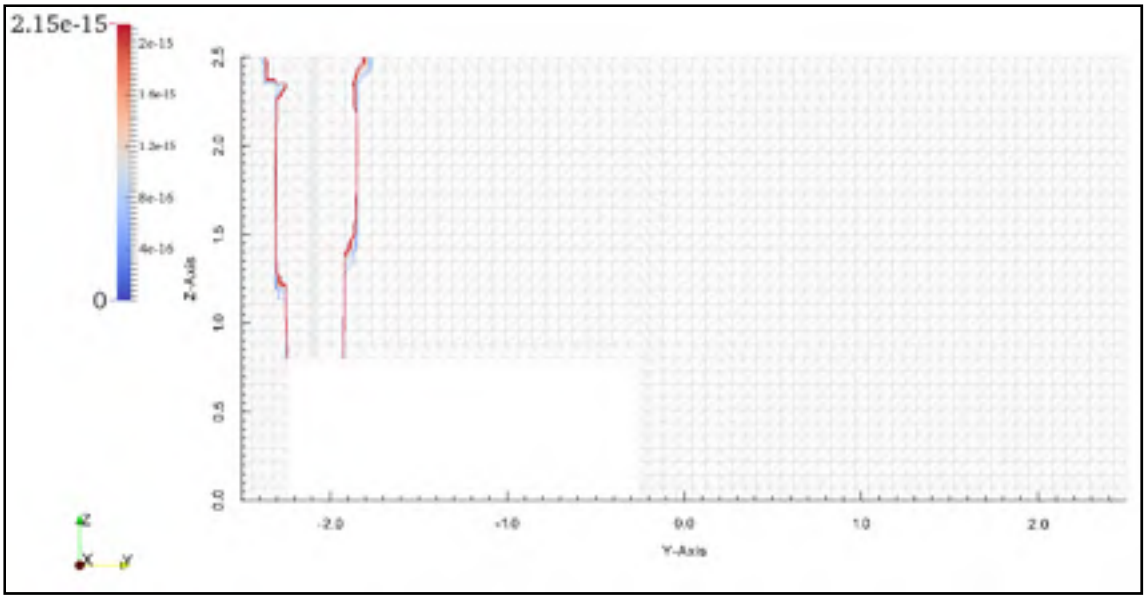

Figure 4-18 Contours of particle concentration in plane A for ACH=24, Θ=45° after 1s of injection

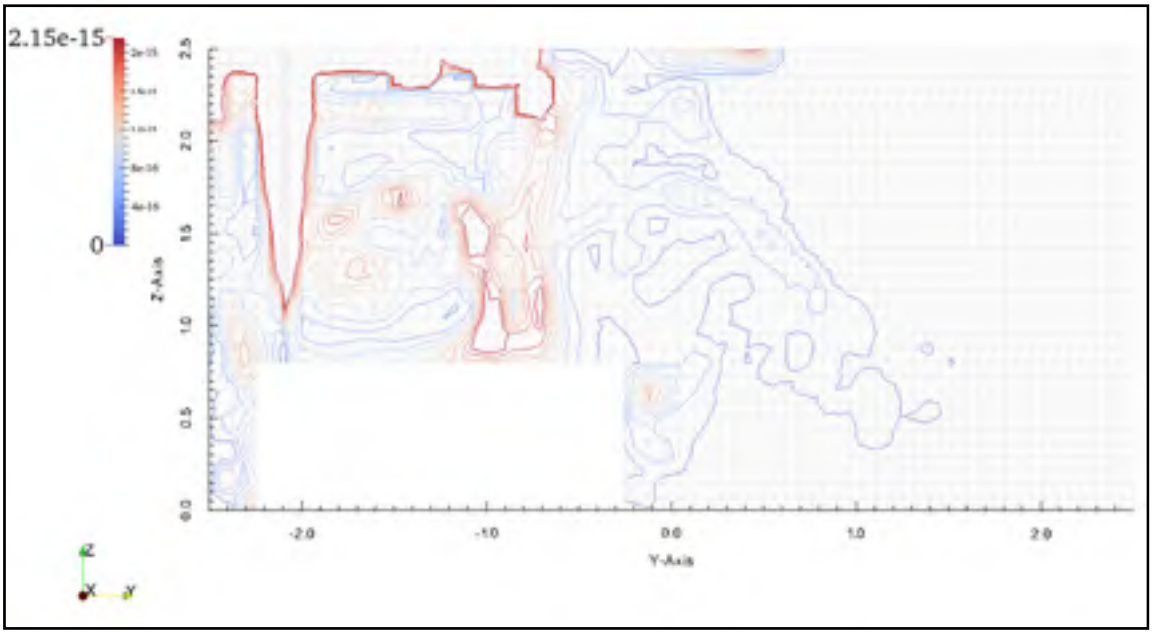

Figure 4-19 Contours of particle concentration in the plane A for ACH=45, Θ=45° after 100s of ventilation

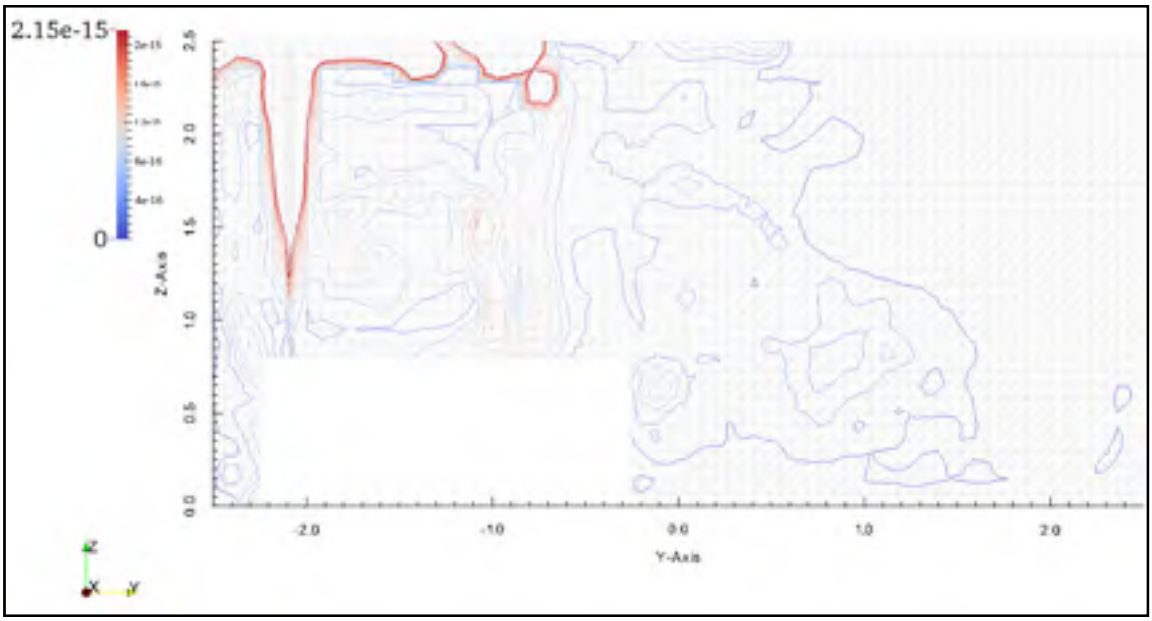

Figure 4-20 Contours of particle concentration in plane A for ACH=24, Θ=45° after 200s of ventilation

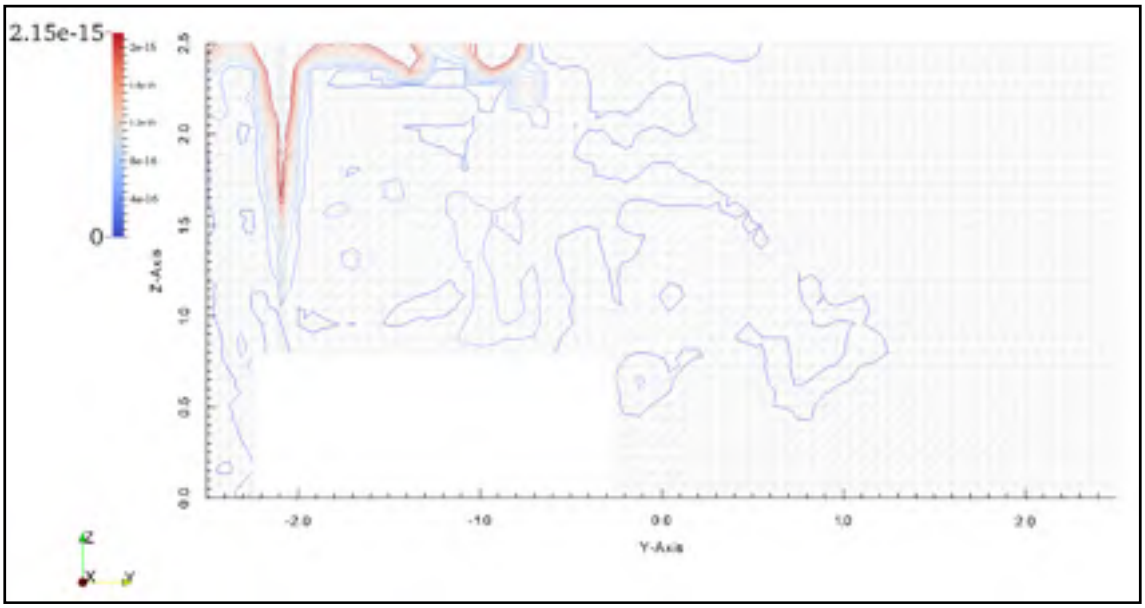

Figure 4-21 Contours of particle concentration in plane A for ACH=24, Θ=45^{o} after 600s of ventilation

4.5 Ventilation effectiveness

To analyze the ventilation effectiveness for six ventilation scenarios, the PRE was calculated for each scenario during the last 200s of a 600s simulation, using the PRE description presented in chapter 3. The last 200s is chosen because at this time the problem is in a stationary state and PRE does not change any more with time. Table 4.3 shows the obtained results for all six scenarios.

To examine whether the PRE variations with ACH are logical or not, we compared the effect of ACH on PRE values, with its effect on time efficiency for contaminants removal in literature [53]. Fig. 4.22 shows the changes of contaminant removal time efficiency with increasing the ACH. From this figure it is concluded that the time removal efficiency for ACH= 15 is 1.1 times the one for ACH=12. Whereas, in this study, the PRE value for ACH 15 is 1.1 times the PRE value for ACH=12. Considering that the rate of changes are relatively close, we can conclude that results are physically reasonable.

For a ventilation strategy that generates perfect mixing conditions, the PRE value is close to one. The PRE value obtained for scenarios number 4 and 6 are significantly smaller than 1, which indicates that these scenarios failed to remove the bioparticles effectively. Scenario 1 with ACH=24 and Θ=45^{o} have the highest value of PRE among the other four scenarios that have PRE values near or bigger than one. Therefore, this scenario is the best among the other scenarios for removing pollutant from the isolation room, based on the PRE values obtained from the simulation results. But increasing ACH causes an increase in energy consumption for cooling or heating the supply air. It also increases the air velocity that patient experiences. According to the ASHRAE standard 55 [82], the air velocity that the patient on the bed is experiencing should be less than 0.25 m/s.

Table 4-3 Comparison of pollutant removal efficiency for different ventilation scenarios

scenarios	θ	ACH	PRE (during the last 200s of a 600s simulation)
Scenario 1	45	24	1.24
Scenario 2	45	15	0.98
Scenario 3	45	12	0.91
Scenario 4	45	9	0.61
Scenario 5	30	24	0.94
Scenario 6	30	9	0.43

Fig. 4.23 shows the air velocity magnitude over line D, above the patient's head for all the six scenarios. In this figure, the yellow line is for the scenario with ACH=9 and Θ=30^{o}, the red line is related to the ACH=9 and Θ=45º, the green line is for ACH=12 and Θ=45º, the black line is for ACH=15 and Θ=45º, the blue line is for ACH=24 and Θ=30º and the purple line is related to the ACH=24 and Θ=45º. For all six scenarios, the air velocity that the patient experienced (at height of 0.8m-1.8m) was less than 0.25 m/s. From the results on this

figure, the ACH augmentation increases the air velocity. For example, at ACH=24, the air velocity over the patient's head is the highest. It is equal to 0.2 m/s approximately. Also, for ACH=24, the air velocity near the ceiling is larger than the recommended air velocity. That could create some problems and bothers the patient. Also the energy consumption increases with increasing the ACH. Therefore, the energy consumption and the air velocity above the patient head create some constraints for increasing the ACH in order to obtain higher PRE values.

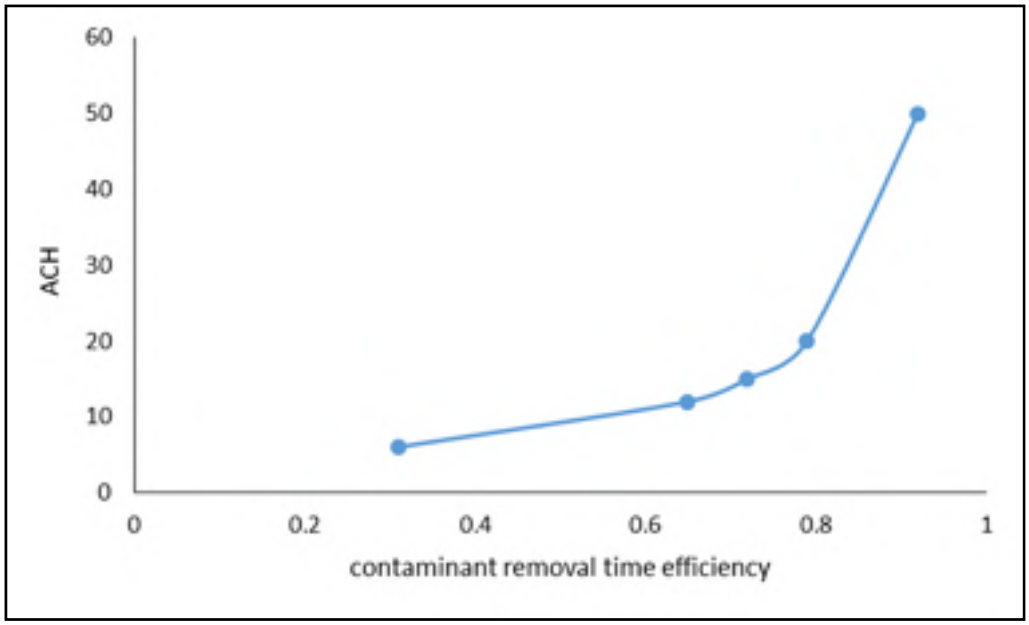

Figure 4-22 Change of time efficiency for contaminants removal with ACH [53]

To compare the ventilation effectiveness more precisely, the normalized bioparticle concentration over line D and E, which are located at the patient and doctor positions respectively, were explored. Fig. 4.24 shows a comparison of normalized bioparticle concentration over line D for 6 scenarios after 600s ventilation. In this figure, the yellow line is for the scenario with ACH=9 and Θ=30°, the red line is related to the ACH=9 and Θ=45°, the green line is for ACH=12 and Θ=45°, the black line is for ACH=15 and Θ=45°, the blue line is for ACH=24 and Θ=30° and the purple line is related to the ACH=24 and Θ=45°. As

observed in this figure, scenarios with an injection angle of 30° (the yellow and the blue lines) have the most particle concentration above the patient's mouth in the breathing zone, at a height of 0.8m-1.5m. Therefore, scenarios with Θ=30° failed to disperse the bioparticles from breathing zone after 600s ventilation, compared to the other scenarios with Θ=45º. The injection angle changes the air flow pattern and the air velocity magnitudes. Considering Fig. 4.23, scenarios with Θ=30° have the lowest air flow velocity over the patient mouth. Low air velocity caused high concentration of the normalized particle in this region. For example, for scenario with ACH=24 and Θ=30°, there is a peak in concentration around z=1.5 m (Fig. 4.24) that could be related to its low air velocity at this height (Fig. 4.23).

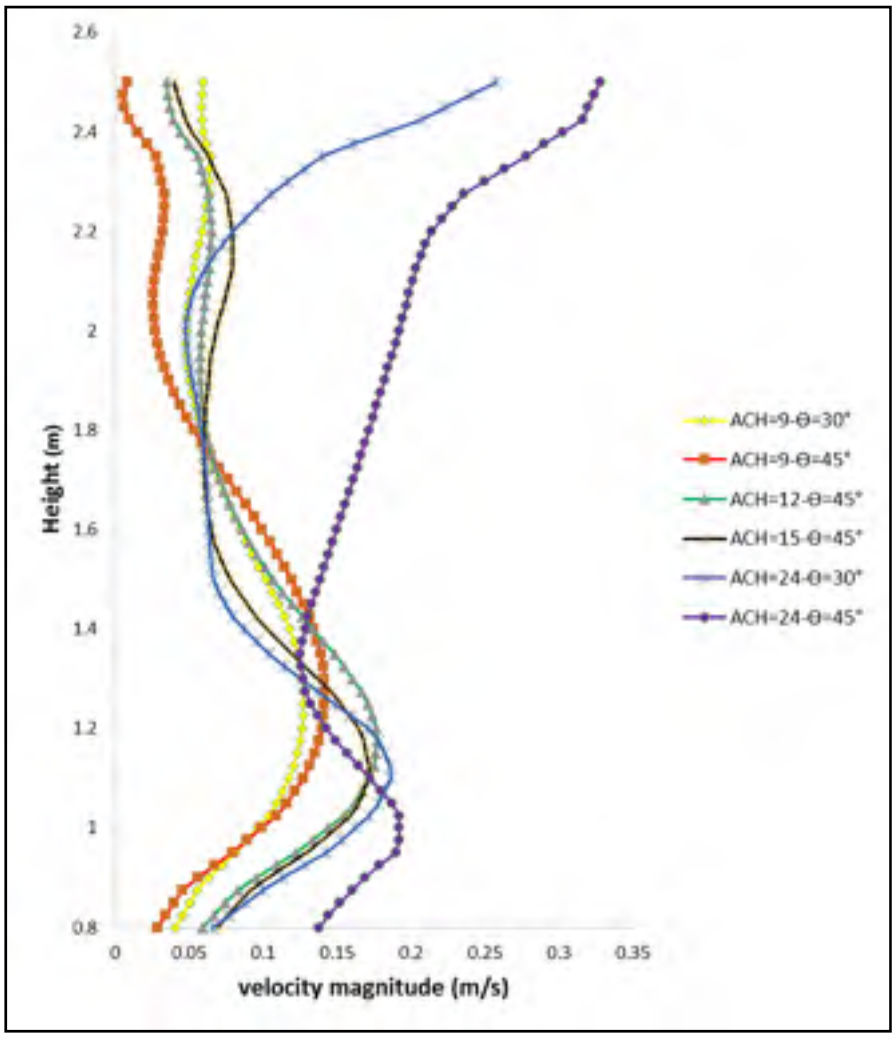

Figure 4-23 Air flow velocity over line D, above the patient mouth for six different scenarios at time = 600s

The other scenarios show the similar value of particle concentration above the patient's mouth in the heights around 0.8m to 2m. The black line which belongs to the ACH=15 dispersed the particles more effectively in the height around 2m-2.3m. Near the ceiling, the purple line with ACH=24 had the lowest particle concentration among the scenarios with Θ=45º.

Fig. 4.25 shows the normalized particle concentration over line E, in the doctor position after 600s ventilation for two scenarios with Θ=30°. As observed in this figure, the yellow and blue lines, which respectively belongs to the scenarios with ACH=9, Θ=30° and ACH=24, Θ=30°, have a high particle concentration at the doctor position. Thus, from this figure, it can be concluded that ventilation scenarios with Θ=30°, were not capable of dispersing the particles from this zone effectively.

Fig. 4.26 shows the normalized particle concentration over line E, at the doctor position after 600s ventilation for four other scenarios with Θ=45º. Each color belongs to one scenario just like in the figure 4.24. The red line is related to the scenario with ACH=9 and Θ=45º. It has three peaks in particle concentration at the height of 1.3m, 1.9m and near the ceiling. Thus, from this figure, it can be concluded that this ventilation scenario was not capable of dispersing the particles from this zone effectively compared to the other scenarios. In addition, the blue line, which belongs to the scenario with ACH=24 and Θ=45°, shows a high particle concentration in the region at heights from 1.5m to 2.5m, compared to the ventilation scenarios with ACH=12 and ACH=15. Therefore, this scenario was not necessarily the most effective ventilation strategy, although its PRE value was the highest one according to the table 4.3. The green and the black line with Θ=45°, have the lowest particle concentration, especially in the doctor breathing zone (height of 1.5m to 2.1m).

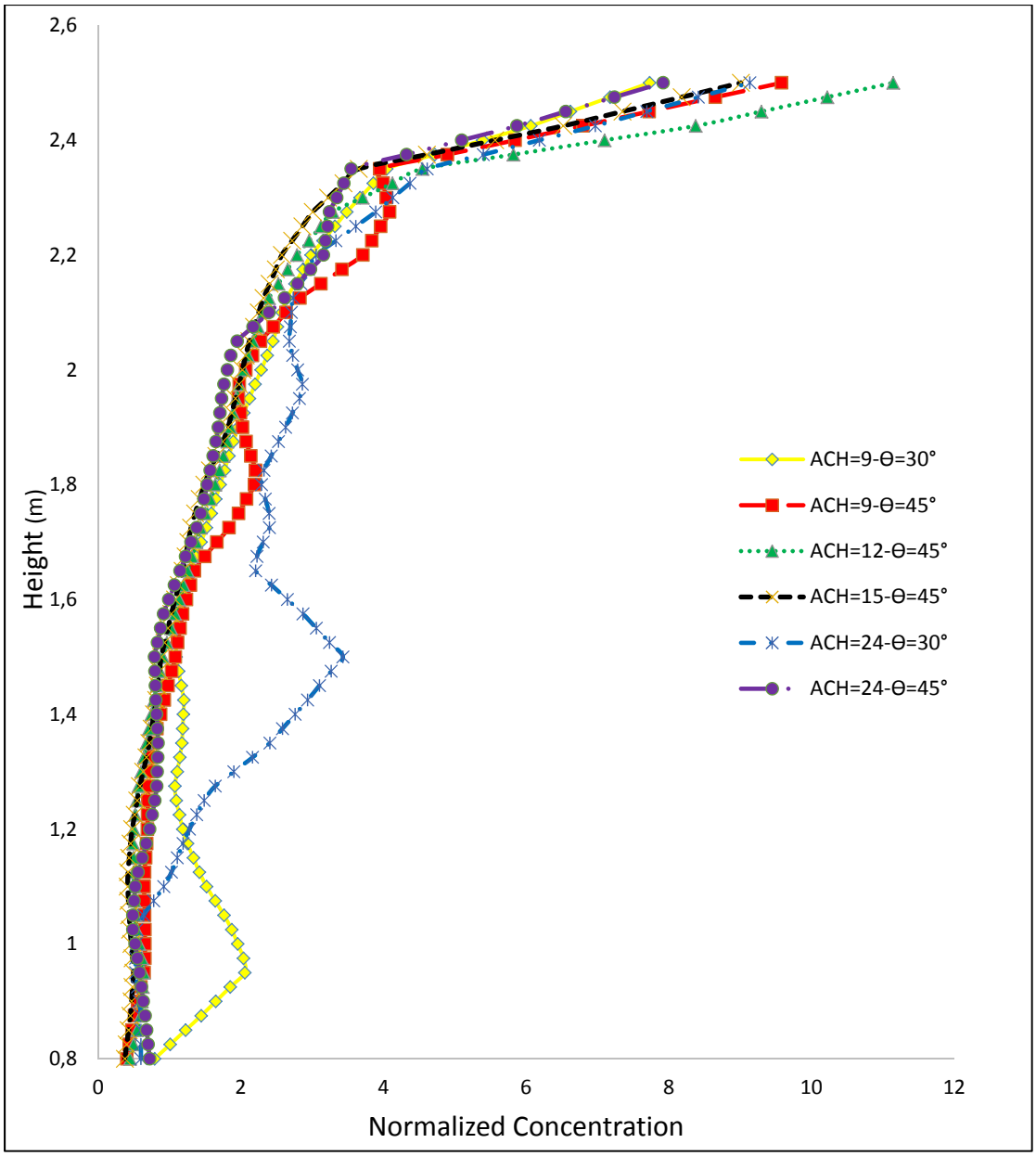

Figure 4-24 Particle normalized concentration over line D, above the patient mouth for six different scenarios after 600s ventilation

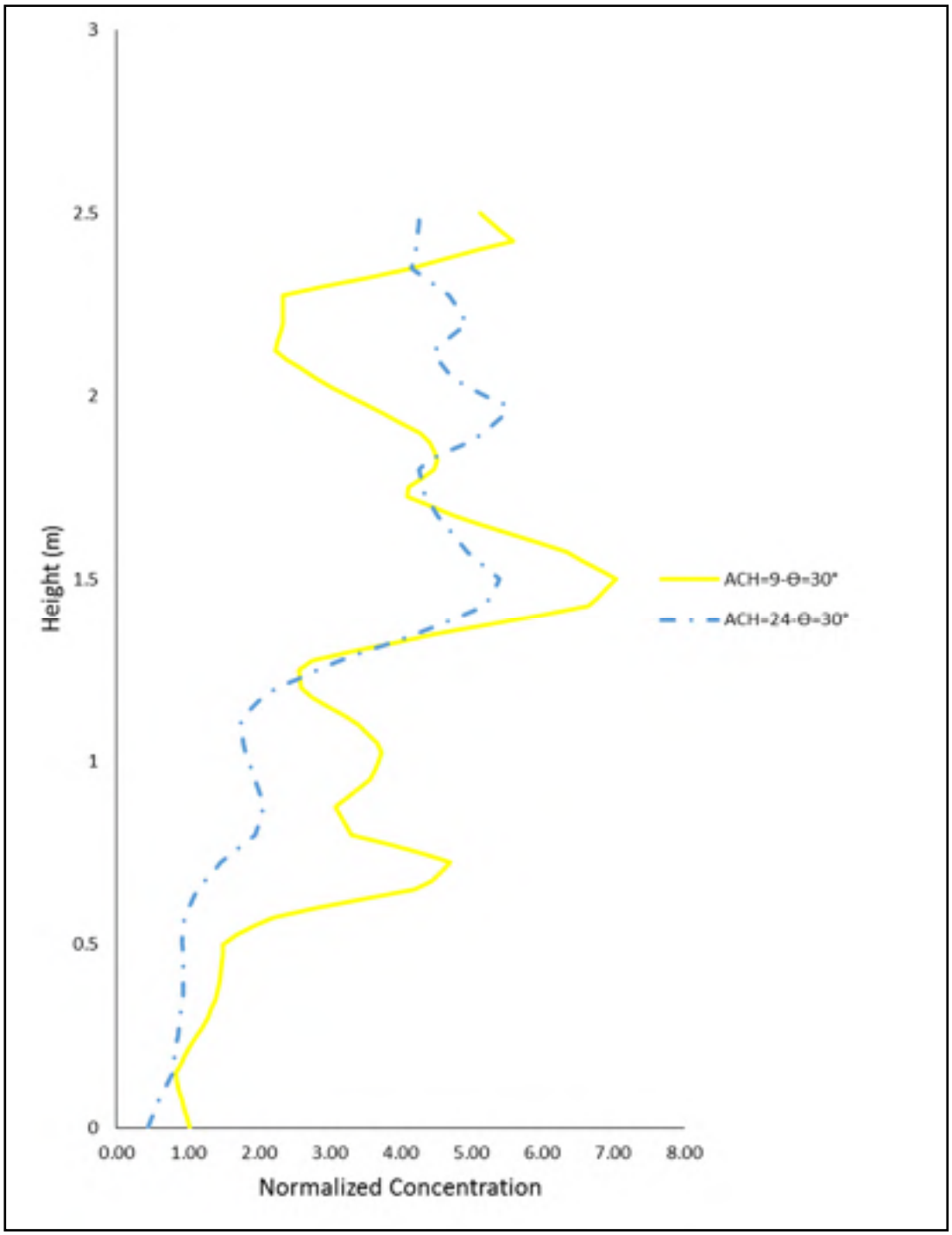

Figure 4-25 Particle normalized concentration over line E, where a doctor may stand, for scenarios with Θ=30°, after 600s ventilation

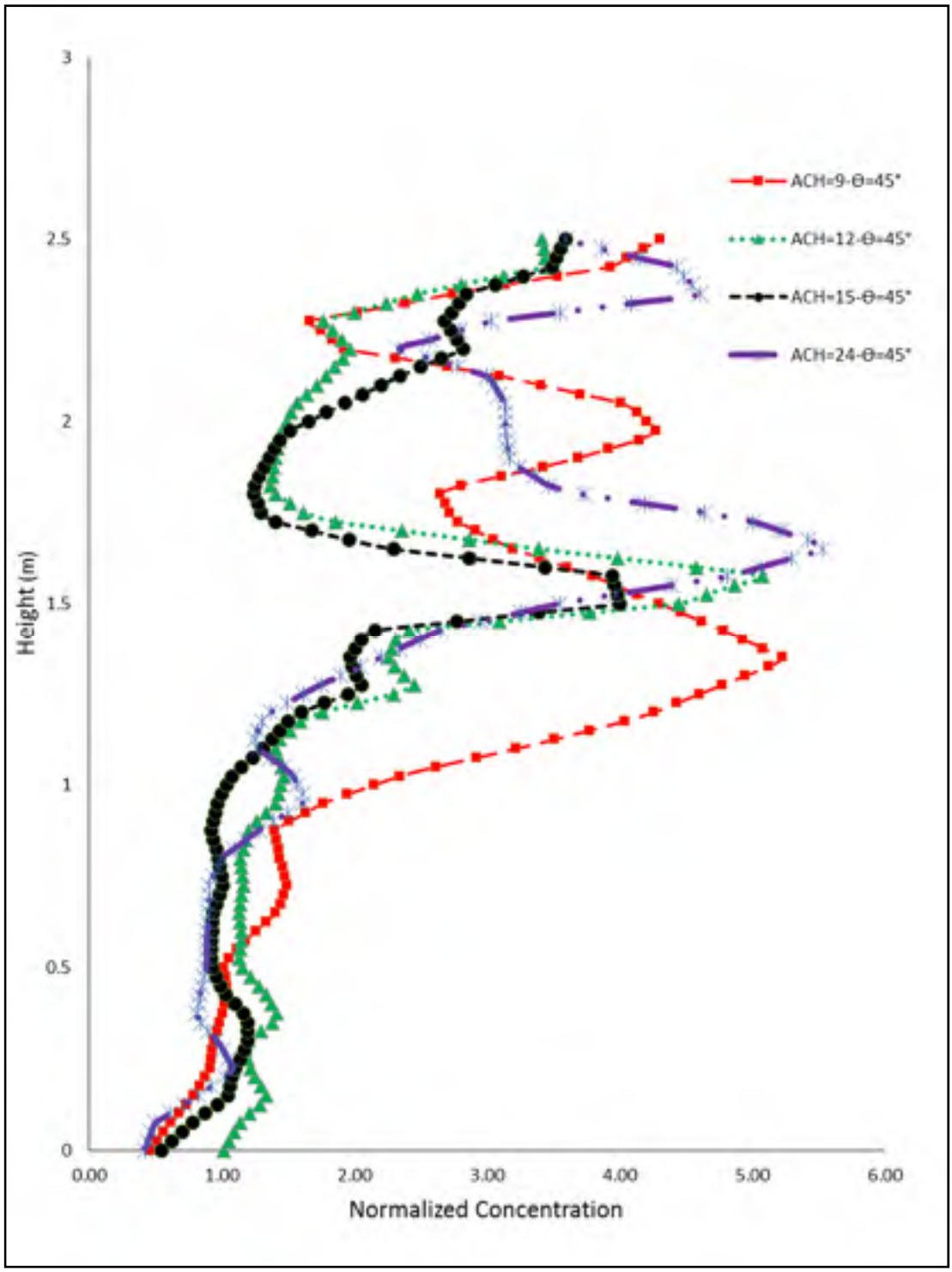

Figure 4-26 Particle normalized concentration over line E, where a doctor may stand, for scenarios with Θ=45°, after 600s ventilation

To investigate the reason of such results, it is helpful to study the air flow pattern in this region. Thus, the velocity vectors for scenarios with Θ=30° are presented in Figures 4.27 and 4.28. They are compared with the velocity vectors for scenario with ACH=15-Θ=45° presented in Fig. 4.29. As observed in these figures, for the two scenarios with Θ=30°, in the doctor position (x=-0.8, y=-2.0) m, the velocity vectors are small compared to the ones for scenario with ACH=15 and Θ=45° (Fig. 4.29). In fact for Θ=30°, the air jet does not arrive to the bed and hit the floor before the bed (Fig. 4.6 (a)). Thus, most of the vortices are formed on the left side of the bed. For scenario with ACH=15 and Θ=45°, some vortices were formed at the doctor position which helped the particles dispersion. But the lack of such vortices at doctor position for the two scenarios with Θ=30°, caused particle stagnation.

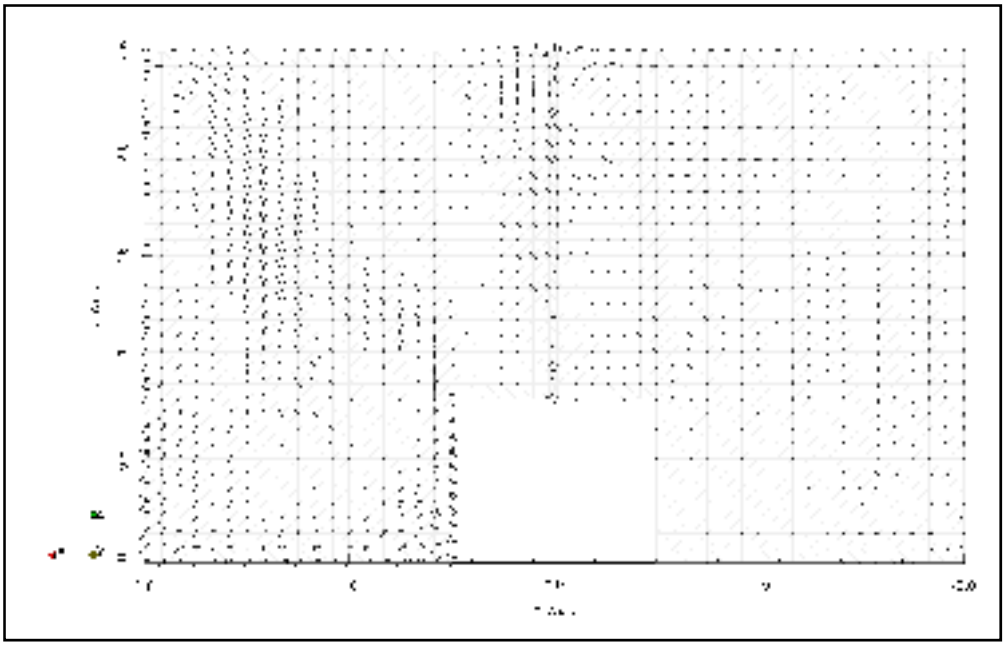

Figure 4-27 Velocity vectors in plane G, with y normal located at y= -2 m (doctor position), for scenario with ACH=9 and Θ=30°, after 600s of ventilation

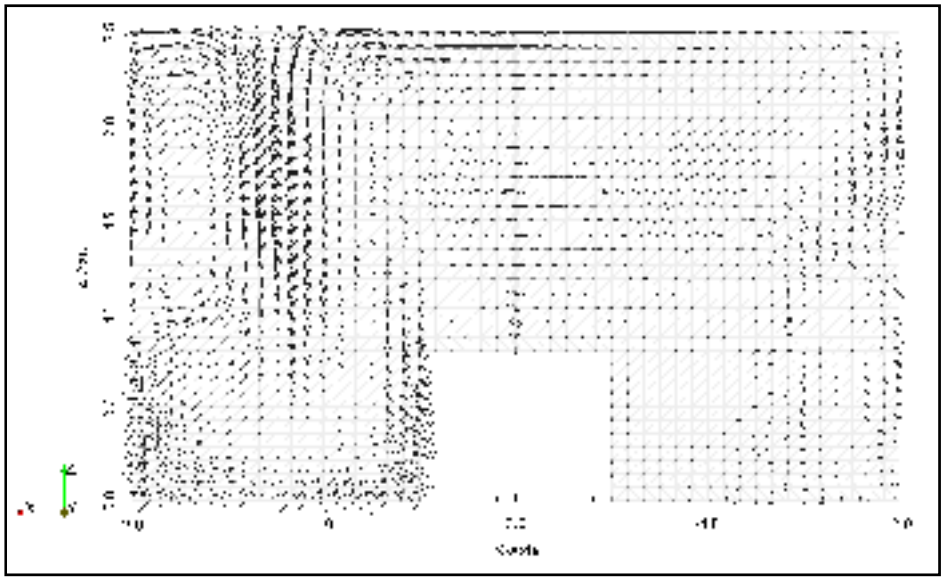

Figure 4-28 Velocity vectors in plane G with y normal located at y= -2 m (doctor position), for scenario with ACH=24 and Θ=30°, after 600s of ventilation

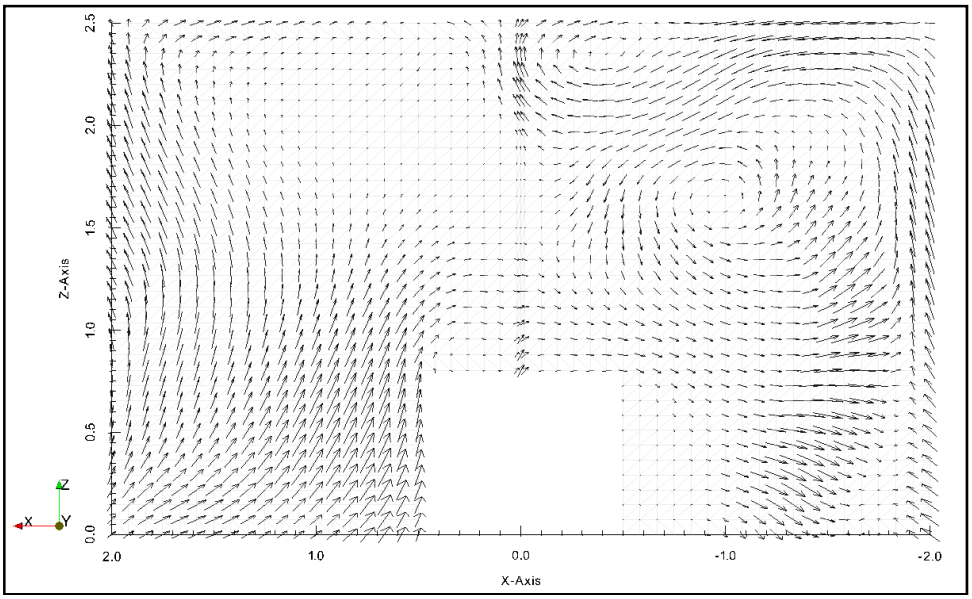

Figure 4-29 Velocity vectors in plane G with y normal located at y= -2 m (doctor position), for scenario with ACH=15 and Θ=45°, after 600s of ventilation

Fig. 4.30 shows the fate of particles after 600s ventilation for different ventilation scenarios. This figure confirmed the previous results that the scenarios with Θ=30° and ACH=9 had the lowest percentage of removed particles, and therefore a low ventilation efficiency. According to this figure, ventilation scenarios with (ACH=24, Θ=45°) and (ACH=15, Θ=45°) have the highest amount of removed particles, respectively. Furthermore, the deposition rate for all ventilation scenarios was approximately the same (between 6-7.2%), except for the ventilation scenario with (ACH=9, Θ=30°) which had a 2% of deposition. This difference in particle deposition for scenario with (ACH=9, Θ=30°), could be due to a lower impact of particles on the floor because of the difference in the air flow pattern. Based on the fact that deposited particles can become airborne again, calculating the deposited amount could be important for the analysis of ventilation efficiency. In this study, the amount of deposited particles was not significant in any of the ventilation scenarios.

Considering the PRE values and the percentage of the removed particles, scenarios with injection angle of 45º and ACH=24, 15 and 12, respectively have the better performance in removing the bioparticles from the isolation room. But for choosing one of these scenarios as the most effective one, it is necessary to consider the particle concentration results in the important zones which suggests the ACH=15 as the best ventilation scenario in decreasing the bioparticles concentration in the breathing zone of the patient and the doctor. Also, from the point of view of energy consumption, ACH=15 is more effective than ACH=24. So the scenario with ACH=15 and Θ=45° is chosen for further investigations on the ventilation strategies with different exhaust locations.

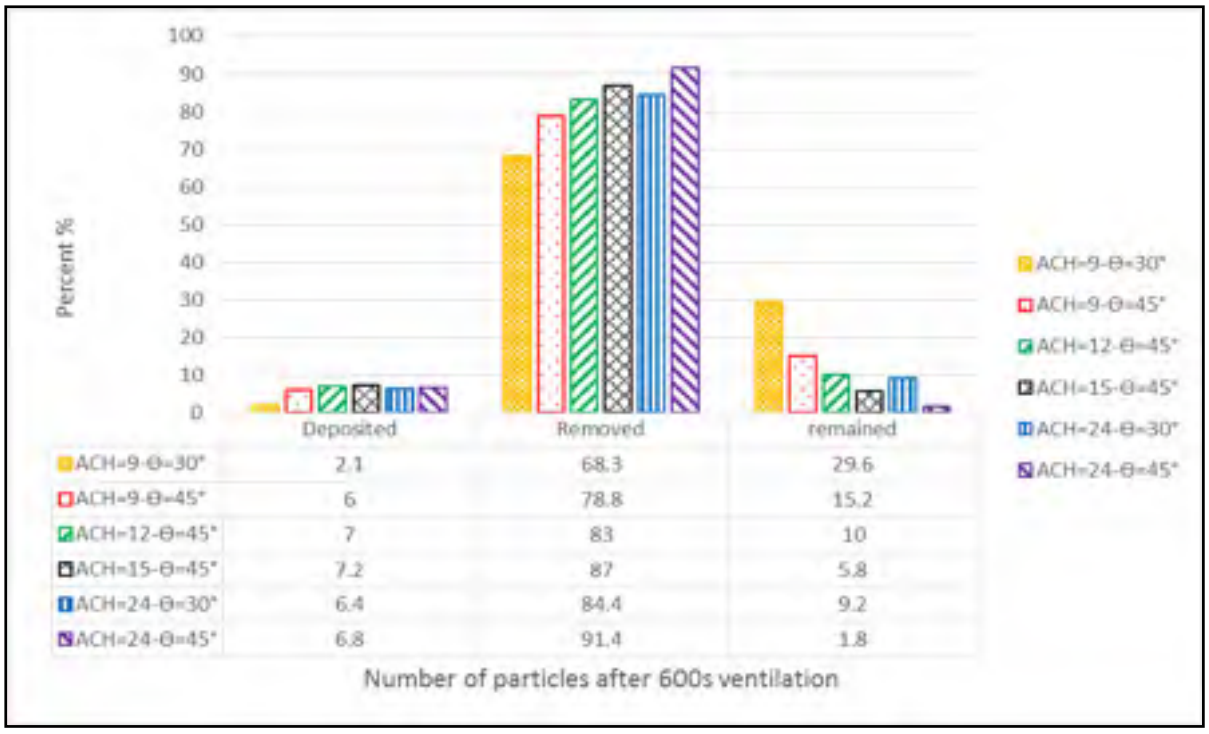

Figure 4-30 Percentage of deposited, removed and remained particles in room after 600s ventilation for different ventilation scenarios

4.6 Ventilation strategies with different exhaust locations

To investigate the effect of exhaust position on ventilation efficiency, the scenario 2 with ACH=15 and Θ=45° was selected. It was the most effective ventilation scenario for the basic configuration. The results of three ventilation scenarios namely; A, B and C, with ACH=15 and Θ=45° and different exhaust positions were compared to see the effect of exhaust position on the ventilation effectiveness. As observed in Table 2.4, the first ventilation strategy is the one selected in the section 4.5 which has an exhaust mounted on the right-side wall with center of (0, 0, 2.35) m which is called scenario A in this section. The second scenario, which is called scenario B, is the ventilation strategy with an exhaust mounted on the north-side wall, near the floor with center of (-1, -2.5, 0.5) m. And the last ventilation strategy, which is called scenario C, has an exhaust located on the ceiling with center of (-

1.2, -1.65, 2.5) m. To investigate the effect of exhaust position on the air flow pattern, the velocity vectors are compared for the three scenarios when the ventilation is started.

4.6.1 Ventilation strategy with an exhaust on the right wall

Fig. 4.31 shows the air flow pattern for scenario A, when the ventilation is started. This figure shows that the air flow jet deflected to the upper areas after hitting the floor and the bed. The flow was then distributed throughout a part of the room between inlet and outlet and a small fraction of the air was extracted via the outlet mounted on the right wall.

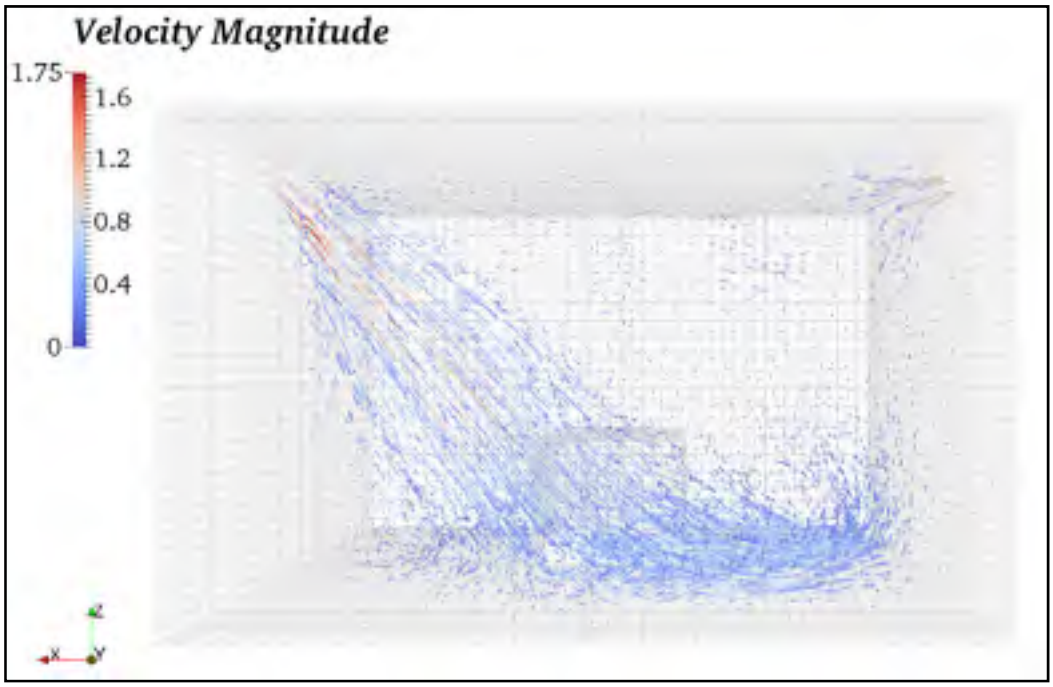

Figure 4-31 Airflow pattern, for ACH=15, Θ=45°, at t=10s of ventilation, for the ventilation strategy with an exhaust mounted on the right wall

4.6.2 Ventilation strategy with an exhaust near the floor

Fig. 4.32 shows the air flow pattern for this ventilation strategy, when the ventilation is started. As observed in this figure, the air flow jet was injected within the isolated room from inlet with an injection angle of 45º, and then deflected by the floor and the bed just like scenario A. But different from scenario A, after deflection, a vortex is created toward the outlet mounted near the floor.

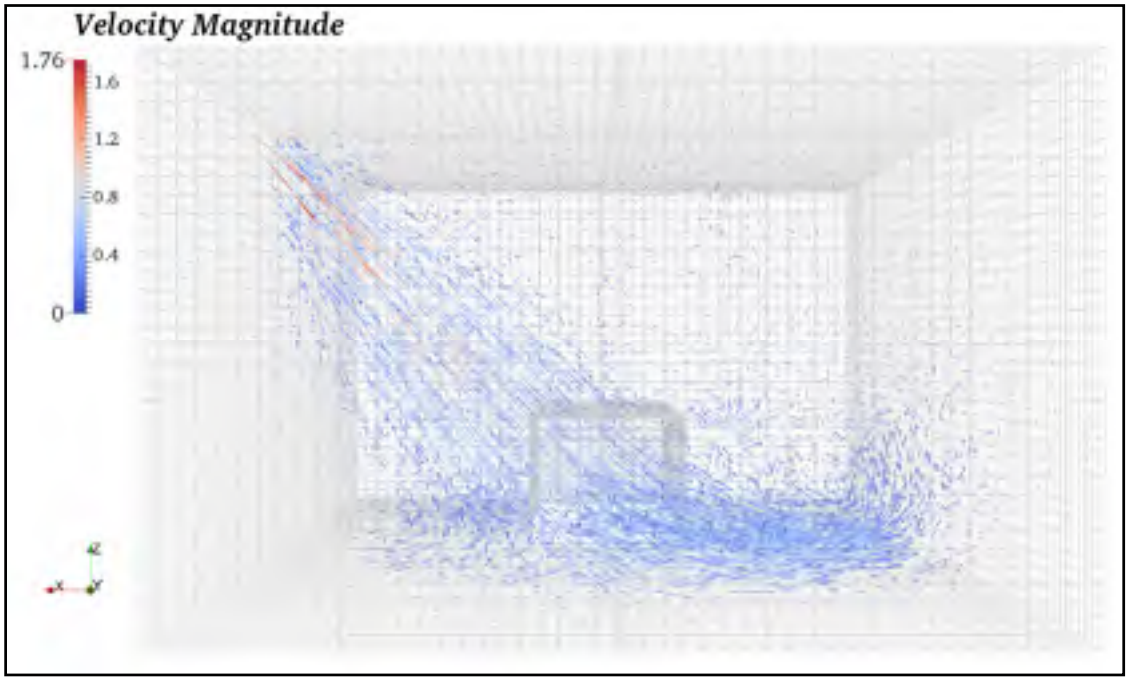

Figure 4-32 Airflow pattern, for ACH=15, Θ=45°, at t=10s of ventilation, for the ventilation strategy with an exhaust near the floor

4.6.3 Ventilation strategy with an exhaust on the ceiling

Fig. 4.33 shows the air flow pattern in the ventilated isolation room with an exhaust on the ceiling when ventilation is started. As observed in this figure the air flow jet came down through the floor and bed just like the two other scenarios. But after impaction with the floor and the bed, the air flow distributed within the room with a different pattern comparing with

two previous scenarios. Finally, the airflow was extracted from the exhaust located on the ceiling.

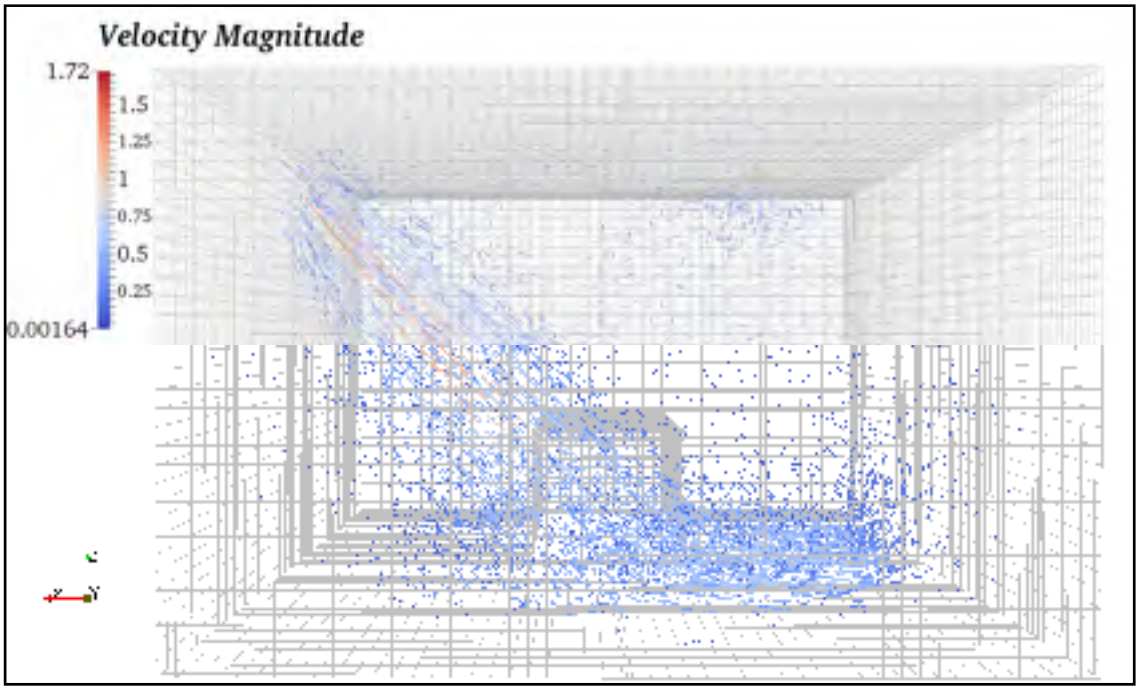

Figure 4-33 Airflow pattern, for ACH=15, Θ=45°, at t=10s of ventilation, for the ventilation strategy with an exhaust located on the ceiling

4.6.4 Comparison of ventilation efficiency for three ventilation strategies with different exhaust positions

To compare the ventilation efficiency of three different ventilation strategies with different exhaust positions, the PRE values, the normalized particle concentration in two important zones as defined before, and the fate of particles are considered.

Table 4.4 shows the PRE values for these three scenarios. As observed in this table, scenario C has the highest pollutant removal efficiency.

Considering the particle dynamic behavior after injection and in the first few minutes of ventilation, shown in Fig. 4.8 and 4.9, it is concluded that most of the particles are accumulated in a region near the ceiling. Also the particle concentration contours in Figs. 4.21 and 4.22, after 200s and 600s of ventilation, shows that the particle concentration near the ceiling is high even after 600s of ventilation. Thus, the scenario C with an exhaust mounted on the ceiling disperses the particles more efficiently.

Table 4-4 Comparison of pollutant removal efficiency for different ventilation strategies

scenarios	θ	ACH	Exhaust position	PRE (during the last 200s of a 600s simulation)
Scenario A	45	15	On the right wall	0.98
Scenario B	45	15	Near the floor	0.96
Scenario C	45	15	On the ceiling	1.19

Fig. 4.34 shows the normalized particle concentration over line D, where the patient's mouth is located, for all the three above-mentioned scenarios. The black and blue lines, which respectively belong to the scenario A and C, have a low normalized particle concentration, above the patient mouth. While the red line, which is related to the scenario B, shows higher normalized concentration compared to the scenarios A and C.

The location of exhaust in scenario B, near the floor, is far from the regions with high particle concentrations. It could be the origin of the weak performance in removing the particles from the isolation room.

Fig. 4.35 shows a comparison of normalized particle concentration over line E, at the doctor position for the three ventilation strategies A, B and C. As observed in this figure, Scenario C with blue line has the lowest particle concentration in this zone compared with the two other scenarios with the black line (scenario A) and the red line (scenario B). In scenario B, there is a high particle concentration in the doctor position. It could be caused by the exhaust position near the floor. As observed in Fig. 4.32, the trend of the air flow was through the exhaust which is located near the floor. Thus, a big fraction of the air flow went out via the exhaust without going up and distribute within the room. Thus, the particle concentration is high in the upper regions. In scenario A, there is a peak at the height of 1.5m. This high concentration could be caused by the air jet, pushing the particles through the right wall where the exhaust is mounted. For scenario C, the particle concentration is low. The reason is that most of the particles are accumulated near the ceiling and the air jet in this scenario just need to push them though the outlet mounted on the ceiling.

Fig. 4.36 shows the fate of the particles after 600s of ventilation for the three scenarios A, B and C. In this figure the black color belongs to the scenario A, the red color belongs to the scenario B and the blue one is related to the scenario C. The scenario C has the higher percent of removed particles and the lowest percent of remained and deposited particles after 600s of ventilation. Considering all the above results, scenario C, with an exhaust mounted on the ceiling, is the most effective ventilation strategy with the highest value of PRE equal to 1.19, the lowest particle concentration in two important breathing zones, the highest percent of removed particle and the lowest percent of the remained an deposited particles compared with the scenario A and B.

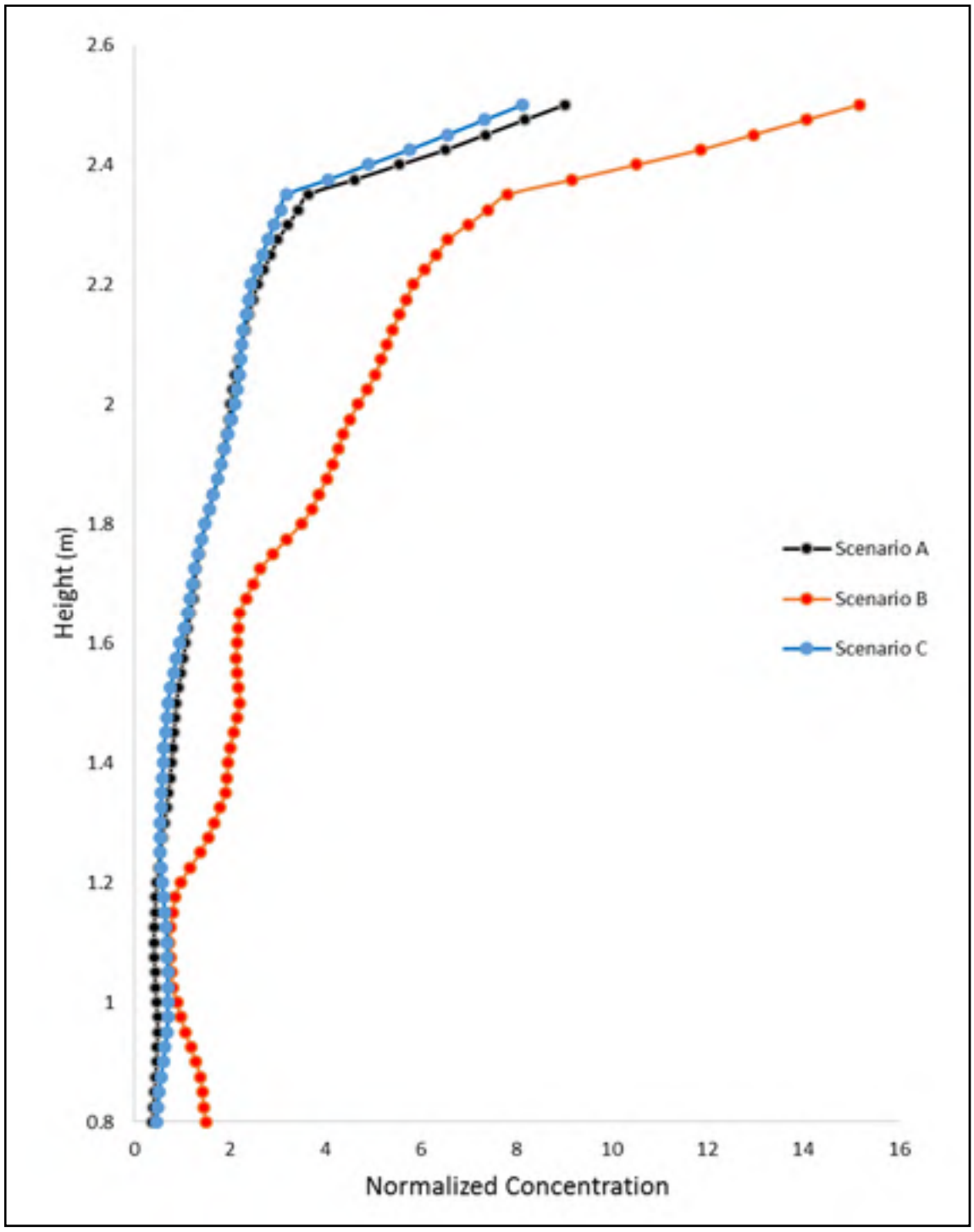

Figure 4-34 Particle normalized concentration over line D, above the patient mouth for three different scenarios after 600s of ventilation

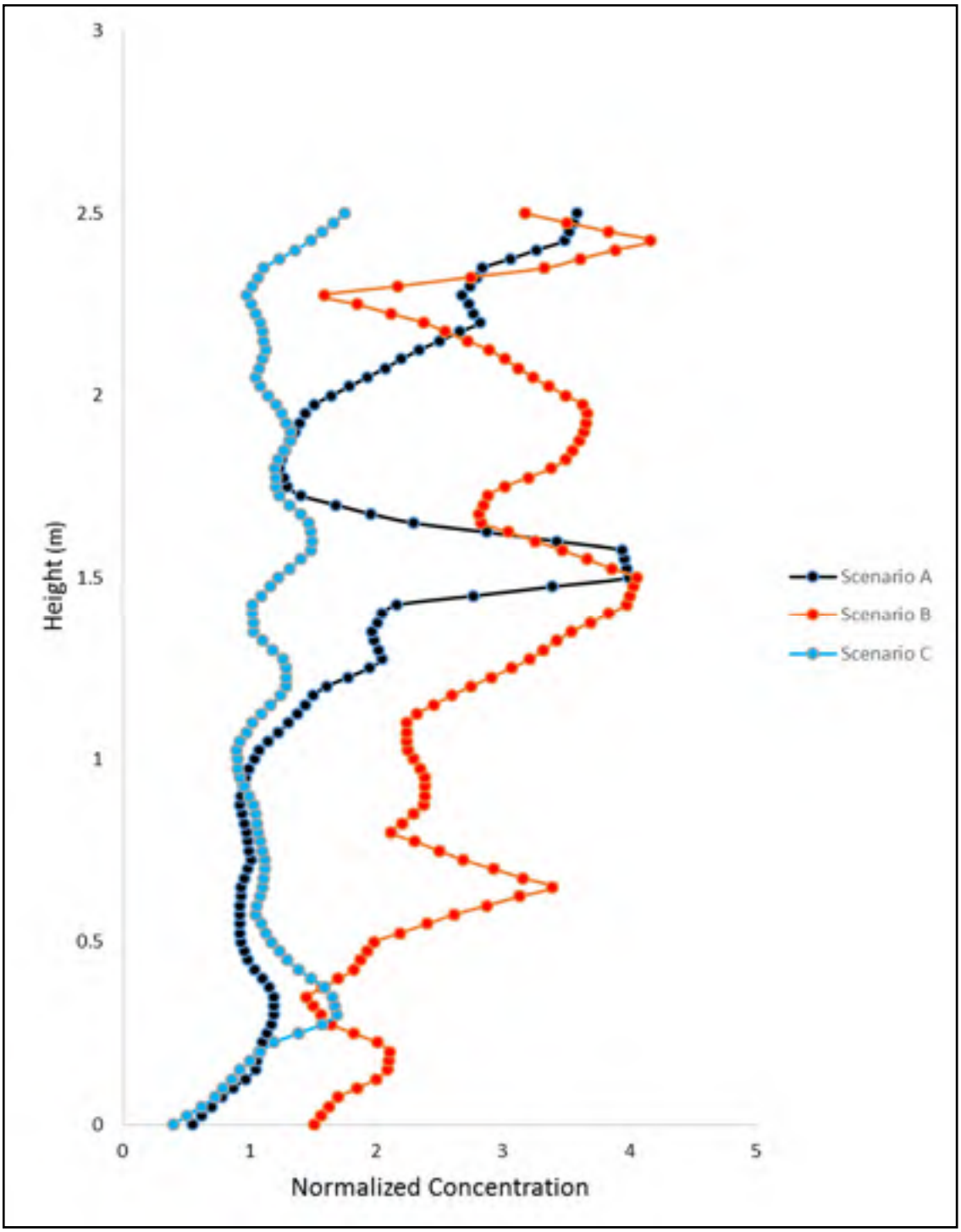
3
2.5
2
1.5
1
0.5
0
Height (m)
0
1
2
3
4
5
Normalized Concentration
Scenario A
Scenario B
Scenario C

Figure 4-35 Particle normalized concentration over line E, where a doctor may stand, for three different scenarios, after 600s ventilation

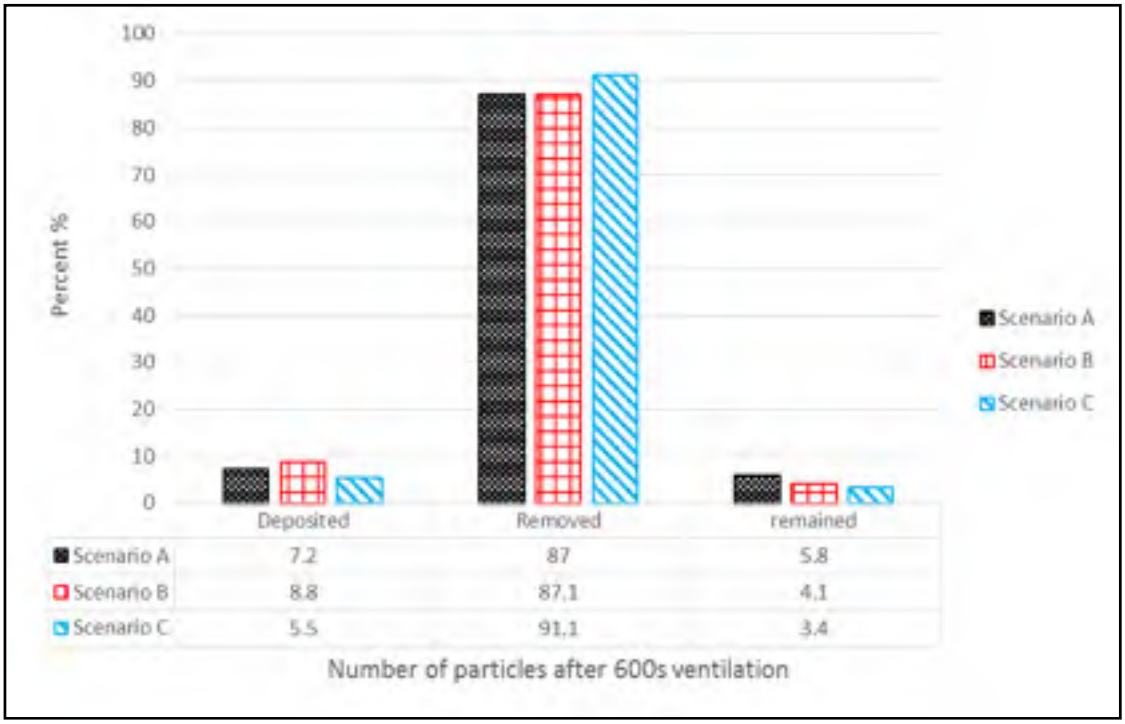

Figure 4-36 Percentage of deposited, removed and remained particles in room after 600s ventilation for different ventilation scenarios A, B and C

The main objective of this chapter was to find the most effective ventilation strategy for removing the bioparticles exhaled from a patient mouth during the coughing process from an isolation room. Among the six defined scenarios with different air change rate and injection angle, we found that the scenario 2 is the most effective one. Then by changing the exhaust position, we tried to find the best ventilation strategy for the defined isolation room. Results show that the most effective ventilation strategy for this isolation room is a ventilation strategy with ACH=15 and Θ=45° and an exhaust mounted on the ceiling.

CONCLUSION

Ventilation is an important engineering control system for infection control in the hospital isolation rooms. The main objective of this study was to select the most effective ventilation scenario for removing bioparticles exhaled by a patient during coughing process. For this purpose, the effect of the air flow velocity, the injection angle and the exhaust position on bioparticles removal was investigated.

The literature review introduced the health risks that airborne bioparticles could represent in enclosed spaces. An appropriate model for the coughing process was determined considering the previous published articles. The literature review helped us to determine the effective parameters in removing bioparticles from such spaces and the methods used for predicting their behavior.

Chapter 2 presented the mathematical model and the methodology used for studying the ventilation effectiveness for defined ventilation scenarios. The problem was defined by a description of the coughing process, the geometry, the mesh, the scenarios and the boundary conditions. Then, Code-Saturne software and the mathematical and numerical methods used were briefly introduced. It is concluded that Code-Saturne is able to predict the trajectory of a discrete phase particle by Lagrangian approach and neglecting the turbulent dispersion for small particles. The six scenarios for investigating the influence of the ACH and the Θ on the ventilation effectiveness were determined. Secondly, three geometrics were defined to investigate the effect of the exhaust position on the ventilation effectiveness.

Chapter 3 showed the validation of Code-Saturne prediction capability for the air flow pattern, particle dispersion and deposition, by comparing the obtained numerical results with the results published in the literature. From this chapter, it is concluded that Code-Saturne is a reliable program for predicting the air flow pattern and the particle dispersion in a 3D chamber, except for the regions close to the floor. For more investigation of Code-Saturne capability in predicting the particle dynamic behavior especially near the walls, the particle

deposition velocity for a range of particles diameter between 1-10 μm was investigated in a 2D channel. The results showed that Code-Saturne is reliable for predicting the particle deposition only when the turbulent dispersion effect is neglected.

Chapter 4 presented the numerical results for the isolation room investigated and discussed them to select the most effective ventilation strategy for removing the bioparticles. In this chapter, the effects of the mesh sizes on the results were shown. Then, the justification for choosing the scenarios in "experimental design results" section is presented. Thereafter the air flow pattern, the bioparticle distribution and the ventilation effectiveness for six defined ventilation scenarios were presented and compared. The most effective scenario among six scenarios was selected after analyzing the results. Finally, the effect of the exhaust position on the ventilation effectiveness was shown and the most effective scenario for the investigated isolation room was selected. The results showed that regardless of the air flow injection angle, ventilation strategies with ACH=9 failed to remove the bioparticles effectively from the room environment. In addition, Θ=30° is not an effective injection angle even at ACH=24. For these conditions, the normalized concentration in important zones such as patient and doctor breathing zones, was high after 600s ventilation.

Considering the PRE values, increasing the ACH from 12 to 24 made a slight increase in the amount of removing particles from the room. But increasing the ACH to 24 did not necessarily introduce a better ventilation strategy due to its higher normalized particle concentration in important zones compared to ACH=12 and ACH=15. Therefore, scenario with ACH=15 and Θ=45° was the most effective ventilation scenario among the six selected ones, due to its lower normalized particle concentration, its high PRE value and its low percentage of remained particle after 600s ventilation. Investigation of the exhaust position effect on the ventilation efficiency was presented at the end of chapter 4. Among the scenarios studied, scenario C (exhaust located on the ceiling) was the most effective ventilation strategy in removing the particles from the isolation room with the highest value

of PRE, the lowest percent of particle deposition and the highest percent of removed particles.

For the future work, it is recommended to investigate the effect of increasing the number of exhaust on the ventilation effectiveness. Also, it could be helpful to simulate the two-phase flow with Eulerian-Eulerian approach and compare the results to obtained numerical results in this study.

LIST OF REFERENCE

1- Fangzhi Chen, Simon C.M. Yu, Alvin C.K. Lai. 2006. "Modeling Particle Distribution and Deposition In Indoor Environments With A New Drift–Flux Model". Atmospheric Environment, vol. 40, Issue 2, p. 357–367.

2- Bin Zhao, Jun Wu. 2007. "Particle Deposition In Indoor Environments: Analysis Of Influencing Factors". Journal of Hazardous Materials, vol. 147, Issues 1–2, p. 439–448.

3- A.P. Jones. 1999. "Indoor Air Quality and Health". Atmospheric Environment, vol. 33, p. 4535-4564.

4- United States environmental protection agency. 1993. "Targeting Indoor Air Pollution, EPA's Approach & Progress". Air and Radiation (6203j).

5- Jones. P. Waters. R. 1993. "The Practical Application of Indoor Airflow Modeling. Modeling Of Indoor Air Quality and Exposure". Niren Nagada, Ed., American Society for Testing and Materials, Philadelphia, p. 173-181.

6- Walkinshaw, D. S. 1992. "Some Engineering Components of Indoor Environmental Investigations". In *Conference Proceedings: IA Q 92: Environments for People. ASHRAE*. San Francisco. p. 59-69.

7- K.W.D. Cheong, S.Y. Phua. 2006. "Development of Ventilation Design Strategy for Effective Removal Of Pollutant In The Isolation Room Of A Hospital". Building and Environment, vol. 41, Issue 9, p. 1161–1170.

8- Zhecho D. Bolashikova, Arsen K. Melikova, Wojciech Kieratb, Zbigniew Popiołekb & Marek Branda, 2012. "Exposure of Health Care Workers and Occupants to Coughed Airborne Pathogens in a Double-Bed Hospital Patient Room with Overhead Mixing Ventilation". HVAC&R Research vol. 18, Issue 4, p. 602-615.

9- Li Y1, Huang X, Yu IT, Wong TW, Qian H. 2005. "Role Of Air Distribution In SARS Transmission During The Largest Nosocomial Outbreak In Hong Kong.". Indoor Air, vol. 15(2), p. 83-95.

10- Hua Qiana, Yuguo Lia, Peter V. Nielsenb, Carl E. Hyldgaard. 2008. "Dispersion of Exhalation Pollutants in A Two-Bed Hospital Ward with A Downward Ventilation Strategy", Building and Environment, vol. 43, Issue 3, p. 344–354.

11- Farhad Memarzadeh. 2008. "Methodology for Minimizing Risk from Airborne Organisms in Hospital Isolation Rooms", ASHRAE Transactions 01/2000.

12- H. Qian, Y. Li. 2010. "Removal of Exhaled Particles by Ventilation and Deposition in a Multi-bed Airborne Infection Isolation Room", Indoor Air, vol. 20, p. 284-297.

13- Anna Kokkonen, Marko Hyttinen, Rauno Holopainen, Kari Salmi, Pertti Pasanen, 2014. "Performance Testing of Engineering Controls of Airborne Infection Isolation Rooms by Tracer Gas Techniques", Indoor and build environment, vol. 23(7), p. 994-1001.

14- Qian, H., Y. Li, P.V. Nielsen, C.E. Hyldgaard, T.W. Wong, and A.T.Y. Chwang. 2006. "Dispersion of Exhaled Droplet Nuclei in a Two-Bed Hospital Ward with Three Different Ventilation Strategies", Indoor Air 16, p. 111–28.

15- Menzies, D. A. Fanning, L. Yuan, J.M. FitzGerald, and the Canadian Collaborative Group in Nosocomial Transmission of TB. 2000. "Hospital Ventilation and Risk for Tuberculous Infection in Canadian Health Care Workers", Annals of Internal Medicine, vol. 133(10), p. 779–89.

16- Li Y1, Leung GM, Tang JW, Yang X, Chao CY, Lin JZ, Lu JW, Nielsen PV, Niu J, Qian H, Sleigh AC, Su HJ, Sundell J, Wong TW, Yuen PL. 2007. "Role of Ventilation

in Airborne Transmission of Infectious Agents in the Built Environment - A Multidisciplinary Strategyatic Review", Indoor Air., vol. 17(1), p. 2-18.

17- Kao, P.H., and R.J. Yang. 2006. "Virus Diffusion in Isolation Rooms". Journal of Hospital Infection, vol. 62, p. 338–45.

18- Noakes, C., L.A. Fletcher, P.A. Sleigh, W.B. Booth, B. Arribas, and N. Tomlinson. 2009. "Comparison of Tracer Techniques for Evaluating the Behavior of Bioaerosols in Hospital Isolation Rooms". In *Proceedings of Healthy Buildings, Syracuse*, NY, vol. 13–17, p. 504.

19- Tung, Y.-C., S.-C. Hu, T.-I. Tsai, and I.-L. Chang. 2009. "An Experimental Study on Ventilation Efficiency of Isolation Room", Building and Environment, vol. 44, p. 271–279.

20- Carla Baloccoa, Pietro Lio. 2011. "Assessing Ventilation Strategy Performance in Isolation Rooms". Energy and Buildings, vol. 43, Issue 1, p. 246–252.

21- Bin Zhao, Caiqing Yangb, Xudong Yanga, Shuangke Liu. 2008. "Particle Dispersion and Deposition in Ventilated Rooms: Testing and Evaluation of Different Eulerian and Lagrangian Models", Building and Environment, vol. 43, Issue 4, p. 388–397.

22- F. Archambeau, N. Mechitoua, M. Sakiz. 2004. "Code_Saturne: A Finite Volume for the Computation of Turbulent Incompressible Flows- Industrial Applications". International Journal of Finite Volumes, p. 10.

23- Christopher R. Buchanan. 1997. "CFD Characterization of a Mechanically Ventilated Office Room: the Effects of Room Design on Ventilation Performance". Ph.D. thesis, University of California, Irvine.

24- I. Eames, D. Shoaib, C. A. Klettner, V. Taban. 2009. "Movement of Airborne Contaminants in a Hospital Isolation Room". Interface focus, p. 319.

25- Xie X, Li Y, Chwang ATY, Ho PL, Seto WH. 2007. "How Far Droplets Can Move In Indoor Environments – Revisiting The Wells Evaporation-Falling Curve", Indoor Air, vol. 17, p. 211-225.

26- Cole E. C., Cook C. E. 1998. "Characterization of Infectious Aerosols in Healthcare Facilities: An Aid to Effective Engineering Controls and Preventative Strategies". Am. J. Infect, Control 26, p. 453–464.

27- Duguid J. P. 1945. "The Numbers And The Sites of Origin of The Droplets Expelled During Expiratory Activities", Edinb. Med. J. vol. 52, p. 385–401.

28- Chao C. Y. H., et al. 2009. "Characterization of Expiratory Air Jets And Droplet Size Distributions Immediately At The Mouth Opening", J. Aero. Sci. vol. 40, p. 122–133.

29- Jennifer Fiegel, Robert Clarke and David A. Edwards. 2006. "Airborne Infectious Disease and the Suppression of Pulmonary Bioaerosols", Drug Discovery Ttoday, volume 11.

30- Shinhao Yang, Grace W. M. Lee, Cheng-Min Chen, Chih-Cheng Wu and Kuo-Pin Yu2. 2007. "The Size And Concentration of Droplets Generated By Coughing In Human Subjects", Journal of Aerosol Medicine, vol. 20, Number 4.

31- Papineni RS, Rosenthal FS. 1997. "The Size Distribution of Droplets in the Exhaled Breath of Healthy Human Subjects", J Aerosol Med., vol.10, Number 2, p. 105-16.

32- Edwards, D.A., J.C. Man, P.Brand, J.P. Katstra, K. Somerer, H.A. Stone, E. Nardell and G. Scheuch. 2004. “Inhaling To Mitigate Exhaled Bioaerosols”, Proceeding of the National Academy of Science, Vol. 101, 50, p. 1783-84.

33- Hyttinen-M; Rautio-A; Pasanen-P; Reponen-T; Earnest-GS; Streifel-A; Kalliokoski-P. 2011. “Airborne Infection Isolation Rooms” *A Review of Experimental Studies*, Indoor Built Environ, vol. 20(6), p. 584-594.

34- Alani A1, Barton IE, Seymour MJ, Wrobel LC., 2001. “Application of Lagrangian Particle Transport Model to Tuberculosis (TB) Bacteria UV Dosing In A Ventilated Isolation Room”, International J Environ Health Res., vol. 11(3), p. 219-28.

35- Bin Zhao, Zhao Zhang, Xianting Li. 2005. "Numerical Study of The Transport of Droplets or Particles Generated By Respiratory Strategy Indoors", Building and Environment, vol. 40, Issue 8, p. 1032–1039.

36- Y. Li, G. M. Leung, J. W. Tang, X. Yang, Y. H. Chao et al. 2007. “Role of Ventilation in Airborne Transmission of Infectious Agents in the Built Environment- a Multidisciplinary Strategyatic Review”, Indoor air, vol.17, p. 2-18.

37- ASHRAE. 2004. *Ventilation for acceptable Indoor Air Quality* (ANSI Approved), Standard 62.1-2004, Atlanta, GA.

38- Beggs, Clive B., Kevin G. Kerr, Catherine J. Noakes, E. Abigail Hathway, P. Andrew Sleigh. 2008. “The Ventilation of Multiple-Bed Hospital Wards: Review and Analysis”. American Journal of Infection Control, vol. 36, no 4, p. 250-259.

39- Andrius Jurelionisa, Laura Gagytėa, Tadas Prasauskasb, Darius Čiužasb, Edvinas Kruglyb Lina Šeduikytėa, Dainius Martuzevičius. 2015. “The Impact of the Air

Distribution Method In Ventilated Rooms On The Aerosol Particle Dispersion And Removal: The Experimental Approach", Energy and Buildings, vol. 86, p. 305–313.

40- Decker, J. 1995. "Evaluation of isolation rooms in health care settings using tracer gas analysis". Applied Occupational Environmental, Hygiene, vol. 10(11), p. 887–91.

41- Meckler, G. HVAC strategy characteristics. 1992. "Ventilation and Energy. Proceedings, Ia Q 92 Environments For People". ASHRAE, San Francisco, p. 327-338.

42- Occupational Safety and Health Administration (OSHA). 1997. *Occupational Exposure to Tuberculosis; Proposed Rule.* Labor, United States.

43- Xianting Li. 2009. "Response Coefficient: A New Concept To Evaluate Ventilation Performance With "Pulse" Boundary Conditions", Indoor and Built Environment, vol. 18, no. 3, p. 189-204.

44- Godish, T. 1989. *Indoor air pollution control*. CRC Press.

45- Spengler, JD, JM Samet, JF McCarthy. 2001. *Indoor air quality handbook*. McGraw-Hill Professional.

46- Sundell, J. 2004. "On The History of Indoor Air Quality and Health", Indoor Air, vol. 14, no 7, p. 51-58.

47- Nguyen, VH, C Beaudry, G Donnini et p Renzi. La qualité de l'air intérieur, 2. Coll, 1999. *La Qualité De L'air Intérieur–Aspects Techniques, Médicaux Et Juridiques*. 356 p.

48- Jianrong Yang, Xianting Li, Bin Zhao. 2004. "Prediction of Transient Contaminant Dispersion and Ventilation Performance Using the Concept of Accessibility". Energy and Buildings, vol. 36, Issue 3, p. 293–299.

49- Bin Zhao, Chun Chen, Zhongchao Tan. 2009. "Modeling of Ultrafine Particle Dispersion in Indoor Environments with an Improved Drift Flux Model", Journal of Aerosol Science, vol. 40, Issue 1, p. 29–43.

50- He, Guoqing, Xudong Yang, Jelena Srebric. 2003. "Contaminant Dispersion from an Area Source with Displacement Ventilation", In *Proceedings of the 4th International Symposium on Heating, Ventilating and Air Conditioning*. Beijing, China: Tsinghua University. p. 339-345.

51- Cai, Hao, Weiding Long, Xianting Li, Lingjuan Kong et Shuang Xiong. 2010. "Decision Analysis of Emergency Ventilation and Evacuation Strategies against Suddenly Released Contaminant Indoors By Considering the Uncertainty of Source Locations". Journal of Hazardous Materials, vol. 178, no 1-3, p. 101-114.

52- American Society of Heating, Refrigerating and Air-Conditioning Engineers, Inc. ASHRAE. 2008. *Ventilation of healthcare facilities* (ANSI Approved), Atlanta, GA: 30329.

53- Centers for Disease Control and Prevention. 1994. *Guidelines for Preventing Transmission of Mycobacterium Tuberculosis in Health-Care Settings*. Morbidity Mortality Weekly Report 43 (RR-13).

54- H. Changa, Sh. Kato, T. Chikamoto. 2004. "Effects of Outdoor Air Conditions on Hybrid Air Conditioning Based On Task/Ambient Strategy with Natural and Mechanical Ventilation in O&Ce Buildings". Building and Environment, vol. 39, p. 153 – 164.

55- M. Behne. 1999. “Indoor Air Quality in Rooms with Cooled Ceilings. Mixing Ventilation Or Rather Displacement Ventilation”. Energy and Buildings, vol. 30, p. 155–166.

56- Ventilation Principles, the Engineering Tool Box. 2015. Online. http://www.engineeringtoolbox.com/ventilation-efficiency-d_124.html.

57- Tardif, Michel. 2007. la ventilation par déplacement. Online. http://www.agpi.org/documents/file/atelier_formation/2007/D2.Michel_Tardif_Ventilation_par_deplacement.pdf .

58- Y.H. Yau, D. Chandrasegaran, A. Badarudin. 2011. “The Ventilation of Multiple-Bed Hospital Wards In the Tropics: A Review”, Building and Environment, vol. 46, p. 1125-1132.

59- Hua Qiana, b, Yuguo Lib, W.H. Setoc, Patricia Chingc, W.H. Chingb, H.Q. Sun. 2010. “Natural Ventilation for Reducing Airborne Infection in Hospitals”. Building and Environment, vol. 45, Issue 3, p. 559–565.

60- Alvin C.K. Lai, F.Z. Chen. 2007. “Comparison of a New Eulerian Model with a Modified Lagrangian Approach for Particle Distribution and Deposition Indoors”. Atmospheric Environment, vol. 41, Issue 25, p. 5249–5256.

61- Z. Zhang, Q. Chen. 2007. “Comparison Of The Eulerian And Lagrangian Methods For Predicting Particle Transport In Enclosed Spaces”, Atmospheric Environment, vol. 41, Issue 25, p. 5236–5248.

62- B. Zhao, Y. Zhang, X. Li, X. Yang, D. Huang. 2004. "Comparison of Indoor Aerosol Particle Concentration and Deposition in Different Ventilated Rooms By Numerical Method". Building and Environment, vol. 39, p. 1-8.

63- Jianbo Jiang, Xinlei Wang. 2012. "On The Numerical Study of Indoor Particle Dispersion and Spatial Distribution", Air, Soil and Water Research, vol. 5, p. 23–40.

64- Loth E. 2000. "Numerical Approaches for Motion of Dispersed Particles, Droplets, and Bubbles". Progress in Energy and Combustion Science, vol. 26, p. 161–223.

65- Shirolkar JS, Coimbra CFM, McQuay MQ. 1996. "Fundamental Aspects of Modeling Turbulent Particle Dispersion in Dilute Flows". Progress in Energy and Combustion Science, vol. 22, p. 363–399.

66- Crowe C, Sommerfeld M, Tsuji Y. 1998. "Multiphase Flows with Droplets and Particles". Boca Raton, Florida, CRC Press.

67- Loomans. M, Lemaire. T. 2002. "Particle Concentration Calculations Using CFD-A Comparison". Proceedings of Indoor Air, p. 153-156.

68- Riddle. A, Carruthers. D, Sharpe. A, McHugh. C, Stocker. J. 2011. "Comparisons Between FLUENT and ADMS for Atmospheric Dispersion Modeling". Atmospheric Environment, vol.38, p. 1029-1038.

69- Code Saturne 4.0.0 Theory Guide, online. http://code-saturne.org/cms/documentation

70- H. K. Versteeg, W. Malalasekera. 1995. "An Introduvtion to Computational Fluid Dynamics, the Finite Volume Method". Longman Group Ltd, England.

71- M. Promtong, P. Tekasakul. 2007. "CFD Study of Flow in Natural Rubber Smoking-Room: I. Validation with the Present Smoking-Room". Appl. Therm. Eng. Vol. 27, p. 2113-2121.

72- Zoran Milas, Damir Vučina & Ivo Marinić-Kragić. 2014." Multi-Regime Shape Optimization of Fan Vanes For Energy Conversion Efficiency Using CFD, 3D Optical Scanning And Parameterization". Engineering Applications of Computational Fluid Mechanics, Vol. 8, No. 3, p. 407–421.

73- Aerosol Technology. 2016. *Properties, Behavior, and Measurement of Airborne Particles, By William C. Hinds*. Second edition.

74- Pope. S. B. 2000. *Turbulent flows*. Cambridge University Press, Cambridge.

75- fPhilippe Nerisson, Olivier Simonin, Laurent Ricciardi, Alexandre Douce, Javaraly Fazileabasse. 2011. "Improved CFD Transport and Boundary Conditions Models for Low-Inertia Particles", Computers & Fluids, vol. 40, p. 79–91.

76- N. P. Gao, J. L. Niu. 2007. "Modeling Particle Dispersion and Deposition in Indoor Environments", Atmospheric Environment, vol. 41, p. 3862-3876.

77- A. C. K. Lai, W. W. Nazaroff. 2000. "Modeling Indoor Particle Deposition from Turbulent Flow onto Smooth Surfaces". Aerosol Science, vol. 31, p. 463-476.

78- Wood, N. B. 1981. "A Simple Method for the Calculation of Turbulent Deposition to Smooth and Rough Surfaces". Journal of Aerosol Science, vol. 12, p. 275–290.

79- B. Zhao, P. Guan. 2007. "Modelling Particle Dispersion in Personalized Ventilated Room", Building and Environment, vol. 42, p. 1099-1109.

80- R. H. Lochner, J. E. Matar. 1990. *Designing for Quality, an Introduction to the Best Of Taguchi And Western Methods Of Statistical Experimental Design*. ASQC Quality press, United States.

81- D. C. Wilcox. 1993. *Turbulence Modeling for CFD*. DCW Industries Inc., Canada, CA.

82- ASHRAE. 2013. *Thermal Environmental Conditions for Human Occupancy.* Standard 55.

83- Magdalena Cortés, Paul Fazio, Jiwu Rao, Waldo Bustamante, Sergio Vera. 2014. "Modelación CFD de casos básicos de convección en ambientes cerrados: Necesidades de principiantes en CFD para adquirir habilidades y confianza en la modelación CFD". Rev. ing. constr., vol. 29, no.1 Santiago.

84- Brian Spangler, Andrea Love, AIA, LEED AP, Charles Klee. 2013. "Ventilation deflation: Reducing HVAC energy consumption in laboratory buildings". Laboratory design, online. http://www.labdesignnews.com/articles/2013/04/ventilation-deflation-reducing-hvac-energy-consumption-laboratory-buildings.

85- Abdallah S. Berrouk, David E. Stock, Dominique Laurence, James J. Riley. 2008. "Heavy particle dispersion from a point source in turbulent pipe flow", International Journal of Multiphase Flow, Vol. 34, p. 916–923.